ENGINEERING OF FUNCTIONALIZED DNA-BASED MATERIALS AND THEIR APPLICATIONS

A Dissertation

Presented to the Faculty of the Graduate School

of Cornell University

In Partial Fulfillment of the Requirements for the Degree of

Doctor of Philosophy

by

Young Hoon Roh

January 2011

ENGINEERING OF FUNCTIONALIZED DNA-BASED MATERIALS AND THEIR APPLICATION

Young Hoon Roh, Ph. D.

Cornell University 2011

DNA has been utilized to engineer the novel functionalized and networked nanostructures in this dissertation. Based on the anisotropicity and multivalency of branched DNA building blocks, a multifunctionalized nanocarrier platform, termed “DNAsomes”, was constructed. These DNAsomes are liposome-like core-shell structures formed by the self-assembly of branched DNA-lipid hybrid molecules. The size and surface charge of self-assembled DNAsomes can be precisely manipulated. Importantly, DNAsomes were introduced as universal multi-functional drug carriers, particularly well-suited for small interfering RNA (siRNA) delivery due to the inherent base-pairing with DNA.

X-shaped DNA (X-DNA) has four branched arms, providing multivalent functionalities that allow for simultaneous multiple crosslinking. By synthesizing four acrylate-functionalized X-DNA monomers, monodisperse and tunable DNA nanospheres were generated via photocrosslinking. The size and surface charge of these nanospheres were precisely controlled in a linear fashion, simply by adjusting the monomer concentration in the reaction. In addition, *in vitro* studies in mammalian cells revealed that these DNA nanospheres demonstrated significant efficacy in the delivery of a hydrophobic small molecule drug that intercalates DNA. These results highlight the potential of using DNA as a material building block to design novel nanocarriers with properties tailored for the delivery of drugs in general.

New methods to construct functionalized DNA hydrogels were also demonstrated. Unlike traditional enzyme-catalyzed method, networked DNA gels were generated by remotely controlled photopolymerization of functionalized X-DNA building blocks. The gelling process was rapidly achieved within several minutes and the mechanical strength of gel matrixes was dramatically improved by adjustment with additional PEG monomers. Various types and shapes of photocrosslinked DNA hydrogels were prepared and further investigated for cell-free protein expression. Fine tuning of each system has its own benefits in terms of protein yield, format, and stability. These results highlight that DNA building blocks can be utilized as novel materials for bio-related applications, particularly in protein engineering.

BIOGRAPHICAL SKETCH

Young Hoon Roh was born and raised on Pusan city in South Korea. From a young age, he had a great interest in education and medicine. After graduating from Naesung high school, he decided to study biological engineering as his major. He received his B.Sc. in Biotechnology at Yonsei University, South Korea in 2002. During his undergraduate years in Korea, he worked to expose himself to interdisciplinary fields of study in addition to his major. Then he entered graduate school at Yonsei University for a master's degree. As a graduate student he found the opportunity to participate in more specific research projects. He achieved his Master's degree at Yonsei University, South Korea in 2004, during which his work was focused on the development of novel biomaterials for drug delivery. In that project he synthesized alginate-carrageenan complex films and examined their physical properties. His research also investigated key factors for enterokinase fermentations using a recombinant *Saccharomyces cerevisiae*.

After gaining his first masters degree, he worked for one year in the Institute of Microbial Cultures. During this time, he developed a novel method for enhancing the efficiency of recombinant protein production in mammalian and microbial cells, using combinatorial libraries of zinc finger protein transcription factors.

In 2006, he joined Professor Dan Luo's group in biological engineering at Cornell University for his Ph.D degree. His research interests lie in the field of DNA nanotechnology to engineer novel functionalized and networked nanostructures with possible bio-related applications towards nucleic acid delivery and protein engineering. After five fruitful years in Luo's group, he will continue exciting postdoctoral work.

To my grandparents, my father, my mother, and my sister

ACKNOWLEDGMENTS

I give special thanks to my academic advisor, Prof. Dan Luo, for inspiration and advice on my research and independent study. He provided and encouraged me with tremendous support and guidance toward completing my Ph.D. study at Cornell University. His passion for research will have a great influence on my future career. I would also like to thank my thesis committee members, Prof. Michael L. Shuler and Prof. Chih-Chang Chu for their valuable advice and comments regarding my research.

I also deliver my thanks to former and present colleagues in Luo research lab, especially Prof. Jay Xu, Prof. Hisakage Funabash, Prof Soong Ho Um, Dr. Nokyoung Park, Dr Jong Bum Lee, Prof. Jong Hwan Sung, Prof. Dayong Yang, Mark Hartman, Pichamon Kiatwuthinon, Shawn Tan, Mike Campolongo, Thua Nguyen Nhi Tran, Jason Kahn, Songming Peng, Roanna Ruiz, Edward Rice, Bojeong Kim, Hyeongsu Park, Ja Eun Lee, Min Kyoung Hwang for their valuable technical support and discussions.

I also appreciate my grandfather, grandmother and sister for their encouragement. Finally, I give special thanks to my parents, Jae Chung Roh and Jung Gum Park, for their endless love and sacrificial support throughout my entire Ph. D. degree. Without their help, I would not have been able to complete the Ph.D. program.

TABLE OF CONTENTS

LIST OF FIGURES

LIST OF TABLES

CHAPTER 1

Engineering DNA-based Materials

*Young Hoon Roh[1], Songming Peng[1], Roanna C. H. Ruiz[1], Michael J. Campolongo[1], Jong Bum Lee[1], Dan Luo[1] "Engineering DNA-based Materials". *Paper in preparation* (2011).

[1]Department of Biological and Environmental Engineering, Cornell University
Ithaca, New York, 14850, USA

1.1. Introduction

Since the DNA structure was determined in 1953 by Watson and Crick,[1] DNA has been addressed in many research areas such as molecular biology, genomics and gene therapy.[2] The invention of the polymerase chain reaction (PCR) further accelerated its wide usage.[3] The unique properties of DNA play a critical role in connecting molecular biology to materials science and engineering.[4] In addition recent progress of DNA nanotechnology provides an excellent capability of DNA as a true polymeric material for the construction of highly complicated nanostructures. Different shapes of DNA as 'material building blocks' have been created to enhance their applicability. Here, various types of DNA-based nanostructures and nanomaterials were introduced including DNA dendrimers, ABC monomer and DNA gels. With these novel DNA materials, real-world applications in diagnostics, protein engineering, and drug delivery were further described.

1.2. Unique properties of DNA as a polymeric material

1.2.1. DNA properties

The meaning of the genetic code is determined by the combination of DNA sequences (A, T, G, and C). DNA can also be recognized as a polymer by the random distribution of repeating units. DNA molecules consist of two major components: a phosphate-deoxyribose backbone consisting of five-carbon sugar molecules tethered together through phosphodiester bonds and four different bases such as adenine (A), thymine (T), guanine (G), and cytosine (C).

Generally these DNA molecules could be found in either single-stranded DNA (ssDNA) or double-stranded DNA (dsDNA). One end of every DNA strand possesses a phosphate group named as the 5' end due to the location of phosphate group (on the 5' carbon of the sugar ring), and the other end is terminated with a hydroxyl group

named as the 3' end (on the 3' carbon of the sugar ring). Two anti-parallel strands (ssDNA) may hybridize into a double helix structure (dsDNA) in opposite directions (from 5' to 3' and from 3' to 5') by following the Watson-Crick base pairing rule (A always pairs with T, and G always pairs with C via hydrogen bonding). Base pairing between G-C gives rise to a more stable structure than A-T because more hydrogen bonds are incorporated (three and two hydrogen bonds, respectively, Figure 1.1a). Furthermore this hybridization is entirely reversible. The double helical structure of dsDNA can be dehybridized into two separated ssDNA under conditions of high pH or temperature. These non-covalent and reversible DNA properties provide important parameters in the DNA sequence design for self-assembly.

1.2.2. DNA as a polymeric material

The unique properties of DNA give it an excellent capability for the building of nanomaterials. Physically, the DNA double helix can exist in either linear or circular forms in nature. One helix turn is made up of ten base pairs with a length of 3.4 nm (hence 0.34 nm per each nucleotide base pair), and the width of the double helix is approximately 2 nm in the B-DNA conformation. This structural property makes DNA an intrinsic nanoscale entity. Mechanically, the flexibility and rigidity of DNA can be easily manipulated by selecting the number of base pairs. DNA can form a rigid structure when the number of sequences is shorter than its persistence length. The persistence length of dsDNA is about 50 nm (corresponds to 150 bp) and ssDNA is about a 1 nm (corresponds to a few bases).[5-9] Furthermore by selecting and designing the combination of ssDNA and dsDNA, the flexibility and rigidity of desired DNA structure can be tailored.[10]

Chemically and biologically, DNA is normally stable, water soluble, and biocompatible making it to be suitable for biomedical applications. Importantly, DNA

can be easily and precisely manipulated by numerous chemical and physical methods with molecular accuracy (at the angstrom level). For example, DNA can be cut at specific sites by restriction enzymes and elongated covalently by ligase enzymes. Under appropriate conditions, DNA molecules can be self-assembled with complementary strands of other nucleic acid. Moreover, DNA molecules can be amplified by using the powerful technique of polymerase chain reaction (PCR) that is a chemical method to increase the amount of specific DNA template exponentially. All the previously mentioned reasons make DNA an excellent and attractive candidate compared to other currently available synthetic and natural polymers for constructing nanomaterials.

1.3. DNA engineering

One of the fundamentally important aspects for designing and engineering DNA is its molecular recognition ability through the Watson-Crick base pairing rules which make DNA hybridization and self-assembly rationally programmable. Normally bulk DNA including genes and DNA fragments can be obtained from bacteria and yeast culture, and shorter DNA sequences can also be achieved commercially by *de novo* synthesis method. The basic steps for DNA engineering include two different assembly processes: self-assembly (hybridization), and enzyme-catalysed assembly (ligation). Two different dsDNA duplexes can be bound together spontaneously by the hybridization of sticky ends (Figure 1.1b). This process is caused by various non-covalent interactions, such as hydrogen bonds, hydrophobic interactions, electrostatics, and base stacking and van der Waals forces. In the next step, nicks between two hybridized dsDNA can be permanently sealed by enzyme ligation, resulting in a single combined duplex.

More importantly, numerous different kinds of enzymes (termed as 'molecular biology tool kits') provide versatility and controllability for DNA engineering including the synthesis, manipulation, and modification of DNA molecules (Table 1.1).[4] In more detail, endonucleases and exonucleases work as 'scissors and sanders' to cut DNA strands at internal sites and from their terminal ends respectively. On the other hand restriction enzymes[11] function as 'table saws' that can precisely recognize and specifically cleave DNA sequences. In addition, nonspecific nucleases functioning as a 'grinder' to degrade both ssDNA and dsDNA into single monomers. Single-stranded endonucleases that can only recognize and cut protruding sequences of ssDNA, function as 'trimmers'. DNA can also be elongated by polymerases such as T4 DNA polymerase and *Taq* polymerase. DNA can be linked together covalently and permanently by ligases that work as a 'glue'. The connection within two dsDNA only occurs when the two protruding ends (named as 'sticky ends') contain complementary sequences.

Another key aspect of DNA engineering is that it can be modified by several chemical methods. Numerous small chemicals including primary amine, thiol, biotin groups, and fluorescent dyes work for conjugation onto either the 5' phosphate or 3' hydroxyl groups during synthesis. These chemically modified DNA can be further attached onto the surface through non-covalent or covalent binding. In the first method, biotin modified DNA strands can be used, which have extraordinary affinity with streptavidin. This biotin-avidin interaction is one of the strongest known noncovalent binding interactions. In the second method, one popular approach for covalent binding is through linkage with Au. DNA labeled with either a disulfide or thiol group can be conjugated with an Au surface.

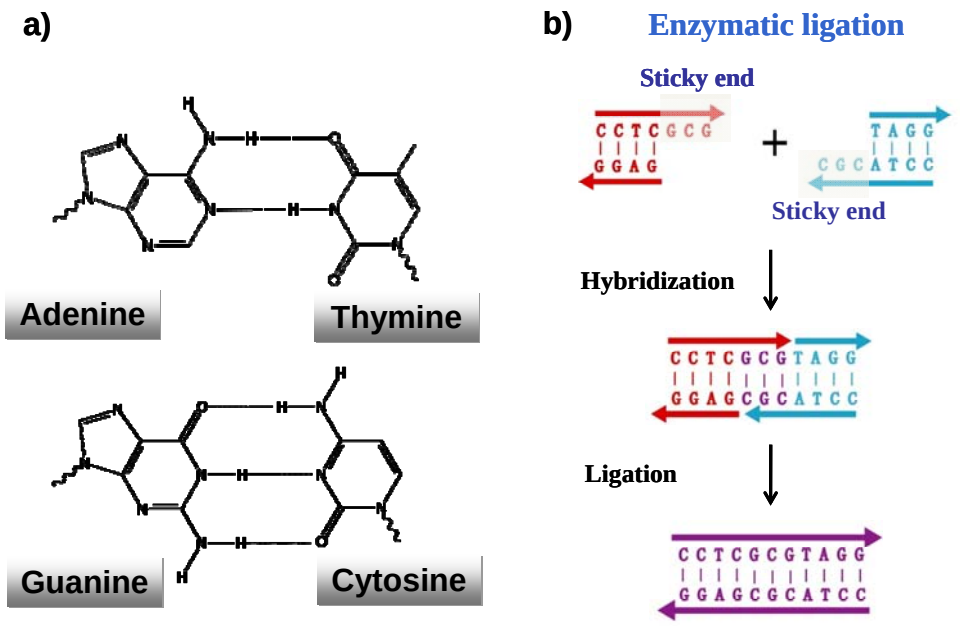

Figure 1.1. Basic Principles of DNA self-assembly. (**a**) The DNA double helix is formed from two single-stranded DNA by obeying the Watson–Crick base-paring rules (adenine (**A**) always pairs with thymine (**T**) and guanine (**G**) always pairs with cytosine (**C**)). (**b**) The two double-stranded DNA (dsDNA) can be connected by the hybridization of sticky ends. The nick between the two dsDNA can be chemically linked by enzyme ligation, resulting in a single dsDNA.

Table 1.1. Molecular biology tool kits for DNA engineering. Reprinted from Materials today, 6, Luo, D., The road from biology to materials, 38-43, Copyright (2003), with permission from Elsevier.

Function			Enzymes	Properties
Elongating DNA or RNA	Polymerization template needed?	Yes	T4 DNA Polymerase	Uses existing DNA as a template and adds deoxynucleotides to the 3'-hydroxy end of the complementary strand. Direction: 5'→ 3'
			E. Coli DNA polymerase I	Same as the above
			Taq polymerase	Same as the above; only works at 72°C Same as the above; only works with a RNA template (i.e. makes DNA from RNA)
			Reverse transcriptase	
		No	Terminal transferase	Adds deoxyribonucleotides directly to the 3'-hydroxy end without any templates
			Poly A polymerase	Adds deoxyribonucleotides (A) to RNA at the 3'-end
	Non-polymerization		T4 DNA ligase	Joins dsDNA together
			E. coli DNA ligase	Joins dsDNA together
			T4 RNA ligase	Joins RNA together
				Joins ssDNA together
Shortening DNA or RNA	Exonucleases	Specific	λ Exonuclease	Cuts DNA from 5'→ 3'
			Exonuclease III	Cuts DNA from 3'→ 5'
			Ribonuclease H	Degrades only RNA in DNA:RNA hybrids
			Mung bean nuclease	Degrades only ssDNA
		Non-specific	Bal 31 nuclease	Cuts DNA from both 5'- and 3'-ends
			Exonuclease VII	Cuts ssDNA from both 5'- and 3'-ends
			Ribonuclease A	Degrades RNA
			Ribonuclease T1	Degrades RNA
			Micrococcal nuclease	Degrades RNA
	Endonucleases	Specific	Restriction enzymes (more than 3000)	Cuts DNA at a specific sequence
		Non-specific	DNase I	Degrades DNA
			Micrococcal nuclease	Degrades DNA
Modifying	At 5' end		T4 polynucleotide kinase	Labels DNA at 5' with phosphate, biotin, etc.
			Klenow fragment	Labels DNA at 5' with phosphate, biotin, etc.
	At 3' end		Terminal transferase	Labels DNA at 3'-end
	At internal sites		Methylase	Methylates DNA

1.4. Anisotropy and multivalency of DNA building blocks

1.4.1. Branched DNA

Naturally, both single-stranded and double-stranded DNA can form only linear or circular structures, which restricts their usefulness as 'material building blocks'. Thus, it is necessary to create different shapes of DNA molecules with multiple dimensions to enhance their applicability. Luo et al. have created the Y-shaped and X-shaped DNA building blocks.[12,13] (Figure 1.2) These branched DNA are designed to contain specific extra sequences, named as sticky ends, which enable them to connect to other specific branched DNA building blocks through enzymatic methods (enzyme ligation). This process makes it possible to grow DNA building blocks into dendrimer-like structures in a precisely controlled fashion. Furthermore each ssDNA can contain different functional moieties, allowing them to form ideal anisotropic/isotropic and multivalent building blocks. These building blocks can be easily and precisely modified with almost any kind of chemical moiety as long as they can be linked with a DNA strand. These multivalent and anisotropic (or isotropic) properties enable branched DNA structures including DNA dendrimers to serve as potential designer materials.

1.4.2. Anisotropy of DNA building blocks

Anisotropic interactions based on physical, chemical, or biological methods are useful to introduce multiple functional moieties within a single building block.[14] This binding selectivity of anisotropic building blocks provides precise control in construction architectures with structural complexity. Although asymmetrically shaped structures have been introduced through other methods [15-17], polydispersity of the constructed structures still inhibit binding sensitivity and selectivity. However, the

anisotropy and monodispersity of DNA building blocks overcomes these barriers, providing excellent controllability and selectivity over intermolecular interactions.

1.4.3. ABC monomer (anisotropic, branched, and crosslinkable monomers)

Based on the multivalency and anisotropicity of branched DNA structures, Luo and colleagues demonstrated a general approach to create multifunctional nanoarchitectures.[18] The ability to attach different functional moieties onto each arm of branched DNA building blocks allows the investigation to form precisely regulated anisotropic, branched and crosslinkable monomers, termed as ABC monomers. Each Y-DNA building block, chemically modified with a functional moiety, served as the donor molecule and X-DNA was utilized as the core acceptor. Anisotropicity was realized by designing unique DNA sequences at each arm of branched X-DNA (sticky-ends). In addition, multifunctionality was achieved by the specifically controlled connection of different donor Y-DNA onto the one acceptor X-DNA. Due to the built-in modularity, the type and number of functional moiety that can be bounded to the core is virtually unrestricted and unlimited. The bridge ssDNA, with a sequence complementary to both donor and acceptor sequences, was designed to link the Y-DNA with the X-DNA.

This approach leads to applications in a DNA-based target-driven polymerization that is photo-polymerized only in the presence of a targeted DNA. To construct DNA-based nanoarchitectures for target-driven polymerization, each ABC monomer was labeled with quantum dots (QDs), a photocrosslinkable group, and single-stranded oligonucleotide probes that contains the complementary sequence code to a specifically targeted pathogen DNA including those from *Bacillus anthracis*, *SARS coronavirus*, or *Ebola* virus. The ABC dimer was formed in the presence of pathogen DNA. Here the pathogen DNA worked as a complementary linker DNA

between two ABC monomers. Upon short UV illumination, these ABC dimer structures formed polymeric aggregates (Figure 1.3). Notably this process only occurred in the presence of a targeted DNA linker. For example with unrelated DNA linker sequence, the process of polymerization did not happen. These target-driven polymeric spheres were further analyzed by epi-fluorescence optical microscopy with their pre-assigned fluorescence color-codes. In this manner, target-driven polymerization provides a rapid and simple signal amplification method for pathogens detection with high sensitivity and selectivity.

1.5. DNA nanotechnology

1.5.1. Self-assemblies of DNA into 2D and 3D structures

Since Seeman pioneered the field of DNA nanotechnology, much progress has been achieved from designing synthetic DNA subunits to constructing highly ordered complex nanostructures.[19] This area, following rules that molecular recognition capability and programmable assembly of DNA, can give rise to the construction of designed nanostructure within precisely controlled nanometer range.[20] Such DNA programmability by following Watson-Crick base pairing makes it possible to find and connect two DNA molecules together via the complementary sequence. Also well-developed synthesis methods allow that any desired DNA base sequence can be easily prepared. The general methods for the sequence design of DNA building blocks has been based on empirical rules.[21] Also recently computer simulations and modeling have been developed to design the structure of DNA building blocks.[22]

In 1998, Seeman first introduced artificial DNA tiles and lattices.[23] These synthetic branched DNA contained fixed and multi-armed junctions.[24] However, the challenge to construct well-ordered two- and three-dimensional DNA assemblies was to generate rigid DNA building blocks. Seeman further developed DNA crossover

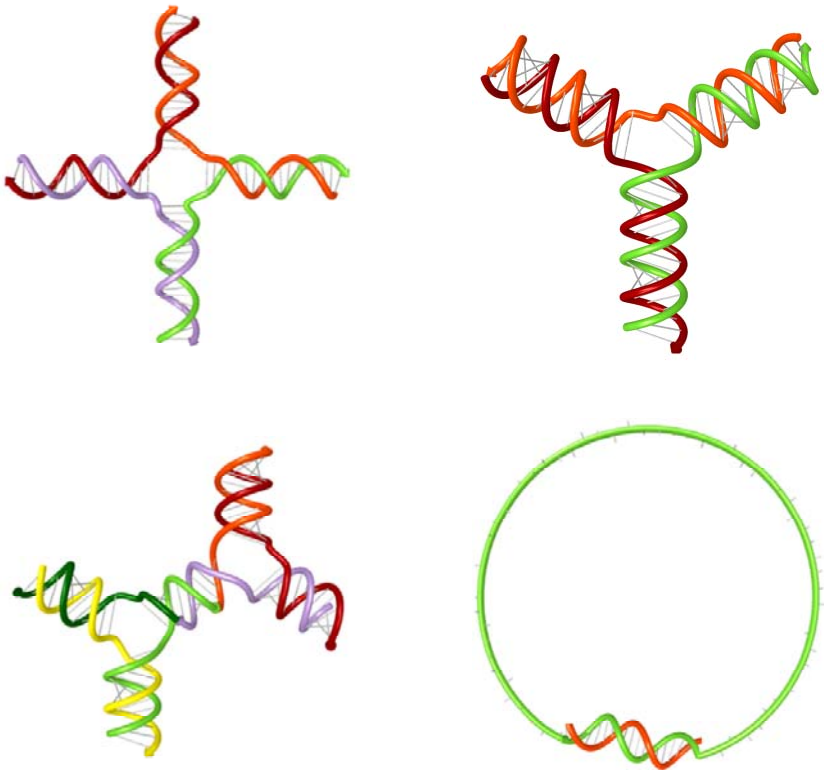

Figure 1.2. DNA building blocks. Schematic illustration of the structure of X-shaped, Y-shaped, dumbbell-shape and circular-shape DNA. Each four or three ssDNA are utilized to synthesize X-DNA and Y-DNA by changing annealing temperature.

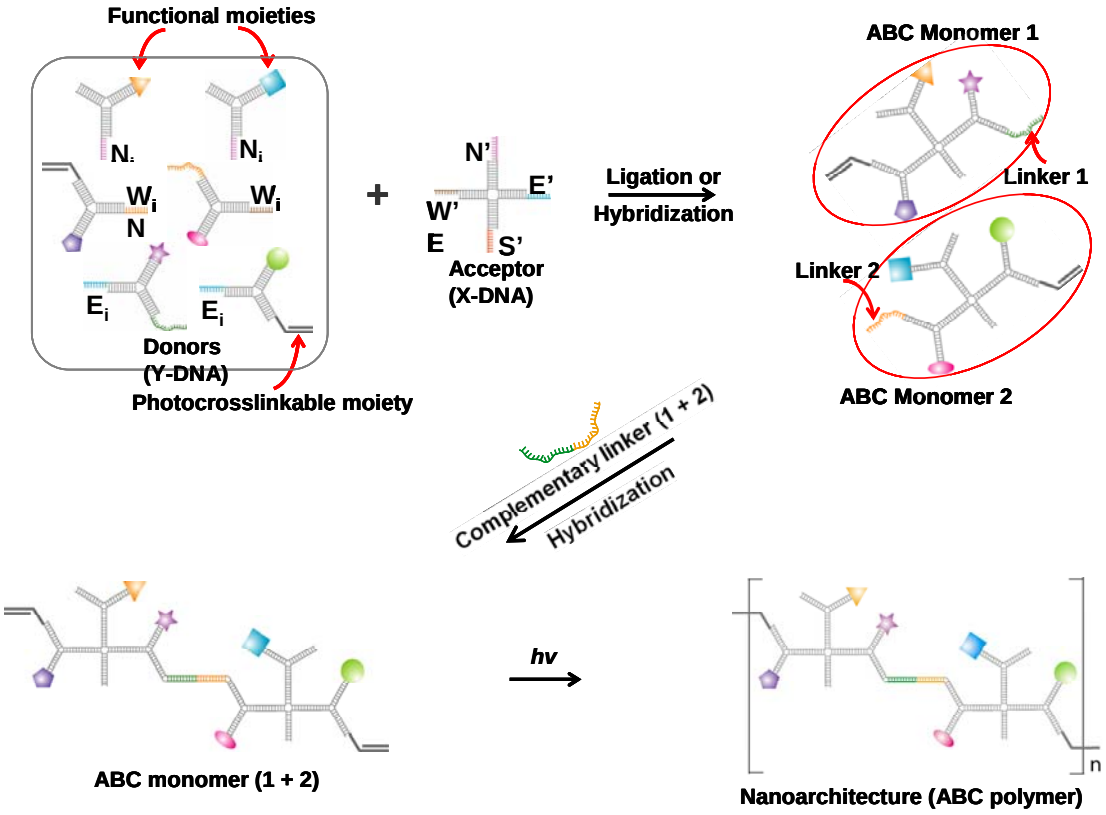

Figure 1.3. Schematic illustration of the general approach to synthesize ABC monomer and target-driven photo-polymerization. Multiple functional moieties are conjugated onto Y-DNA donors. The ABC monomer is formed when the functionalized Y-DNAs are linked into corresponding end-sequences of acceptor X-DNA. ABC monomers 1 and 2 are linked together via hybridization with a bridge pathogen DNA as a linker. Then ABC monomers (1 + 2) are photo-polymerized under the short UV illumination. Reprinted by permission from Macmillan Publishers Ltd: Nature nanotechnology (18), copyright (2009).

tiles (e.g. a double-crossover (DX) and triple-crossover (TX)) to improve rigidity.[23-32] These self-assembled 'double crossover' building blocks guide the two dimensional complex arrays of nanocomponents with nanometer precision.[33, 34]

The field of structural DNA nanotechnology has been further developed to create more complex nanostructures including two-dimensional patterns[35] as well as three-dimensional shapes. Rothemund significantly improved this concept with the demonstration of scaffolded DNA origami structures.[36] Using a long and single-stranded DNA as a scaffold material, this simple 'one-pot' approach enables one to generate nanometer-scale and two-dimensional sheets with a desired surface pattern such as stars, smiley faces and even more complicated shapes (Figure 1.4).

Furthermore three-dimensional DNA assemblies have been reported. Seeman first demonstrated 3D DNA cubes[37], truncated octahedron[38] and octahedron with a long ssDNA[39] which are a closed polyhedral DNA structure. Luo and colleagues also reported a three-dimensional DNA hydrogel matrix from branched DNA by enzymatic ligation.[40] Recently Mao successfully demonstrated polyhedron DNA structures (tetrahedron, dodecahedron and buckyball DNA structures (Figure 1.5).[41] These complicated DNA structures were synthesized via one-pot assembly by changing the flexibility and concentration of the motifs. Anderson et al also reported a 3D DNA polyhedron box with programmed opening of the box lid (Figure 1.6).[42] In addition Douglas et al have introduced a general methodology to construct and design three-dimensional DNA nanostructure (Figure 1.7).[43]

1.6. DNA hydrogel

DNA hydrogels entirely made by pure DNA or chemically crosslinked with other polymer materials have been demonstrated. These gels have been further introduced in a broad range of biomedical applications especially in drug delivery and

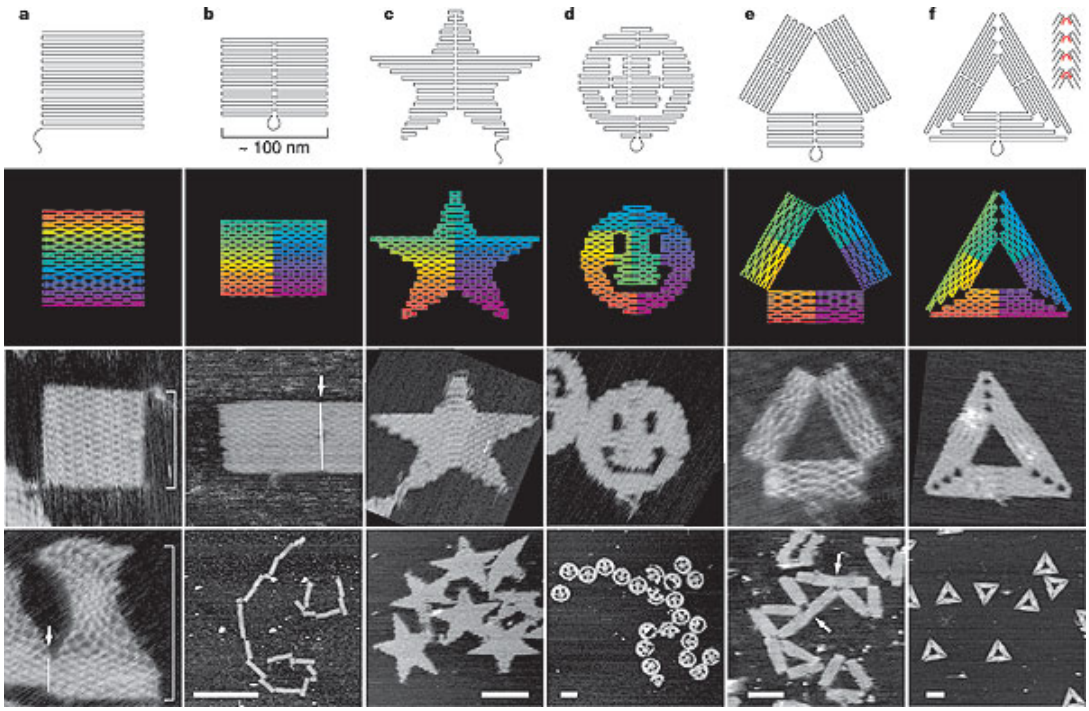

Figure 1.4. Various shapes of two-dimensional scaffolded DNA origami structures. Top row, folding paths. **a**, square; **b**, rectangle; **c**, star; **d**, disk with three holes; **e**, triangle with rectangular domains; **f**, sharp triangle with trapezoidal domains and bridges between them (red lines in inset). Dangling curves and loops represent unfolded sequence. Second row from top, diagrams showing the bend of helices at crossovers (where helices touch) and away from crossovers (where helices bend apart). Colour indicates the base-pair index along the folding path; red is the 1st base, purple the 7,000th. Bottom two rows, AFM images. All images and panels without scale bars are the same size, 165 nm ×165 nm. Scale bars for lower AFM images: **b**, 1 μm; **c**–**f**, 100 nm. Reprinted by permission from Macmillan Publishers Ltd: Nature (36), copyright (2006).

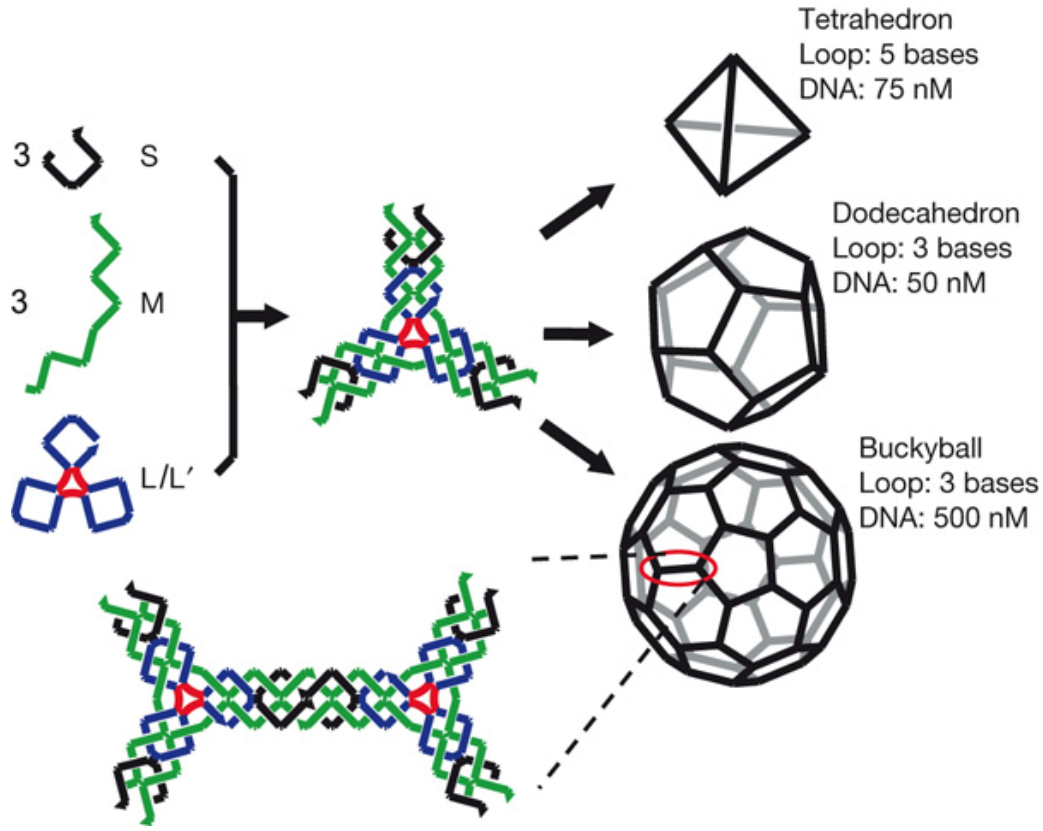

Figure 1.5. Self-assembly of DNA polyhedra. Three different types of DNA single strands stepwise assemble into symmetric three-point-star motifs (tiles) and then into polyhedra in a one-pot process. There are three single-stranded loops (coloured red) in the centre of the complex. The final structures (polyhedra) are determined by the loop length (3 or 5 bases long) and the DNA concentration. Reprinted by permission from Macmillan Publishers Ltd: Nature (41), copyright (2008).

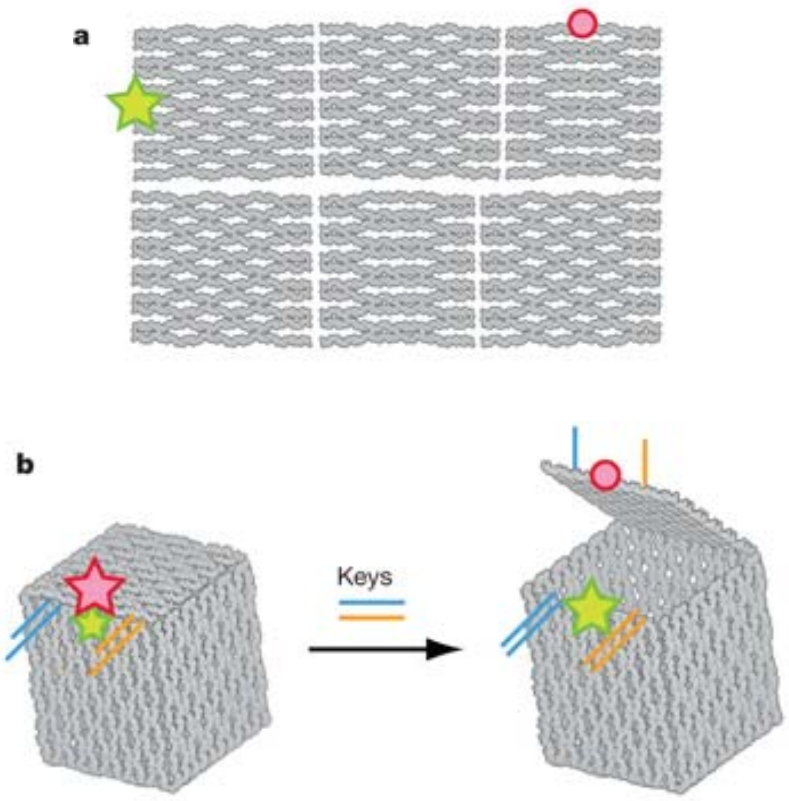

Figure 1.6. Programmed opening of the box lid. Illustrations of the unlinked faces of the box (**a**) and the controlled opening of the box lid (**b**). The emission from the Cy5 and Cy3 fluorophores are marked with red and green stars, respectively. Loss of emission from Cy5 is denoted by a red circle and the independent lock–key systems are indicated in blue and orange. Reprinted by permission from Macmillan Publishers Ltd: Nature (42), copyright (2009).

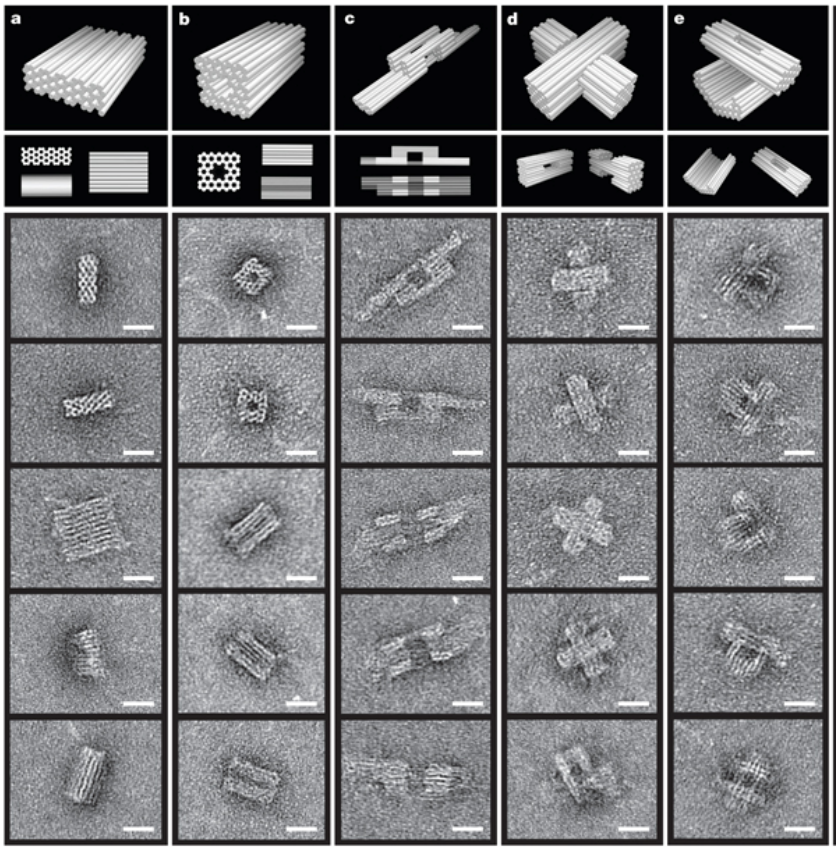

Figure 1.7. Three-dimensional DNA origami shapes. The first and second rows show perspective and projection views of cylinder models, with each cylinder representing a DNA double helix. **a**, Monolith. **b**, Square nut. **c**, Railed bridge. **d**, Slotted cross. **e**, Stacked cross. Rows three to seven show transmission electron microscope (TEM) micrographs of typical particles. Reprinted by permission from Macmillan Publishers Ltd: Nature (43), copyright (2009).

tissue engineering, as well as cell-free protein engineering.[44] There are several approaches to synthesize a DNA hydrogel matrix.

The first method to produce DNA hydrogels is through enzyme ligation. Luo et al demonstrated biodegradable, biocompatible, and inexpensive hydrogels that can be easily manipulated into any desired form for biomedical applications especially in controlled drug delivery and tissue engineering.[40] Here different shapes of branched DNA building blocks (X-DNA, Y-DNA and T-DNA) were designed and prepared as a starting material. The cross-shaped branched DNAs with "sticky ends" were further annealed to each other by enzyme-catalyzed ligation to create a three dimensional hydrogel matrix (Figure 1.8). The reported gelling processes were accomplished at physiological condition (without high temperatures or harsh chemicals), allowing encapsulated material to be introduced in the gel matrix *in situ*. Due to the fact that these gel matrixes consist of entirely synthetic DNA, an immune response can be avoided,[45, 46] enabling the encapsulation of proteins and even live cells. By choosing the types of branched DNA and the concentration of DNA in the reaction mixture, their rigidity and absorbency of gel matrixes can be easily tailored. More recently, these enzyme-ligased DNA hydrogels were further applied for stimuli-responsive approach.[47] Y-DNA building blocks were designed and assembled via the conformation of intermolecular structures (i-motif). The networked DNA hydrogel contains a phase switchable ability in minutes by simply adjusting environmental pH.

A second method is, instead of using enzyme-catalyzed approach to link neighbor DNA building blocks together, to introduce chemically crosslinked DNA hydrogels.[48-52] A third approach is the physically entangled method to make stable DNA networks. Instead of using any crosslinking agent and chemical/enzymatic covalent method, DNA hydrogel fibers were prepared by physical entanglements of very flexible linear DNA.[53, 54] Compacted interwined toroids were further entangled to

form DNA hydrogel fibers during the wet spinning. Room-temperature hydrophilic ionic liquids (RTILs) were used as condensing agent to enhance coagulation during wet spinning process. These DNA hydrogel fibers revealed the resistance to the wide range of pH and digestion of DNases.

1.7. Cell-free protein producing DNA gel (P-gel)

Recently DNA-based hydrogel networks were introduced as a general platform for protein production in a cell-free system (Figure 1.9).[55, 56] Such a system can easily and efficiently express all proteins, including toxic proteins or even multiple proteins from protein-producing nucleic acid gel matrices (termed as "P-gel") without any living organisms or cells. Moreover, gene mutations can be directly investigated without further transformation and selection at the protein level. In addition this cell-free system eliminates the complicated process of purification of final protein products. In terms of protein yield, the production of protein is expected to be efficiently high. Also the protein production cost can be low because of the reusability of both enzymes and P-gel matrices, and can be further reduced by eliminating additional processes including live cells feeding, reactors maintenance, and post-expression purification steps.

A P-gel matrix is made up of two classes of nucleic acid molecules. First, branched DNA building blocks are prepared as a structural supporter. Second part is that linearized nucleic acids contain encoding a protein of interest. This part can be specifically designed one or more encoding to provide protein-encoding matrix that can produce one or multiple proteins. Those two categories are connected together by enzyme ligation for the construction of protein-producing and three-dimensional networked structures.

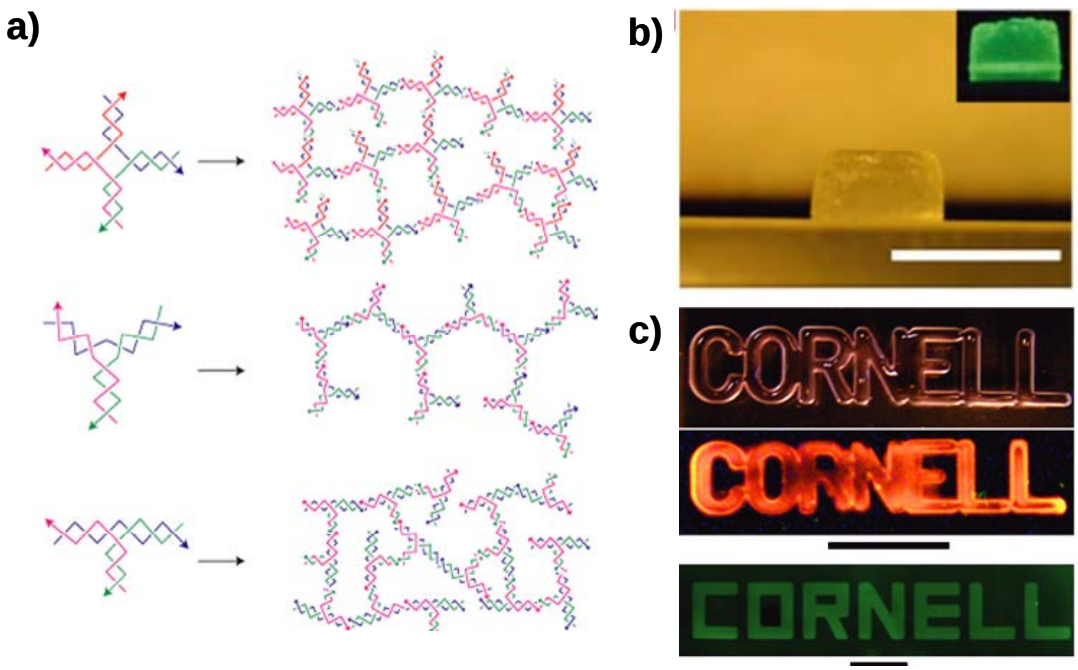

Figure 1.8. DNA hydrogel from branched DNA building blocks by T4 DNA ligation. (**a**) X-, Y- and T-DNA shaped building blocks serve as crosslinkers to form networked gels. (**b**) A swollen X-DNA hydrogel fabricated in a cylindrical mould. The size is 7.0 mm in diameter and 3.0 mm in height. The scale bar is 1 cm. The inset shows the DNA gel stained with SYBR I. (**c**) X-DNA gels patterned in CORNELL shapes at centimetre scale (top and middle rows, the scale bar is 1 cm) and micrometre scale (bottom row, the scale bar is 500 μm). They were stained with two different, DNA-specific fluorescent dyes: ethidium bromide (red, the middle row) and SYBR I (green, the bottom row). Reprinted by permission from Macmillan Publishers Ltd: Nature materials (40), copyright (2006).

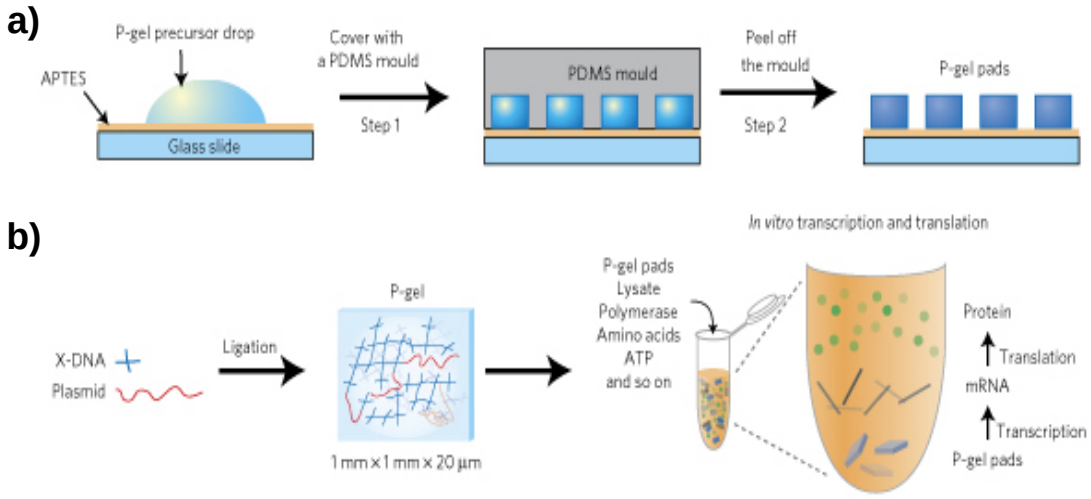

Figure 1.9. Protein producing DNA hydrogel (P-gel). (**a**) The formation of P-gel micropads. The P-gel precursor drop, which includes X-DNA, genes and T4 DNA ligase, was confined within a PDMS mould with precisely pre-defined dimensions to control the exact gene amount within the P-gel scaffolding and also to obtain a higher surface-to-volume ratio of P-gel (Step 1). After gelation, the PDMS mould was peeled off from the substrate (Step 2), and P-gel micropads were formed. (**b**) A schematic diagram of the gelation process through enzymatic crosslinking and cell-free expression with P-gel pads. Reprinted by permission from Macmillan Publishers Ltd: Nature materials (54), copyright (2009).

1.8. Significance of this dissertation

The excellent programmability and molecular recognition capability of DNA has allowed the engineering of novel functional nanomaterials. Much research in the field of DNA nanotechnology has improved the construction of various DNA-based nanostructures and networks, including ordered supramolecular assemblies, DNA origami, and three-dimensional objects. However, the study of using DNA as anisotropic and multivalent building block, and its applications in the biomedical field still needs to be investigated. The second chapter in this dissertation demonstrates the novel multifunctional nanocarrier platform assembled from anisotropic and branched DNA building blocks, termed as "DNAsomes". These self-assembled DNAsomes can be engineered to specific sizes and surface charges on demand. Furthermore, DNAsomes are introduced as multi-drug carriers, particularly well-suited for siRNA delivery due to the inherent base-pairing with DNA. The third chapter addresses a rapid and simple synthesis method of functionalized X-DNA building blocks which can be further photocrosslinked to form monodisperse DNA nanospheres with tunable properties. The fourth chapter describes the new types and formats of DNA hydrogels synthesized by photopolymerization of DNA building blocks. Four different types of photocrosslinked DNA hydrogels from branched DNA building blocks were engineered. In addition, their application in cell-free protein expression will be discussed. Each system has its own benefits in terms of protein yield, format, and stability. These results emphasize that our branched DNA building blocks can be utilized as novel material for biomedical application, particularly in drug delivery and protein engineering fields.

REFERENCES

1. Watson, J. D. & Crick, F. H. C. A structure for deoxyribose nucleic acid. *Nature* **171,** 737-738 (1953).
2. Seeman, N. C. DNA nanotechnology. *Mater. Today* **6,** 24-29 (2003).
3. Saiki, R. K. *et al.* Enzymatic amplification of beta-globin genomic sequences and restriction site analysis for diagnosis of sickle cell anemia. *Science* **230,** 1350-1354 (1985).
4. Luo, D. The road from biology to materials. *Mater. Today* **6,** 38–43 (2003).
5. Smith, S. B., Cui, Y. & Bustamante, C. Overstretching B-DNA: the elastic response of individual double-stranded and single-stranded DNA molecules. *Science* **271,** 795-799 (1996).
6. Vologodskaia, M. & Vologodskii, A. Contribution of the intrinsic curvature to measured DNA persistence length. *J. Mol. Biol.* **317,** 205-213 (2002).
7. Bouchiat, C. *et al*. Estimating the persistence length of a worm-like chain molecule from force-extension measurements. *Biophys. J.* **76,** 409-13 (1999).
8. Tinland, B., Pluen, A., Sturm, J. & Weill, G. Persistence length of single-stranded DNA. *Macromolecules* **30,** 5763-5765 (1997).
9. Toth, K., Sauermann, V. & Langowski, J. DNA curvature in solution measured by fluorescence resonance energy transfer. *Biochemistry* **37,** 8173-8179 (1998).
10. Yang, D. *et al*. Novel DNA materials and their applications. *Advanced Review* **2,** 648–669 (2010).
11. Roberts, R. J. & Macelis, D. REBASE—restriction enzymes and methylases. *Nucl. Acids Res.* **29,** 268-269 (2001).
12. Li, Y. *et al*. Controlled assembly of dendrimer-like DNA. *Nature Mater.* **3,** 38-42 (2004).

13. Um, S. H., Lee, J. B., Kwon, S. Y., Li, Y. & Luo, D. Dendrimer-like DNA-based fluorescence nanobarcodes. *Nature Protoc.* **1,** 995-1000 (2006).

14. Glotzer, S. C. & Solomon, M. J. Anisotropy of building blocks and their assembly into complex structures. *Nature Mater.* **6**, 557-562 (2007).

15. Chen, S., Wang, Z. L., Ballato, J., Foulger, S. H. & Carroll, D. L. Monopod, bipod, tripod, and tetrapod gold nanocrystals. *J. Am. Chem. Soc.* **125,** 16186–16187 (2003).

16. Lee, S. M., Jun Y. W., Cho, S. N. & Cheon, J. Single-crystalline star-shaped nanocrystals and their evolution: programming the geometry of nano-building blocks. *J. Am. Chem. Soc.* **124,** 11244–11245 (2002).

17. Tang, Z., Wang, Y., Shanbhag, S., Giersig, M. & Kotov, N. A. Spontaneous transformation of CdTe nanoparticles into angled Te nanocrystals: from particles and rods to checkmarks, X-marks, and other unusual shapes. *J. Am. Chem. Soc.* **128,** 6730–6736 (2006).

18. Lee, J. B. *et al.* Multifunctional nanoarchitectures from DNA-based ABC monomers. *Nature Nanotech.* **4**, 430-436 (2009).

19. Seeman, N. C. DNA Nanotechnology: Novel DNA Constructions. *Annu. Rev. Biophys. Biomol. Struct.* **27,** 225–248 (1998).

20. LaBean, T.H. Nanotechnology: another dimension for DNA art. *Nature* **459**, 331-332 (2009).

21. Seeman, N. C. De novo design of sequences for nucleic acid structural engineering. *J. Biomol. Struct. Dyn.* **8,** 573-581 (1990).

22. Barish, R. D., Rothemund, P. W. K. & Winfree, E. Two computational primitives for algorithmic self-assembly: copying and counting. *Nano Lett.* **5,** 2586-2592 (2005).

23. Seeman, N. C. Nucleic acid junctions and lattices. *J. Theor. Biol.* **99,** 237-247 (1982).

24. Seeman, N. C. DNA in a material world. *Nature* **421**, 427-431 (2003).

25. Seeman, N. C. DNA engineering and its application to nanotechnology. *Trends Biotechnol.* **17,** 437-443 (1999).

26. Seeman, N. C. DNA components for molecular architecture. *Acc. Chem. Res.* **30,** 357-363 (1997).

27. Seeman, N. C. *et al*. Designed two dimensional Holliday junction arrays. *Biophys. J*. **78,** 308a (2000).

28. Sha, R. J., Liu, F., Millar, D. P. & Seeman, N. C. Atomic force microscopy of parallel DNA branched junction arrays. *Chem. Biol.* **7,** 743-751 (2000).

29. LaBean, T. H. *et al*. Construction, analysis, ligation, and self-assembly of DNA triple crossover complexes. *J. Am. Chem. Soc.* **122,** 1848-1860 (2000).

30. Yang, X. P., Wenzler, L. A., Qi, J., Li, X. & Seeman, N. C. Ligation of DNA triangles containing double crossover molecules. *J. Am. Chem. Soc*. **120,** 9779-9786 (1998).

31. Mao, C. D., Sun, W. & Seeman, N. C. Assembly of borromean rings from DNA. *Nature* **386,** 137-138 (1997).

32. Sa-Ardyen, P., Vologodskii, A. V. & Seeman, N. C. The flexibility of DNA double crossover molecules. *Biophys. J.* **84,** 3829-3837 (2003).

33. Pinto, Y. Y. *et al.* Sequence-encoded self-assembly of multiple-nanocomponent arrays by 2D DNA scaffolding *Nano Lett.* **5,** 2399–2402 (2005).

34. Zheng, J. *et al.* Two-Dimensional nanoparticle arrays show the organizational power of robust DNA motifs. *Nano Lett.* **6,** 1502–1504 (2006).

35. Park, S. H. *et al.* Finite-size, fully-addressable DNA tile lattices formed by hierarchical assembly procedures. *Angew. Chem.* **118**, 749–753 (2006).

36. Rothemund, P. W. Folding DNA to create nanoscale shapes and patterns. *Nature* **440**, 297-302 (2006).

37. Chen, J. & Seeman, N. C. The synthesis from DNA of a molecule with the connectivity of a cube. *Nature* **350**, 631–633 (1991)

38. Zhang, Y. & Seeman, N. C. Construction of a DNA truncated octahedron. *J. Am. Chem. Soc.* **116**, 1661–1669 (1994).

39. Shih, W. M. , Quispe, J. D. & Joyce, G. F. A 1.7-kilobase single-stranded DNA that folds into a nanoscale octahedron. *Nature* **427**, 618–621 (2004).

40. Um, S. H. *et al.* Enzyme-catalyzed assembly of DNA hydrogel. *Nature Mater.* **5**, 797-801 (2006).

41. He, Y. *et al.* Hierarchical self-assembly of DNA into symmetric supramolecular polyhedra. *Nature* **452**, 198-201 (2008).

42. Andersen, E. S. *et al.* Self-assembly of a nanoscale DNA box with a controllable lid. *Nature* **459**, 73-76 (2009).

43. Douglas, S. M. *et al.* Self-assembly of DNA into nanoscale three-dimensional shapes. *Nature* **459**, 414-418 (2009).

44. Feldkamp, U., Saccá, B. & Niemeyer, C. M. Dendritic DNA building blocks for amplified detection assays and biomaterials. *Angew. Chem. Int. Ed.* **48**, 5996-6000 (2009).

45. Nishikawa, M., Matono, M., Rattanakiat, S., Matsuoka, N., Takakura, Y. Enhanced immunostimulatory activity of oligodeoxynucleotides by Y-shape formation. *Immunology* **124**, 247-255 (2008).

46. Rattanakiat, S., Nishikawa, M., Funabashi, H., Luo, D., Takakura, Y. The assembly of a short linear natural cytosine-phosphate-guanine DNA into

dendritic structures and its effect on immunostimulatory activity. *Biomaterials* **29**, 5701-5706 (2009).

47. Cheng, E. *et al.* A pH-triggered, fast-responding DNA hydrogel. *Angew. Chem. Int. Ed.* **48,** 7660-7663 (2009).

48. Cho, Y. J. *et al.* Spectroscopic characterization of interstrand carbinolamine cross-links formed in the 5‘-CpG-3‘ sequence by the acrolein-derived γ-OH-1,N^2-propano-2‘-deoxyguanosine DNA adduct. *J. Am. Chem. Soc.* **127,** 17686-17696 (2005).

49. Horkay, F. & Basser, P. J. Osmotic observations on chemically cross-linked DNA gels in physiological salt solutions. *Biomacromolecules* **5,** 232-237 (2004).

50. Liu, W. G. *et al.* A novel pH-sensitive gelatin–DNA semi-interpenetrating polymer network hydrogel. *Polym. Int.* **53**, 675–680 (2004).

51. Murakami, Y. & Maeda, M. DNA-responsive hydrogels that can shrink or swell. *Biomacromolecules* **6,** 2927-2929 (2005).

52. Murakami, Y. & Maeda, M. Hybrid hydrogels to which single-stranded (ss) DNA probe is incorporated can recognize specific ssDNA. *Macromolecules* **38,** 1535-1537 (2005).

53. Lee, C. K. *et al.* DNA hydrogel fiber with self-entanglement prepared by using an ionic liquid. *Angew. Chem*. **120,** 2504–2508 (2008).

54. Liedl, T., Dietz, H., Yurke, B. & Simmel, F. Controlled trapping and release of quantum dots in a DNA-switchable hydrogel. *Small* **3,** 1688–1693 (2007).

55. Park, N. *et al.* High-yield cell-free protein production from P-gel. *Nature Protoc.* **4**, 1759-1770 (2009).

56. Park, N., Um, S. H., Funabashi, H., Xu, J. & Luo, D. A cell-free protein-producing gel. *Nature Mater.* **8**, 432-437 (2009).

CHAPTER 2

DNAsomes: Multifunctional DNA-based Nanocarriers*

*Young Hoon Roh[1], Jong Bum Lee[1], Pichamon Kiatwuthinon[1], Mark R. Hartman[1], Judy J. Cha[2], Soong Ho Um[3], David A. Muller[4], Dan Luo[1] "DNAsomes: Multifunctional DNA-Based Nanocarriers". *Small DOI: 10.1002/smll.201000752* Online published (2010).

[1]Department of Biological and Environmental Engineering, Cornell University Ithaca, New York, 14850, USA and [2]Department of Materials Science and Engineering, Stanford University, Stanford, California, 94305, USA and [3]Department of Materials Science and Engineering, Gwangju Institute of Science and Technology, Gwangju, 500-712, Korea and [4]Department of Applied and Engineering, Physics, Cornell University, Ithaca, New York, 14850, USA

2.1. Abstract

Multifunctional DNAsomes: DNA-lipid amphiphiles self-assemble into novel "DNAsomes" – liposome-like core-shell structures with subunits composed of branched DNA-lipid hybrid molecules. These DNAsomes can be precisely tuned over a wide range in terms of both size and surface charge. More importantly, DNAsome is a natural carrier of small interfering RNA (siRNA) due to DNA-RNA base-pairing, enabling efficient co-delivery of drug and siRNA. The DNAsome represents a universal multi-functional drug vector for simultaneous delivery of drugs, tracer dyes, or antibodies, along with genes, siRNA, or antisense nucleic acids.

2.2. Introduction

Non-viral drug delivery systems,[1-3] traditionally based on synthetic carriers such as polymeric materials and liposomes offer valuable possibilities for disease prevention and treatment.[4-12] Such systems are now being extended to achieve the co-delivery of multiple drugs and/or nucleic acid drugs, which can lead to synergistic effects.[13, 14] However, due to the fact that most building blocks of polymeric materials and liposomes are isotropic and polydisperse, it remains challenging to rationally engineer building blocks with multiple functionalities within a single molecule for tailored multi-drug delivery. The powerful molecular recognition capabilities of DNA[15-20] has enabled the controlled assembly of anisotropic building blocks, leading to multifunctional DNA nanostructures.[21]

Recently, we have developed DNA-based **a**nisotropic, **b**ranched, **c**rosslinkable (ABC) monomers that can carry multiple moieties on a single molecule with precise control.[22-26] These ABC monomers are particularly suited for multifunctionalization due to their multivalency, anisotropicity, monodispersity, and the rich chemistry of DNA bioconjugation. Here, inspired by these ABC monomers, we rationally design a

DNA-lipid amphiphile that self-assembles into novel "DNAsomes" – liposome-like core-shell structures with subunits composed of branched DNA-lipid hybrid molecules. Unlike traditional liposomes, these DNAsomes can be precisely tuned over a wide range in terms of both size (from 100 to 5000 nm) and surface charge (from -10 to -35 mV). More importantly, our DNAsome is a natural carrier of small interfering RNA (siRNA) due to DNA-RNA base-pairing, enabling efficient co-delivery of drug and siRNA to mammalian cells. The DNAsome represents a universal multi-functional drug vector for simultaneous delivery of drugs, tracer dyes, or antibodies, along with genes, siRNA, or antisense nucleic acids.

2.3. Materials and Methods

2.3.1. Synthesis of Y-DNA building blocks

All chemicals utilized in this study were obtained from Sigma-Aldrich (St. Louis, Missouri) unless otherwise mentioned. The Y-DNA building blocks were designed and synthesized according to the previous papers published by our group.[23-26] All oligonucleotides including fluorescent labeled oligonucleotide strands were commercially synthesized with standard desalting (Integrated DNA Technologies, Coralville, Iowa). Table 2.1 and Table 2.2 show oligonucleotide sequences utilized in this experiment. Briefly, oligonucleotides were dissolved in annealing buffer (10 mM Tris, pH = 8.0, 1 mM EDTA and 50 mM NaCl) with a final concentration of 0.2 mM. Y-DNA was synthesized by mixing the same molar amount of corresponding oligonucleotide strands. The nomenclature is as follows: Y_{01}, Y_{02}, and Y_{03} are the three corresponding single oligonucleotide chains that form a Y-DNA. Hybridizations were performed according to the following procedures: (1) Denaturation at 95 °C for 2 min. (2) Cooling at 65 °C and incubation for 2 min. (3) Annealing at 60 °C for 5 min. (4) Further annealing at 60 °C for 0.5 min with a continuous temperature decrease at a

rate of 1 °C per min. The annealing steps were repeated a total of 40 times. The final annealed products were stored at 4 °C.

2.3.2. Construction of DNA-lipid amphiphiles and DNAsome

Succinyl NGPE (0.3 mg), 0.5 ml of 0.016 M octylglucoside in MES buffer (pH 5.5), EDC (2 mM) and NHS (5 mM) were then reacted with shaking for 10 min and centrifuged at 2.5 kG for 60 sec, followed by 20 µl of 0.1 M NaOH (pH 8.0) with repeated shaking and centrifugation. Mixtures were then added to the prepared Y-DNA products, and incubated for 4 hours at room temperature. High performance liquid chromatography (HPLC) was performed to remove non-reacted products and the impurities. The running conditions were as follows: XBridge C18 column equipped with a photo-diode array detector (Waters Corp, Milford, Massachusetts), The gradient used was 0–50% acetonitrile in 0.1 M triethylammonium acetate (TEAA, pH 7.0) as the mobile phase within 30 min at a flow rate of 1.0 mL/min with UV detection (260 nm). The functionalized Y-DNA-lipid amphiphiles was further dialyzed to prepare DNAsomes against 100 ml of aqueous solution for 48 hrs using a cellulose membrane bag. After dialysis, DNAsomes were collected and frozen using a freeze-dryer system (Labconco Corp, Kansas City, Missouri) to achieve final products.

2.3.3. Fourier transform infrared spectroscopy (FT-IR)

To characterize the conjugation of lipid and Y-DNA, FT-IR microspectra were used with Galaxy series FT-IR 5000 (GL5020, Mattson, Arizona). The spectra were scanned in the transmission mode from 4000 to 500 cm^{-1} with 100 scans per point and resolution of 4 cm^{-1}. Each sample of 100 µl was squeezed between two BaF_2 windows.

Table 2.1. Oligonucleotide sequences of the Y-DNA building blocks with fluorescent dyes for DNAsome synthesis

Strand		Sequence
Y-DNA (FRET)	**Y_{01}**	5'-/NH_2/ CTT ACG GCG AAT GTC ATG CGG ATC CA-3'
	Y_{02}	5'-/Cys 3(●)/ GGT CAT CCA TGA CAA CTT TAG GCT GAT TCG GTC ATT CGC CGT AAG-3'
	Y_{03}	5'-/Cys 3(●)/ TGG ATC CGC ATG AAC CGA ATC AGC CT-3'
Y-DNA (FRET)	**Y_{01}**	5'-/NH_2/ CTT ACG GCG AAT GTC ATG CGG ATC CA-3'
	Y_{02}	5'-/Cys 5 (●)/ AGG CTG ATT CGG TCA TTC GCC GTA AG-3'
	Y_{03}	5'-/Cys 5 (●)/ TGG ATC CGC ATG AAC CGA ATC AGC CT-3'
Y-DNA (Confocal)	**Y_{01}**	5'-/NH_2/ CTT ACG GCG AAT GTC ATG CGG ATC CA-3'
	Y_{02}	5'-AGG CTG ATT CGG TCA TTC GCC GTA AG-3'
	Y_{03}	5'-/BODIPY 630/650 (●)/ TGG ATC CGC ATG AAC CGA ATC AGC CT-3'
Y-DNA (Control)	**Y_{01}**	5'-/NH_2/ CTT ACG GCG AAT GTC ATG CGG ATC CA-3'
	Y_{02}	5'-AGG CTG ATT CGG TCA TTC GCC GTA AG-3'
	Y_{03}	5'-TGG ATC CGC ATG AAC CGA ATC AGC CT-3'

Note that the labeled fluorescent dye is represented by a dot with the same color. The same colored sequences represent complementary pairs.

Table 2.2. Oligonucleotide sequences of the siRNA and Y-DNA building blocks for siRNA delivery

Strand		Sequence
GAPDH siRNA		5'-**rArArA rGrUrU rGrUrC rArUrG rGrArU rGrArC rCrUrU**-3'
GAPDH siRNA (Confocal)		5'-/Cys 5 (●)/ **rArArA rGrUrU rGrUrC rArUrG rGrArU rGrArC rCrUrU**-3'
Bcl-2 siRNA		5'-**rCrArC rArUrC rUrCrC rCrArC rArUrC rCrCrA rCrUrC rGrUrA rGrCrC rUrU**-3'
Negative siRNA		5'-**rCrCrG rUrArU rCrGrU rArArG rCrArG rUrArC rUrUrU**-3'
Y-DNA (GAPDH)	**Y_{01}**	5'-/NH_2/ CTT ACG GCG AAT GTC ATG CGG ATC CA-3'
	Y_{02}	5'-**GGT CAT CCA TGA CAA CTT T**AG GCT GAT TCG GTC ATT CGC CGT AAG-3'
	Y_{03}	5'-TGG ATC CGC ATG AAC CGA ATC AGC CT-3'
Y-DNA (Bcl-2)	**Y_{01}**	5'-/NH_2/ CTT ACG GCG AAT GTC ATG CGG ATC CA-3'
	Y_{02}	5'-**CTA CGA GTG GGA TGT GGG AGA TGT G**AG GCT GAT TCG GTC ATT CGC CGT AAG-3'
	Y_{03}	5'-TGG ATC CGC ATG AAC CGA ATC AGC CT-3'
Y-DNA (Negative)	**Y_{01}**	5'-/NH_2/ CTT ACG GCG AAT GTC ATG CGG ATC CA-3'
	Y_{02}	5'-**AGT ACT GCT TAC GAT ACG G**AG GCT GAT TCG GTC ATT CGC CGT AAG-3'
	Y_{03}	5'-TGG ATC CGC ATG AAC CGA ATC AGC CT-3'

Note that the labeled fluorescent dye is represented by a dot with the same color. The same colored sequences represent complementary pairs.

2.3.4. Morphology study of DNAsome

For the STEM imaging experiment, samples were prepared as follows: approximately 1 µl of DNAsomes was mixed with 100 µl of Tris (30 mM, pH 8.0) before 2.5 µl of 5 % 2, 4, 6 Tri(dimethylaminomethyl phenol) (DMP) 30 was added to the mixture. A drop of the mixture (50 µl) was placed onto a sheet of parafilm and covered with a petri dish for 7 minutes at room temperature. The DNA molecules were then picked up by touching the drop with a formvar/carbon-coated TEM grid (Electron Microscopy Sciences, Fort Washington, Pennsylvania), and were left covered with a petri dish for another 3 minutes. The sample was then stained with 2 % uranyl acetate (negative staining reagent) for 1 minute. The grid was then blotted with a filter paper and allowed to dry in air. The grids were visualized at a voltage of 100 kV using a FEI Philips TECNAI 12, after rotary coated with Pt/Pd

2.3.5. Critical Micelle Concentration measurement (CMC)

The CMC of Y-DNA-lipid amphiphile in buffer/solvent was analyzed by fluorescence spectroscopy using pyrene as a hydrophobic fluorescence probe. Aliquots of pyrene solutions in acetone (20 µL of 30 µM pyrene) were added to empty tubes, and the acetone was allowed to evaporate overnight. Then, 90 µL of aqueous Y-DNA-lipid amphiphile solution with concentrations ranging from 0.01 nM to 2190 nM was added to the tubes. The solutions were equilibrated for 24 hours at room temperature. When Y-DNA-lipid amphiphile concentrations reach above the CMC, pyrene preferentially partitioned into the hydrophobic part of the assembled core/shell structures. As pyrene moved from hydrophilic to hydrophobic environment, its excitation and emission spectra both exhibited a shift. The fluorescent spectra of the samples were recorded with an SLM 8000c Spectrofluorimeter (SLM) at room temperature (20^{o}C). The excitation spectra were recorded from 280 to 360 nm with an

emission wavelength of 395 nm. The CMC of Y-DNA-lipid amphiphile was determined by plotting the intensity (peak height) ratio of the 339 nm peak to the 334 nm peak from the emission spectra versus the logarithm of polymer concentration. The CMC value was taken from the intersection of the tangent to the curve at the inflection with the horizontal tangent through points at low concentrations.

2.3.6. Förster resonance energy transfer (FRET)

To confirm the formation of DNAsome, Cy3 (donor) and Cy5 (acceptor) were choose for fluorescence resonance energy transfer (FRET) experiments because of the large spectral overlap between emission spectrum of Cy3 and excitation spectrum of Cy5. Two Cy3 or Cy5 were labeled on a single Y-DNA. With 540 nm laser light, FRET tests were performed by checking fluorescence intensity changes before conjugation of lipid and fluorescence dye labeled Y-DNA and after conjugation of lipid on Y-DNA upon emission at 565 nm and 665 nm.

2.3.7. Cell culture

CHO cells were cultured at 37 °C with 5% CO_2 in Ham's F-12K Nutrient Mixture, Kaighn's Mod, F-12K (Mediatech, Manassas, Virginia) supplemented with L-Glutamine, 10% fetal bovine serum (FBS, Mediatech, Manassas, Virginia), and 1% penicillin/streptomycin (P/S, Mediatech, Manassas, Virginia).

2.3.8. Fluorescence labeling and imaging of cell

CHO Cells (2×10^4 cells) were cultured in a 25 cm^3 flask and plated on the day of experiments by reverse transfection method.[27] CHO cells in suspension media were then transfected and added to the well just before adding the 30 nM fluorescently labeled GAPDH siRNA-hybridized DNAsome in the presence of serum-free media

(OPTi-MEM I, Invitrogen, Carlsbad, California) in each well on Lab-Tek chamber slides (8 wells, Permanox slide, Nunc) for overnight (24 hours) at 37°C. Cells then were washed three times with PBS and fixed with 4% paraformaldehyde. Staining cells by two fluorescence dyes were mentioned previously.[26] Briefly, actin filaments and nuclei were stained with Alexa Fluor488 phalloidin (Invitrogen, Carlsbad, California) and DAPI (40,6-diamidino-2-phenylindole) with an antifade reagent (Invitrogen, Carlsbad, California) according to the supplier's protocol. Fluorescence images of the cells were achieved by Zeiss LSM 510 Meta confocal microscope.

2.3.9. Transfection studies

The antisense strand of Glyceralhehyde-3-Phosphate Dehydrogenase (GAPDH) siRNA's and non-complementary siRNA's sequences were obtained (Ambion, Inc., Austin, Texas) and synthesized as a single-stranded siRNA from IDT (Coralville, Iowa). The sequences are (5'-rArArA rGrUrU rGrUrC rArUrG rGrArU rGrArC rCrUrU-3') for GAPDH siRNA and (5-rCrCrG rUrArU rCrGrU rArArG rCrArG rUrArC rUrUrU-3') for non-complementary siRNA respectively. The single-straned siRNA was hybridized to the DNAsome at the sticky end of the Y-DNA as described above. After hybridization, the siRNA-DNAsome complex was diluted in serum-free media (OPTi-MEM I, Invitrogen, Carlsbad, California) to 5 μL final volumes for each siRNA's amount. The amounts of GAPDH siRNA were varied at 10, 30, 90, and 180 nM. The molar ratio of DNAsomes and single-stranded siRNAs was 1:1. After CHO cells (1 x 10^4 cells in 95 μL P/S –free media) were plated in each well of a 96-well plate, 5μL of prepared samples at different siRNA amount were added and then mixed gently. The cells were incubated in the controlled-temperature at 37 °C with 5% CO_2 incubator for 4 hours before all complex media were replaced by 200 μL of fresh serum-contained F-12K media. The plate was further incubated until 48

hours and was measured remaining GAPDH protein level by using KDalert™ GAPDH Assay Kit (Ambion, Inc., Austin, Texas) as the kit's protocol. Briefly, the supernatant was removed and washed three times with 1 x PBS buffer. 200 µL KDalert lysis buffer was added to each sample well. The plate was then kept at 4 °C for 20 minutes. After the cells were lysed, 10 µL of each sample was transferred to a clean 96-well plate. Next, 90 µL of KDalert Mix was quickly added and the fluorescence emitting was immediately measured every one minute by the real-time kinetic mode from a Synergy 4 Hybrid multi-mode microplate reader (Biotek Instrument, Inc., Winooski, Vermont) using a 560 nm excitation and a 590 nm emission filter. The kinetic reaction was run for 4 minutes.

2.3.10. Investigation of endocytosis mechanism of DNAsomes uptake

To investigate the cellular endocytosis mechanism of DNAsomes, CHO cells (1x 10^4 cells) were trypsinized and plated in each well of 96-well plate. Then, cells were pre-incubated with three endocytosis inhibitors for one hour at 37 ºC with 5 µg/mL of filipin complex, 5 µg/mL of cytochalasin B, and 10 µg/mL of Nocodazole, and 10% of DMSO only as a positive control. Cells were cultured with GAPDH and negative siRNA (30 nM) conjugated DNAsomes respectively for 4 hours. The new media was replaced and additionally incubated until 48 hours. An inhibition of endocytosis was determined by the KDalert GAPDH assay (Ambion, Inc., Austin, Texas).

2.3.11. Cell cytotoxicity evaluation (MTT)

The cytotoxicity of the DNAsome and siRNA-hybridized DNAsome was determined by MTT (3-(4, 5-dimethylthiazolyl-2)-2, 5-diphenyltetrazolium bromide) cell viability assay (ATCC, Manassas, Virginia). CHO cells were plated in 96-well

plate at 8,000 cells per well. Next, the DNAsome and siRNA-hybridized DNAsome at different concentration was added and incubated for 24 hours. Then, the supernatant was replaced by 120 μL of freshly full media and additionally incubated for 24 hours. After 48 hours incubation, 12 μL MTT reagent was added and cells were incubated for 2 hours and purple precipitate was observed. 100 μL of detergent reagent was then added and incubated in the dark at room temperature for another 2 hours. Absorbance was measured with a specific monochrome filter at 570 nm by the Synergy 4 Hybrid multi-mode microplate reader (Biotek Instrument, Inc., Winooski, Vermont). The cytotoxicity (%) of each sample was compared to control cells in full media.

2.3.12. Drug loading and *In vitro* drug release measurements

Two drug candidates (Bcl-2 siRNA and DOX) were selected to evaluate in vitro drug release profiles. To load model drugs, Cy5 labeled siRNA solution (60 μM, IDT, Coralville, Iowa) and a doxorubicin (DOX) solution (20 ng/μL), which intercalates DNA, was prepared and incubated with DNAsome in 300 μL of distilled water for 48 hrs at room temperature under gentle shaking to allow both drugs to be encapsulated into DNAsome. After loading process, each reaction solution was centrifuged at 14000 rpm for 20 min and the supernatant was removed to separate the unloaded drug from DNAsome. The DNAsome was then re-dispersed into 300 μL of PBS solution (pH 7.4) with a gentle and continuous shaking (100 rpm) at 37 °C. The amount of DOX or siRNA released from the DNAsome was measured by fluorescence intensity (Doxorubicin excitation 480 nm, emission 550 nm and Cy5-siRNA excitation 650 nm, emission 670 nm). Cumulative drug release profiles were calculated based on Equation below

$$\text{Cumulative Drug Release [\%]} = (Mt / Mo) \times 100$$

where Mt is the amount of accumulated drug released from the DNAsome at time t, and M_0 is the amount of drug loaded into the DNAsome. Here, M_0 was calculated by subtracting the amount of unloaded drug from initial drug fed.

2.4. Results and Discussions

2.4.1. Design of DNA-lipid amphiphiles and DNAsome

We designed the DNAsomes from Y-shaped DNA subunits, each of which was constructed from three single-stranded DNAs (ssDNA) with the following specific functional modifications (Figure 2.1). One ssDNA was functionalized with a lipid molecule (N-glutaryl phosphatidylethanolamine, NGPE, Figure 2.2), resulting in a branched DNA-lipid hybrid molecule with amphiphilic properties, capable of self-assembly into liposome-like DNAsomes. The remaining two ssDNAs were functionalized with two different moieties including tracers (fluorescent dyes) and capture sequences that were complementary to a therapeutic siRNA. Subsequently, these ssDNAs were annealed to form Y-shaped DNA-lipid hybrids with defined functional groups. After this process, the Y-DNA amphiphiles self-assembled in aqueous solution to form DNAsomes.

2.4.2. Evaluation of construction of Y-DNA-lipid amphiphiles

Gel electrophoresis was performed to confirm the synthesis of the HPLC-purified Y-DNA amphiphile (HPLC = high-performance liquid chromatography) (Figure 2.3a). We observed an orange smear band (Figure 2.3b, Lane 2), which was stained by both DNA-specific (Gel Green) and lipid-specific (Nile Red) dyes, corresponding to the successfully-synthesized Y-DNA amphiphile. As a negative control, Y-DNA alone did not show a smear band and was stained only with green dye (Figure 2.3b, Lane 1). Furthermore, a simple mixture of DNA and lipid showed non-

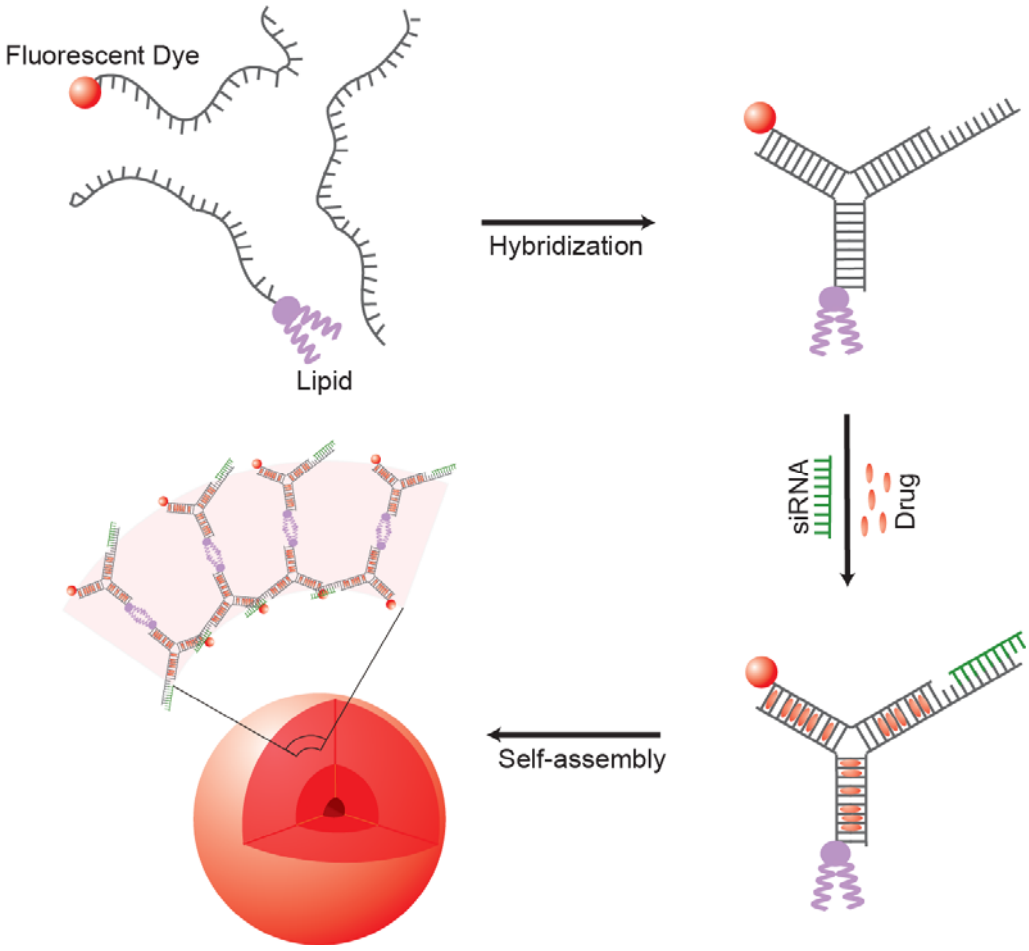

Figure 2.1. Schematic illustration of the construction of DNAsome for the delivery of RNAi agents. DNAsomes and functional groups are not drawn to scale. The resultant DNAsome possesses not only capability and capacity to store drug and siRNA, but also molecular probe ability.

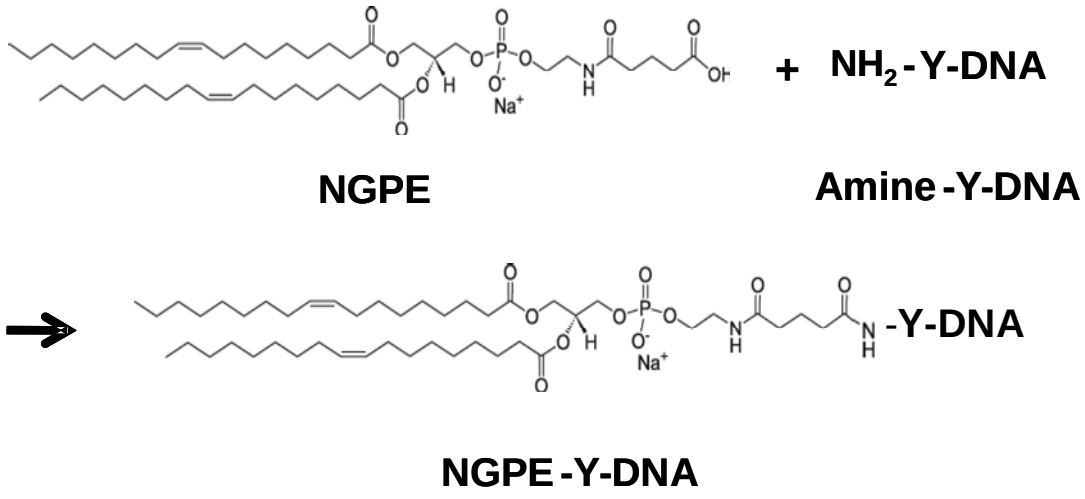

Figure 2.2. Synthesis of Y-DNA-lipid amphiphiles. The Y-DNA-lipid conjugates were achieved through reactions between the amine modified groups of Y-DNA and the activated ester groups of the lipid molecules. The final products were obtained by performing HPLC purification to ensure removal of unreacted reagents as well as impurities.

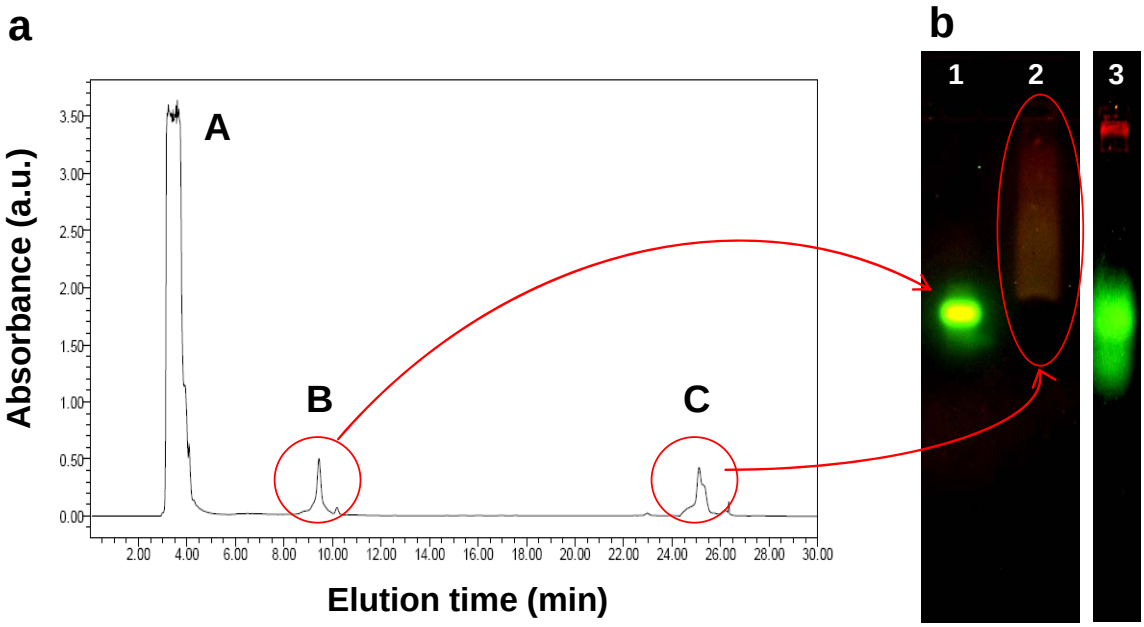

Figure 2.3. (**a**) HPLC chromatogram of products formed in the reaction of Y-DNA and lipid. The separation of unreacted lipid (A), NH_2-Y-DNA (B), and Y-DNA-lipid conjugate (C) were achieved by a gradient elution. The elution time (min) is on the x-axis; the ultraviolet absorbance at 260 nm (mV) is on the y-axis. (**b**) Mobility shift of Y-DNA and lipid conjugates. Gel electrophoresis of HPLC fractions was conducted at a constant voltage of 90 volts for 60 min. (3 % agarose gel) Lanes 1 2 and 3 indicate NH_2-Y-DNA, Y-DNA-lipid conjugate and Y-DNA + lipid mixture, respectively.

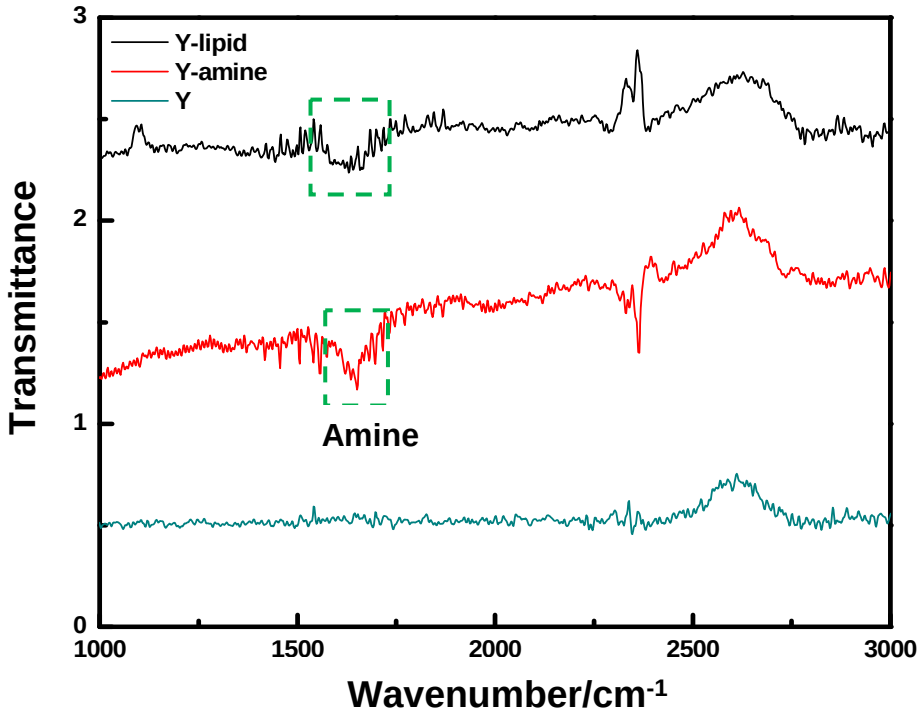

Figure 2.4. FT-IR spectroscopy. FT-IR spectrum of Y-DNA-lipid conjugates revealed transmission bands from amide bond. The IR spectrums of lipid conjugated Y-DNA confirm the presence of amide I band (C=O stretching vibration) and amide II band (N-H bending vibration) at around 1660 cm^{-1} and 1590 cm^{-1} (black line). These results show carboxylated lipid and amine modified Y-DNA formed amide bonding through reaction between carboxylic group and amine group. However, amine modified Y-DNA shows only N-H bending vibration at around 1630 cm^{-1} (red line) and Y-DNA do not show any band (blue line).

smeared, distinct bands (Figure 2.3, Lane 3). Fourier transform infrared (FT-IR) spectroscopy revealed the presence of a new amide bond, further confirming DNA-lipid conjugation (Figure 2.4).

2.4.3. Characterization of DNAsomes

2.4.3.1. Morphology characteristic of DNAsomes

To characterize the DNAsome morphology, confocal microscopy was employed to identify the internal structure of the DNAsomes self-assembled from dye-modified Y-DNA amphiphile (Figure 2.5a). Interestingly, DNAsomes were core/shell structures consisting of a hollow region surrounded by a dense core and a lower-density shell. The scanning transmission electron microscope (STEM) image also shows similar spherical structures with dense cores (Figure 2.5b). Phosphorus (electron energy loss spectroscopy, EELS) from the cores of the spherical structures suggests that the core contains DNA (Figure 2.6).[28]

2.4.3.2. The controllability of DNAsomes

In addition, the size of the DNAsomes was controlled by varying the concentration of Y-DNA amphiphiles. Two different concentrations of Y-DNA amphiphiles led to two different sizes of DNAsomes (with approximate diameters 460 ± 45 nm and 5000 ± 430 nm), as observed with scanning electron microscopy (Figure 2.7). Dynamic light scattering (DLS) was utilized to further explore the effect of Y-DNA amphiphile concentration on DNAsome size, unexpectedly demonstrating a striking linear relationship with DNAsome average diameters ranging from 110.7 ± 12.9 nm to 1102.5 ± 91.2 nm (Figure 2.8). Over the same range of concentrations, zeta potential measurements also show a linear relationship between anionic charge (ranging from -10.77 ± 0.81 mV to -35.60 ± 1.27 mV) and Y-DNA amphiphile

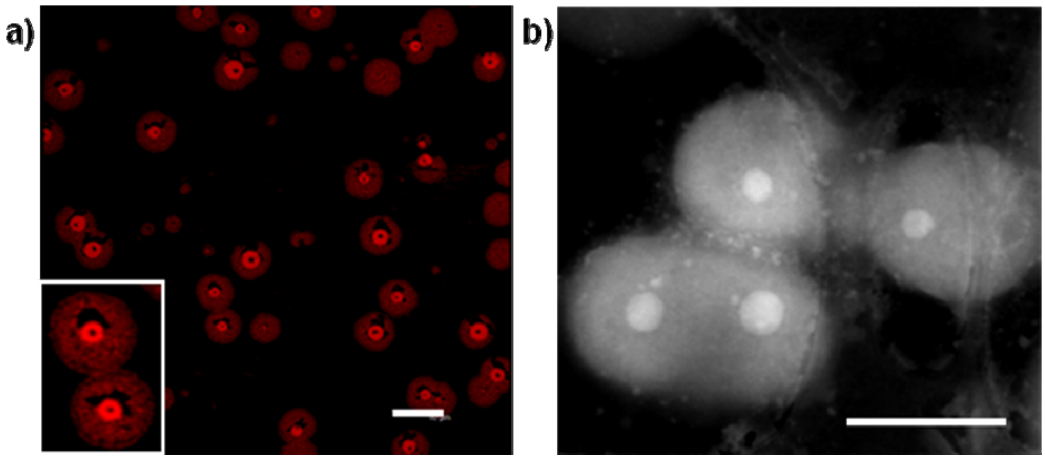

Figure 2.5. (**a**) Confocal microscopy image of self-assembled DNAsome. The scale bar is 5 µm. (**b**) ADF-STEM image of DNAsome. The Annular Dark Field Scanning Transmission Electron Microscopy (ADF-STEM) image shows the spherical shape of the DNAsome that contain a dense core. The scale bar is 500 nm.

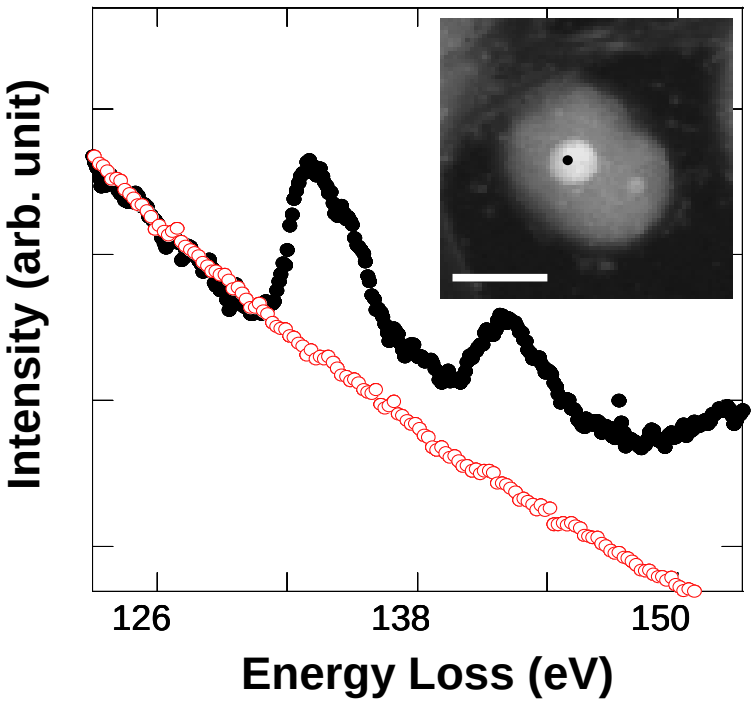

Figure 2.6. Phosphorus EELS spectra of DNAsome. Phosphorus signal is detected in the core of DNAsome. Raw EELS spectra from a DNAsome (inset) are shown where the black spectrum is taken from the core. The spectra are scaled so that the pre-edge intensity is the same. The scale bar is 500 nm.

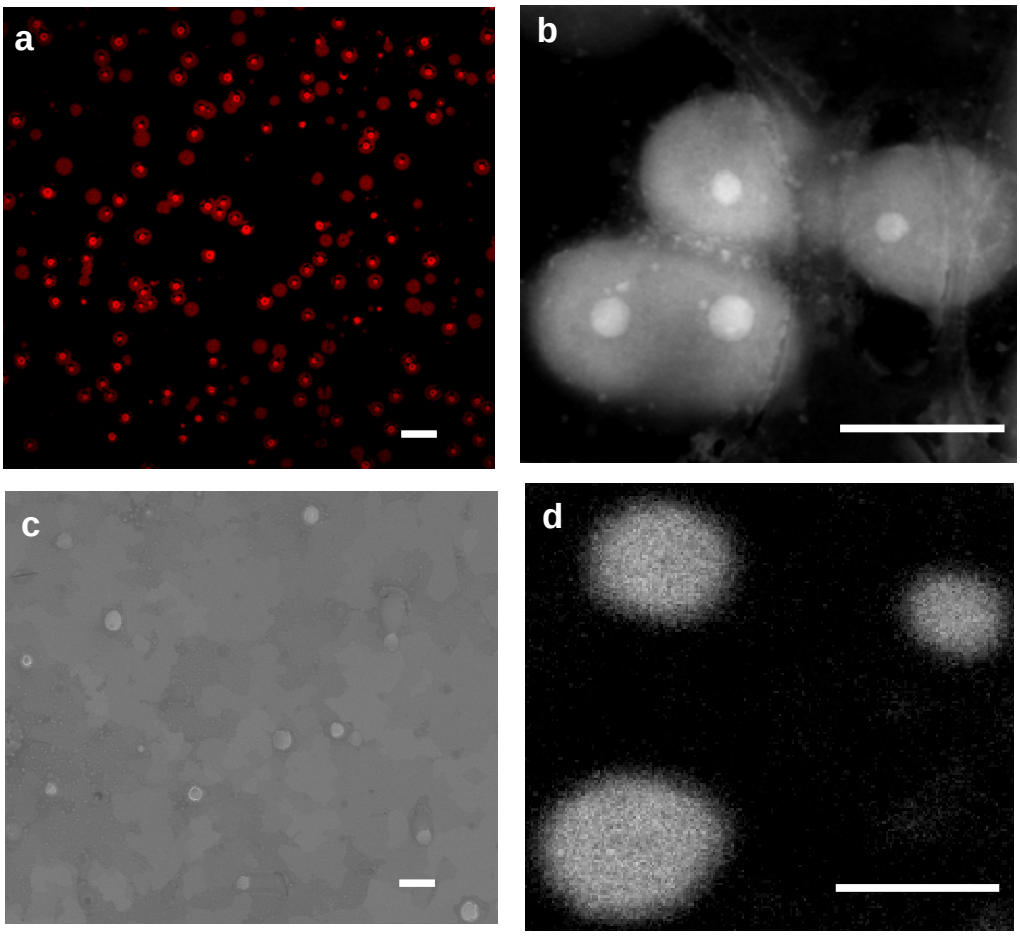

Figure 2.7. (**a**) Confocal microscopy image of self-assembled DNAsome. The scale bars is 5000 nm. (**b**) ADF-STEM image of DNAsome. The Annular Dark Field Scanning Transmission Electron Microscopy (ADF-STEM) image shows the spherical shape of the DNAsome that contain a dense core. The scale bars is 500 nm. (**c-d**) SEM images of DNAsome depending on particles size. The scale bars are 5000 nm (c) and 500 nm (d) respectively.

concentration. We note that as the concentration of DNA amphiphile increases, both the surface area per particle and the volume per particle increase more rapidly than the zeta potential. Thus, the charge per unit area (and per unit volume) decreases with increasing Y-DNA amphiphile concentration, and consequently the DNAsomes become less repulsive to the free Y-DNA amphiphiles. These results suggest that, unlike conventional liposomes, the size of our DNAsomes can be precisely controlled over a wide range simply by adjusting the concentration of Y-DNA amphiphile.

2.4.3.3. Determination of Critical Micelle Concentration

At very low concentrations, however, we did not observe DNAsome formation. To determine the critical micelle concentration (CMC) of Y-DNA amphiphile, we employed fluorescence spectroscopy using pyrene as a hydrophobic fluorescent probe.[29, 30] We obtained a CMC of 17 nM, above which the DNA-lipid conjugates self-assembled into DNAsomes (Figure 2.9).

2.4.3.4. Conformation of internal structure of DNAsomes by FRET

To obtain further insight regarding the internal packaging of Y-DNA amphiphile within the DNAsome structure, Fluorescence resonance energy transfer (FRET) was used with a FRET pair dye: green (Cy3) and red (Cy5) fluorophores.[31] The effect of FRET was compared for the following 1) a control, a simple mixture of dye-labeled Cy3-Y-DNA, Cy5-Y-DNA, and unlabeled free lipids, and 2) DNAsomes assembled from dye-labeled Y-DNA amphiphiles (Cy3-Y-DNA-lipid and Cy5-Y-DNA-lipid). The intensity ratio I_R/I_G, where I_R and I_G were fluorescence intensities of Cy5 and Cy3, respectively, was 3.2 times higher for the DNAsome than for the control (Figure 2.10). This result suggests that the internal structure of DNAsomes consists of Y-DNA amphiphiles that are closely-packed within FRET distance (< 10 nm).

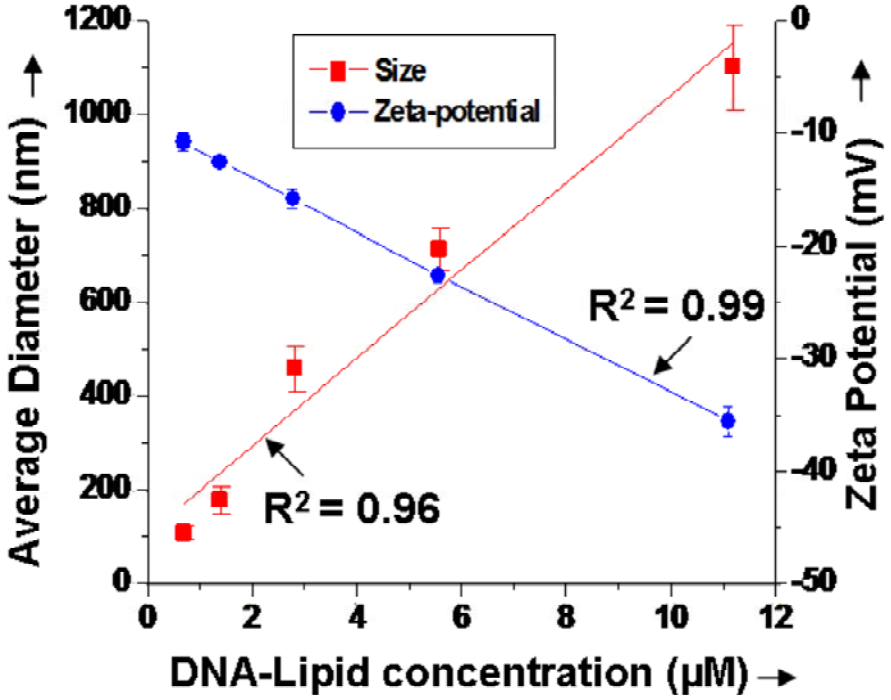

Figure 2.8. Zeta potential and size distribution of DNAsome as a function of Y-DNA amphiphile concentrations.

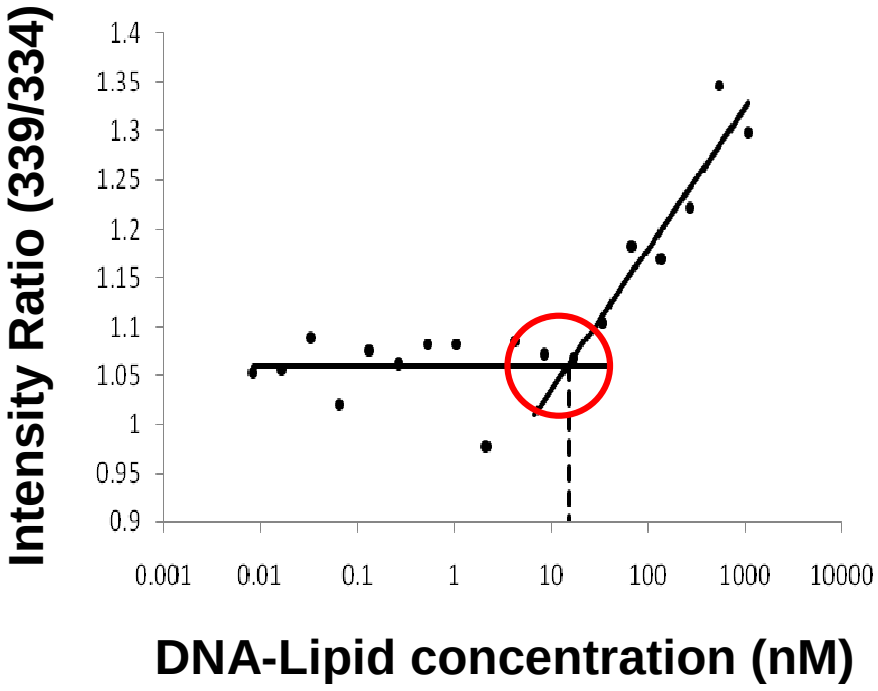

Figure 2.9. Critical Micelle Concentration (CMC). The concentration of Y-DNA amphiphile was varied from 0.01 nM to 2190 nM. Here, pyrene was used as a fluorescent probe (no other fluorescent dyes were used in these experiments to prevent interference).

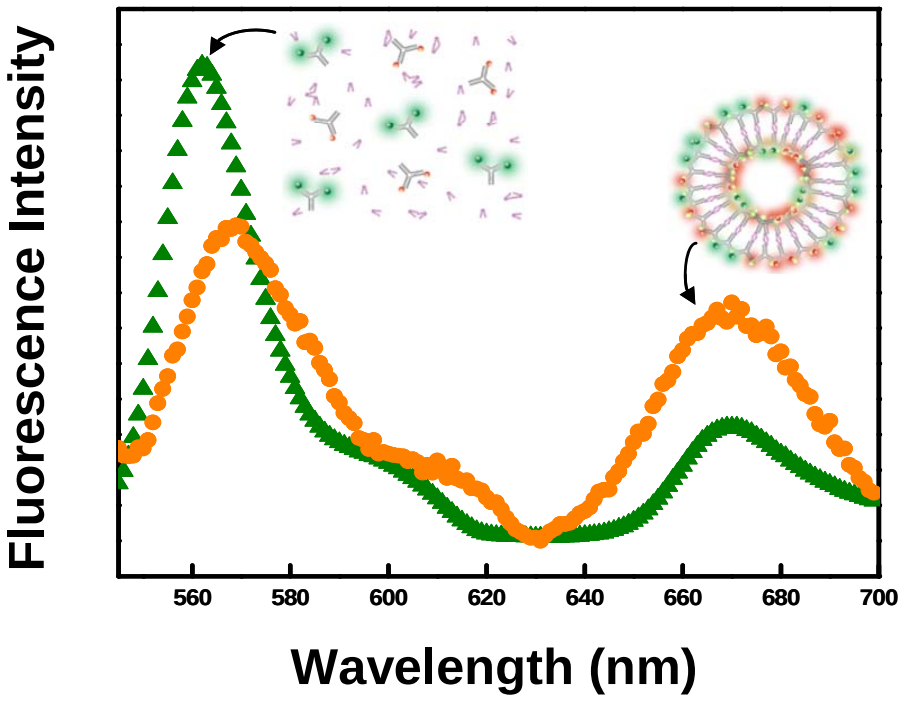

Figure 2.10. Fluorescence resonance energy transfer (FRET). Fluorescence intensity of a free lipids and Y-DNA mixture (▲) and DNAsome made by Y-DNA amphiphile (●) was compared.

2.4.4. Application of DNAsomes

2.4.4.1. Evaluation of intracellular delivery of siRNA using DNAsomes

DNAsomes possess the unique advantage of inherent base-pairing between RNA and DNA, and thus can be used to facilitate siRNA delivery, which has been a challenge in the field of drug delivery.[32-36] To explore the use of DNAsomes as siRNA delivery vectors, DNAsomes were first hybridized with fluorescence-labeled siRNA[37-38] and then delivered to Chinese hamster ovarian (CHO) cells. Confocal microscopy images revealed intracellular localization of siRNA in CHO cells (Figure 2.11 and Figure 2.12). This cellular uptake was attributed to endocytosis because no fluorescence was observed inside the cells when endocytosis was inhibited by incubation at 4 °C. We further investigated the specific endocytosis mechanisms involved in DNAsome delivery by measuring glyceraldehyde 3-phosphate dehydrogenase (GAPDH) gene knockdown in the presence of various inhibitors (Figure 2.13). Filipin complex was found to totally avert GAPDH knockdown, revealing that the pathways for DNAsome endocytosis are predominantly caveolae-mediated. Furthermore, cytochalasin B partially averted GAPDH knockdown, suggesting that actin-based endocytosis also plays a role in DNAsome uptake.

2.4.4.2. Evaluation of DNAsomes as drug delivery nanocarriers

Notably, the fluorescence-labeled siRNA was observed throughout both nucleus and cytoplasm, suggesting that DNAsomes are capable of delivering siRNA to the entire cell. Delivery throughout the entire cell is particularly beneficial for multi-drug delivery, since the target will vary depending on the drug. The use of DNAsomes for siRNA delivery was further investigated by varying the amount of siRNA to optimize delivery efficiency. CHO cells, after transfection with GAPDH siRNA-hybridized DNAsomes, exhibited substantial gene knockdown. Under optimum

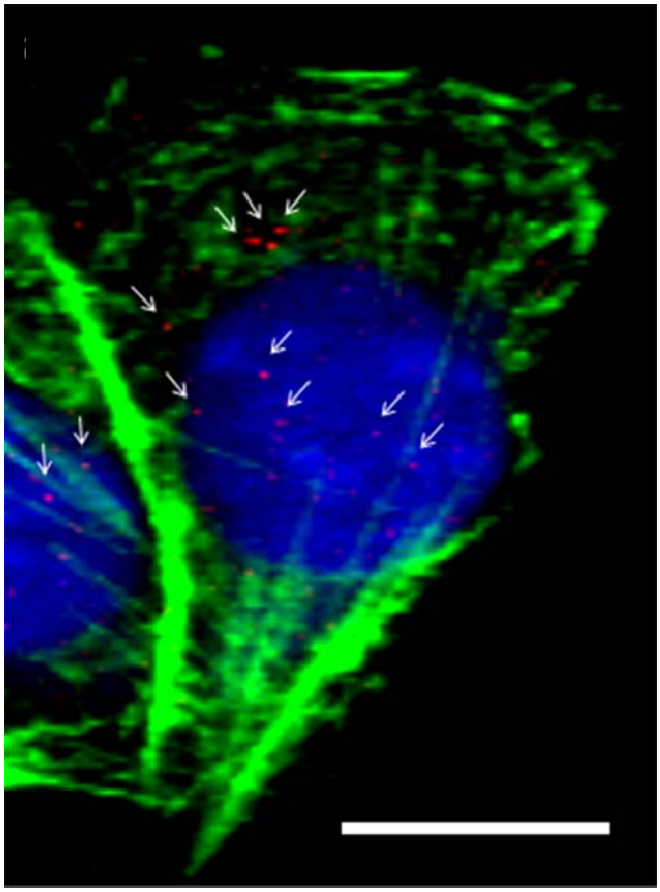

Figure 2.11. Z-directional sliced confocal microscopy image of DNAsome hybridized with fluorescence-labeled siRNA (red) transfected into CHO cells (blue, nuclei; green, actin), exhibiting the intracellular delivery of siRNA-DNAsomes. The scale bar is 10 μm.

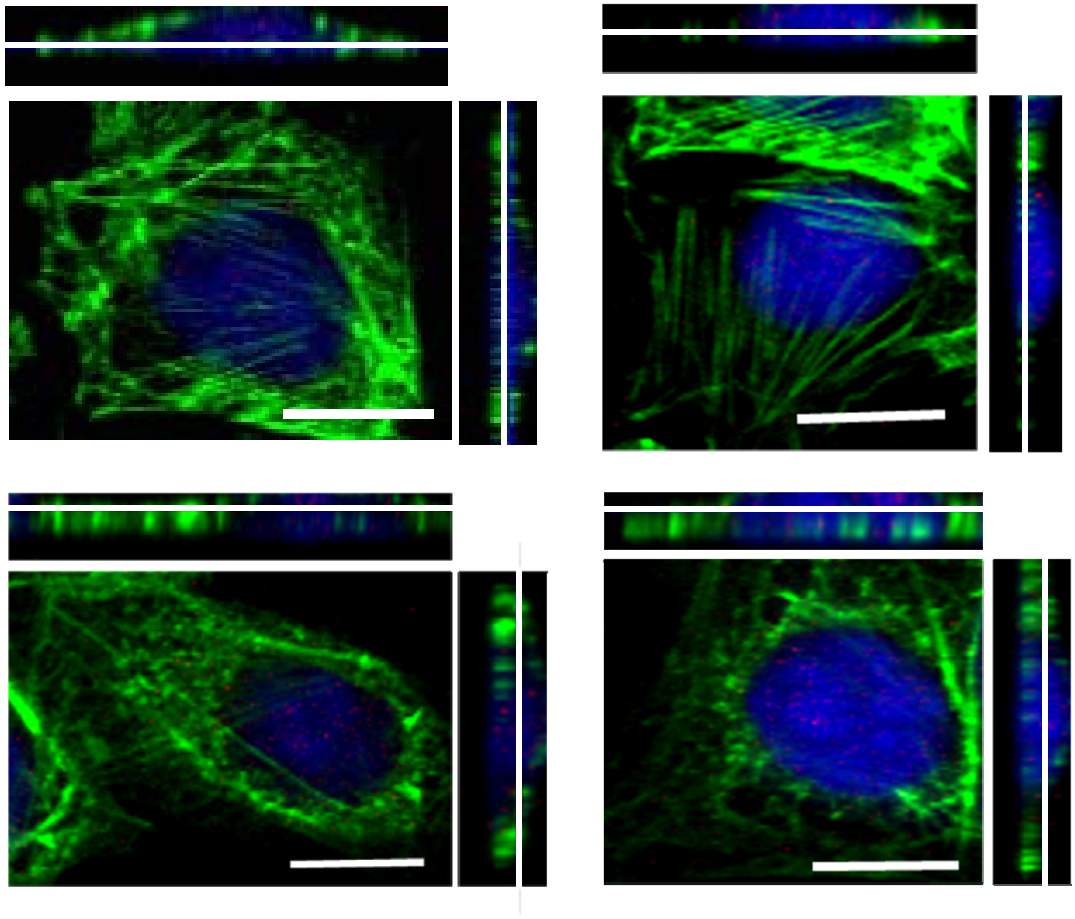

Figure 2.12. Confocal microscopy images of DNAsomes delivered to CHO cells. (**a-d**) DNAsomes were hybridized with fluorescence-labeled siRNA (red) and transfected into CHO cells (blue, nuclei; green, actin) at 37 ºC overnight. Confocal images were used to project side views (Z-directional slices) of CHO cells, exhibiting the intracellular delivery of siRNA-labeled DNAsomes. The scale bars are 10 μm.

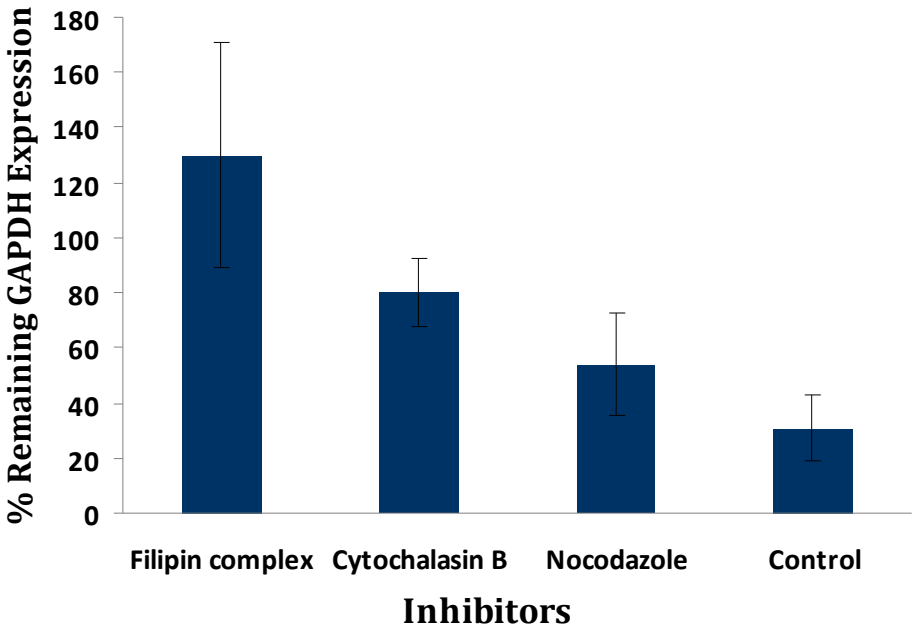

Figure 2.13. Investigation of the endocytosis mechanism for DNAsomes. The cellular endocytosis mechanism of our DNAsome was investigated by endocytosis inhibition studies. Cells were incubated with filipin complex to inhibit caveolae-mediated endocytosis.[43] Cytochalasin B and nocodazole were also used to disrupt actin-mediated and microtubules dependent endocytosis pathway, respectively.[44] The control contained no inhibitors.

conditions (Figure 2.14), GAPDH expression was significantly decreased with 46 % gene knockdown (Figure 2.15). Compared with the commercially-available transfection reagents Lipofectamin2000 and DOTAP, DNAsomes achieved much higher cell viability (approximately 100%) while still demonstrating significant transfection efficiency (Figure 2.16-2.19). It has been suggested that many cationic polymers and liposomes exhibit significant cytotoxicity.[39-42] In contrast, our DNAsomes are innately negatively-charged (due to DNA), and exhibit low cytotoxicity, which is further confirmed by additional cytotoxicity assays with CHO cells (Figure 2.20 and Figure 2.21).

2.4.4.3. Evaluation of DNAsomes as multi-drug delivery vectors

In order to investigate the use of DNAsomes for multi-drug delivery, we combined two model drugs, Doxorubicin (Dox, a hydrophobic apoptosis-inducing anticancer drug) and Bcl-2 siRNA (an inhibitor of the anti-apoptotic gene Bcl-2) into the DNAsome structure (Figure 2.22 and Figure 2.23). We carried out an *in vitro* release study to confirm that both Dox and Bcl-2 siRNA could be loaded into the DNAsome and released gradually (Figure 2.24). We note that distinct release profiles were observed, due to the different binding affinities of siRNA (bound to the DNAsomes via DNA-RNA base pairing) and Dox (bound to the DNAsomes via intercalation). Successful co-delivery of these two drugs should cause a synergistic effect due to enhanced apoptosis via loss of the anti-apoptotic Bcl-2 gene expression. The combined drug efficacy was subsequently measured by carrying out the MTT (3-(4,5-dimethylthiazol-2-yl)-2,5-diphenyltetrazolium bromide) assay. As controls, we also treated CHO cells with free Dox and Dox-loaded DNAsomes. As expected, the IC_{50} of Dox-loaded DNAsomes was lower than free Dox. (5 μM versus 59 μM) More importantly, DNAsomes loaded with both Dox and Bcl-2 siRNA demonstrated much

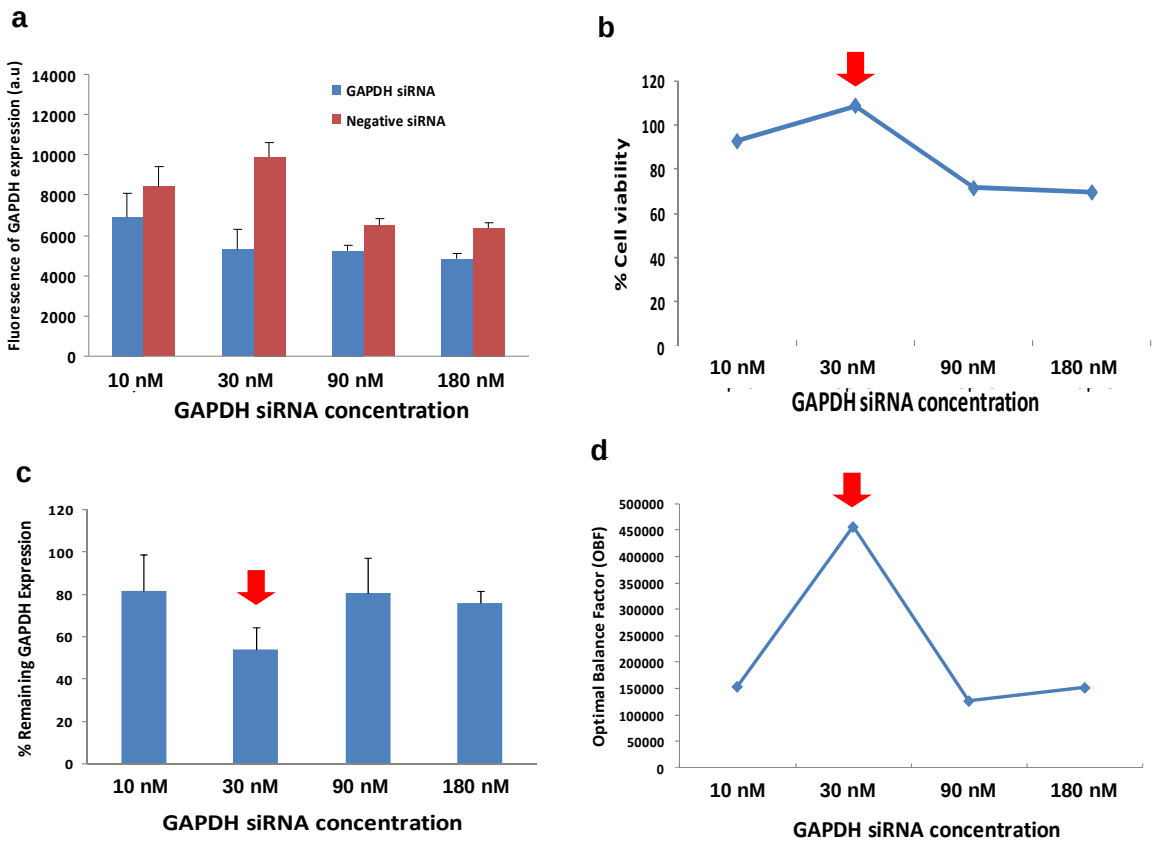

Figure 2.14. Optimization of siRNA-based DNAsome transfection efficiency. (**a**) GAPDH activity in arbitrary fluorescence units for samples plated at 10,000 cells per well. (**b**) % Cell viability associated transfection toxicity. GAPDH activity in negative siRNA-loaded DNAsome culture, relative to that in untreated cell control culture. (**c**) % Remaining GAPDH expression. GAPDH activity in GAPDH siRNA-loaded DNAsome transfected culture compared to that in negative siRNA-loaded DNAsome transfected culture. (**d**) Optimization of siRNA delivery by DNAsome. Optimal Balance Factor (OBF) used to determine the transfection efficiency for each transfection condition. Arrow indicates the best transfection conditions for this mammalian cell line (CHO cells).

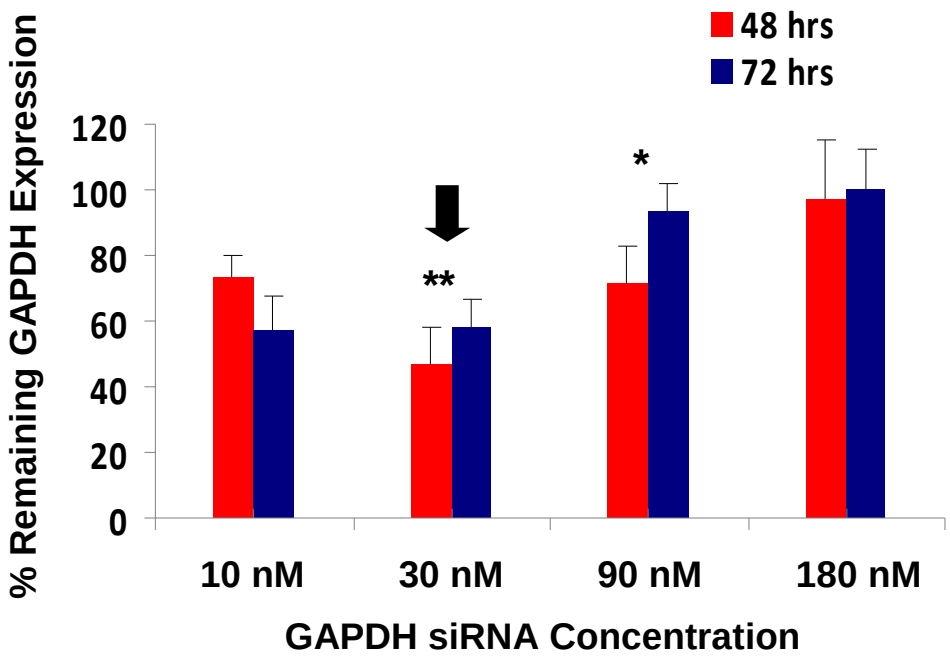

Figure 2.15. Remaining GAPDH activity in GAPDH siRNA-transfected cultures, relative to negative control transfections. Arrow indicates transfection condition resulting in the highest target knockdown. Each bar represents the mean standard deviation (SD). Statistical analyses were performed by Student's *t* test. * $P < 0.05$, ** $P < 0.01$ when compared with negative control cells.

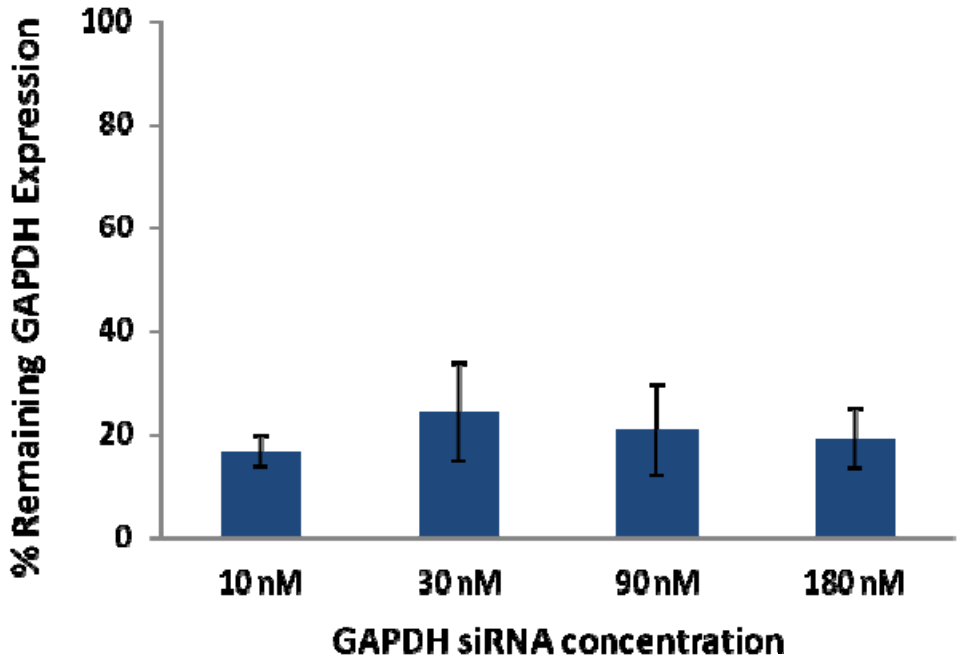

Figure 2.16. Transfection efficiency of siRNA-based transfection reagents. Remaining GAPDH expression from CHO cells. GAPDH activity in GAPDH siRNA-loaded DOTAP transfected cultures was compared to that in negative siRNA-loaded DOTAP transfected culture, respectively.

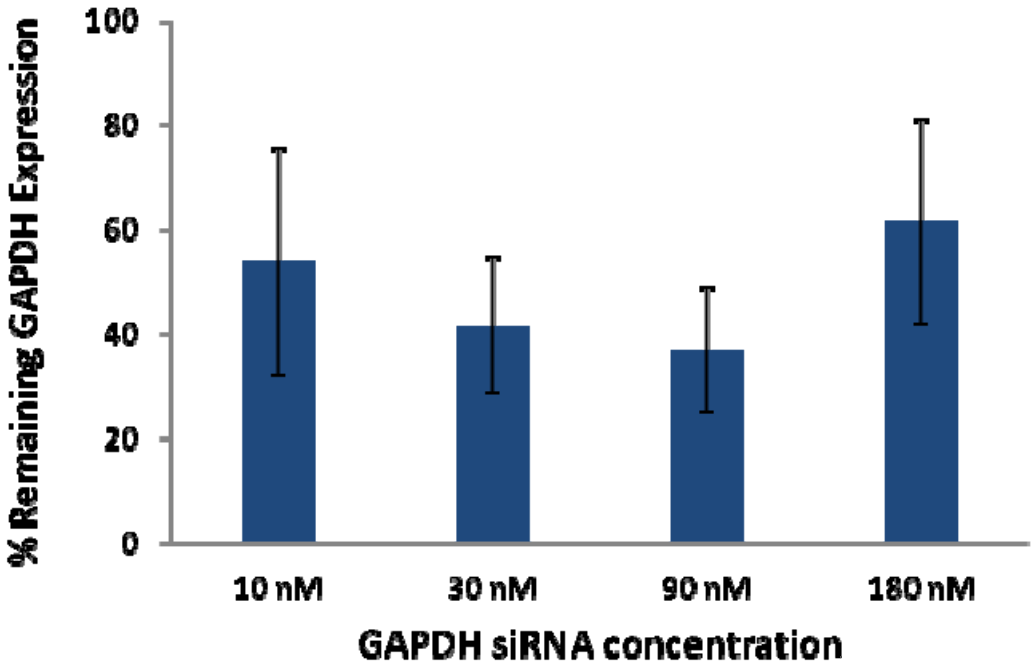

Figure 2.17. Transfection efficiency of siRNA-based transfection reagents. Remaining GAPDH expression from CHO cells. GAPDH activity in GAPDH siRNA-loaded Lipofectamin2000 (L2K) transfected cultures was compared to that in negative siRNA-loaded L2K transfected culture, respectively.

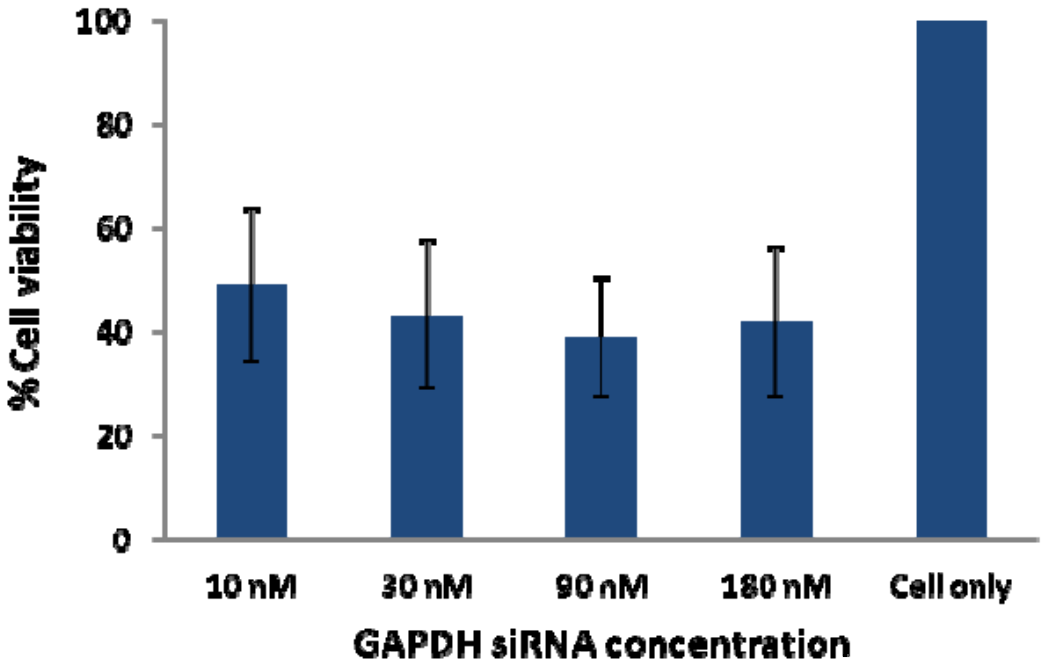

Figure 2.18. Cell viability associated with transfection toxicity. GAPDH activity in negative siRNA-loaded DOTAP transfected cultures, relative to that in untreated cell control culture.

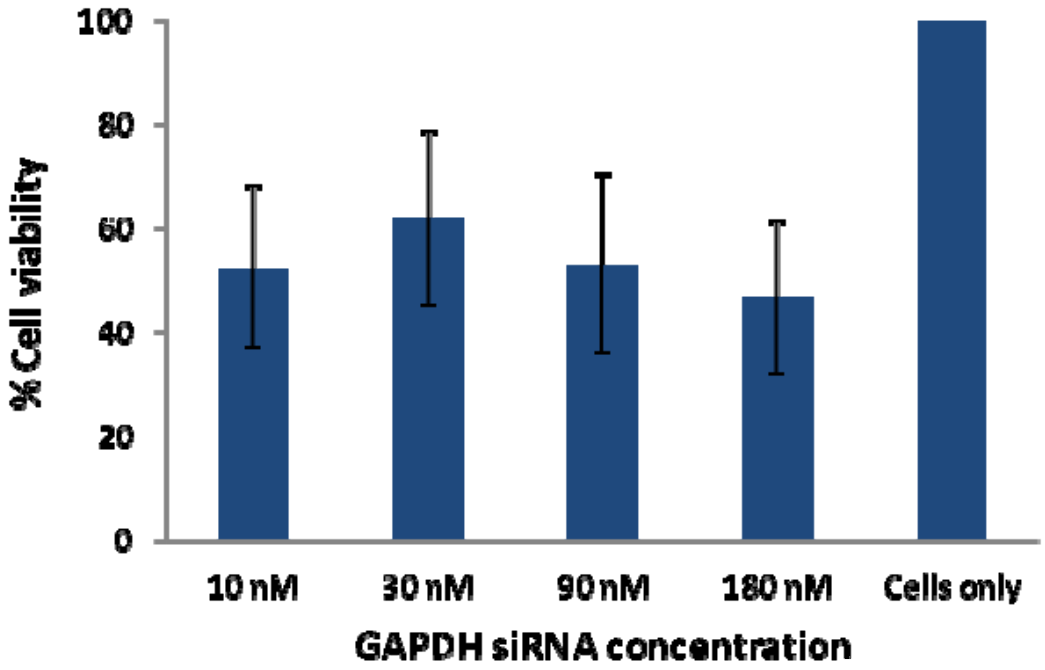

Figure 2.19. Cell viability associated with transfection toxicity. GAPDH activity in negative siRNA-loaded L2K transfected cultures, relative to that in untreated cell control culture.

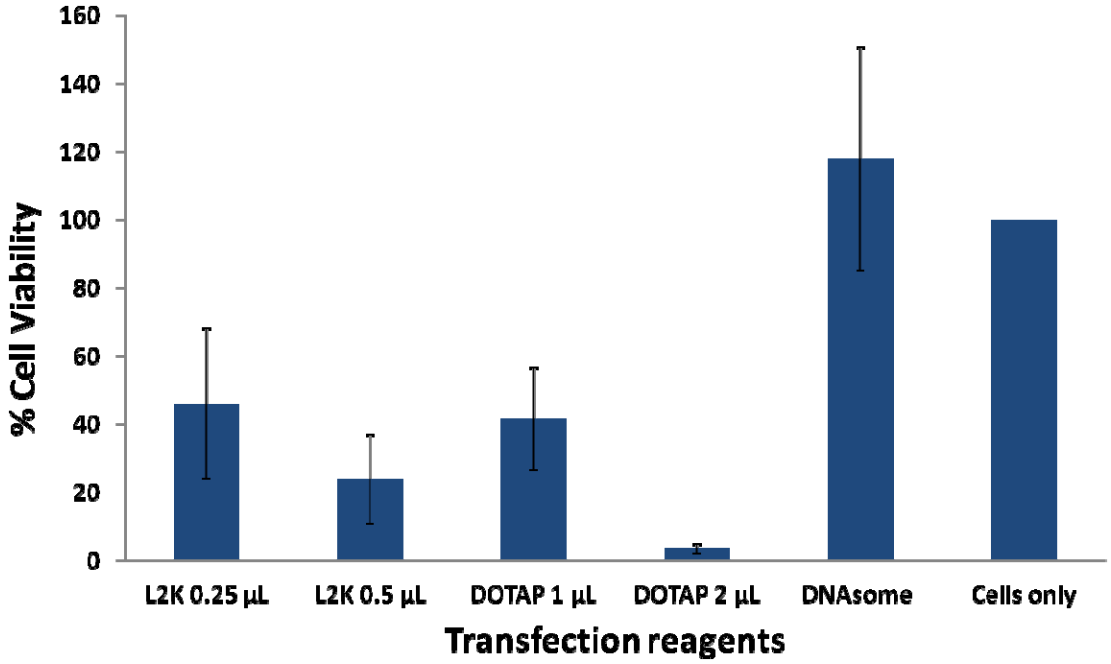

Figure 2.20. Cell viability of transfection reagents. Viability of CHO cells after incubation with the various transfection reagents (Lipofectamin2000, DOTAP, and DNAsome) as evaluated by measuring the remaining GAPDH protein level using KDalert^{TM} GAPDH assay. Only the transfection reagents (with no siRNA or drugs) were used for this assay.

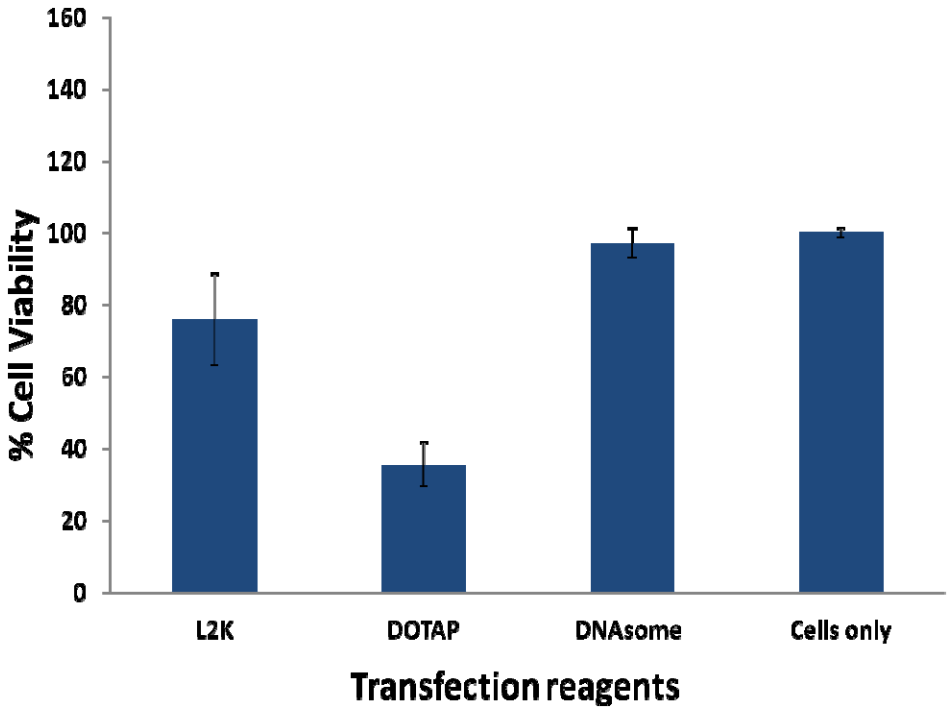

Figure 2.21. Cell viability of transfection reagents. Viability of CHO cells after incubation with the various transfection reagents (Lipofectamin2000, DOTAP, and DNAsome) as determined by the MTT assay. Only the transfection reagents (with no siRNA or drugs) were used for this assay.

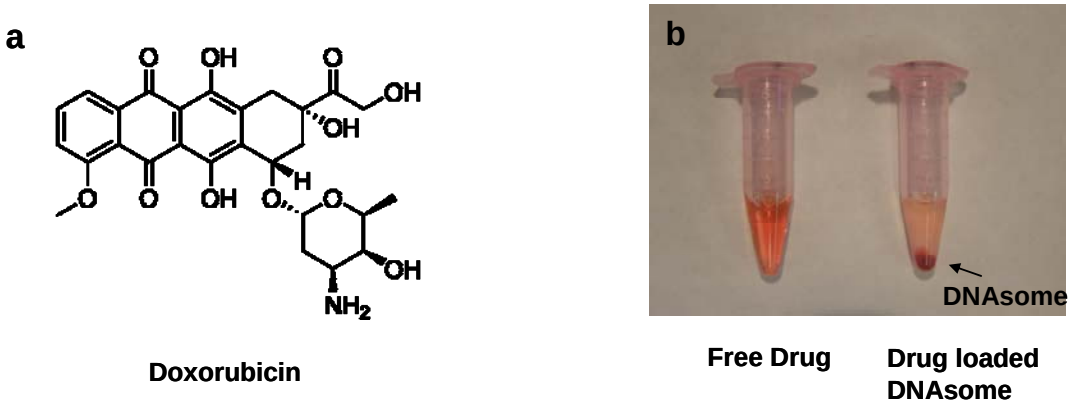

Figure 2.22. Drug loading of DNAsome. (**a**) Chemical structure of doxorubicin (**b**) Photograph of tubes containing doxorubicin solution and drug-loaded DNAsome.

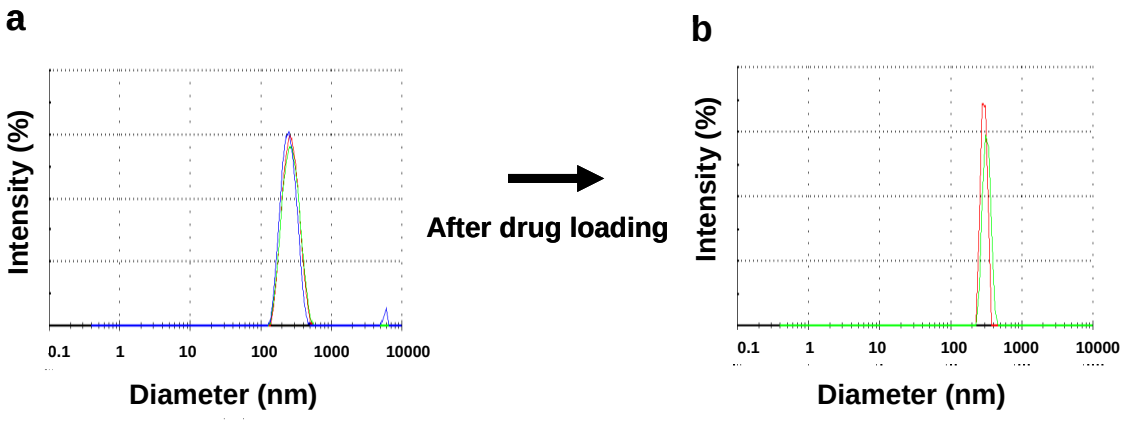

Figure 2.23. Drug loading of DNAsome (**a**) The average size of DNAsome before drug loading is 254 nm. (**b**) The average size of DNAsome after drug loading is 322 nm.

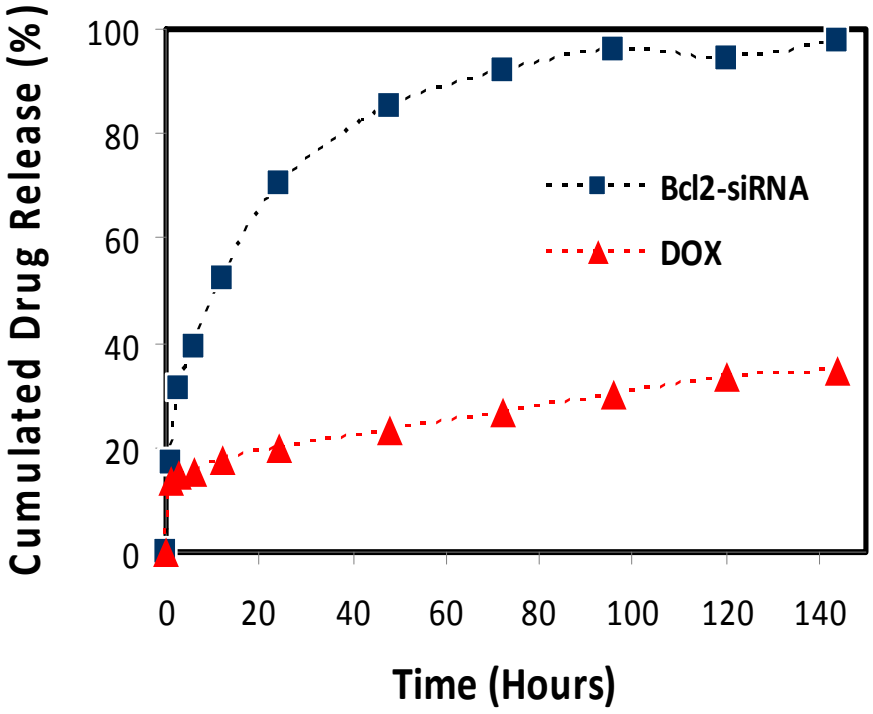

Figure 2.24. Drug release profiles from Bcl2-siRNA (■) and doxorubicin (▲) loaded DNAsomes.

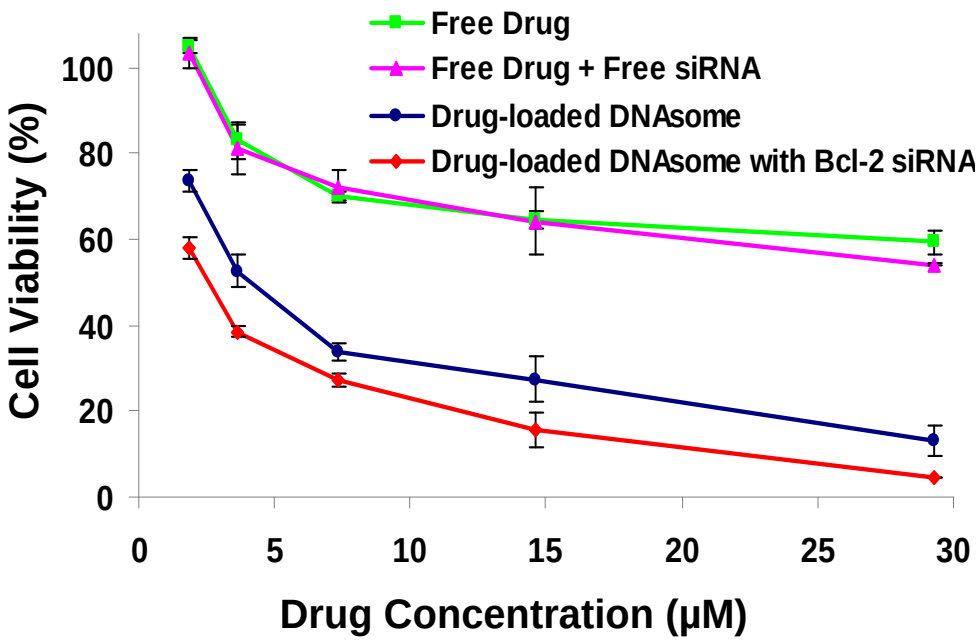

Figure 2.25. Co-delivery of siRNA and drug. Viability of CHO cells after incubation with free Dox, free Dox and free siRNA, Dox-loaded DNAsome, and Dox-loaded DNAsome hybridized with Bcl-2 siRNA, respectively.

lower IC_{50} compared with Dox-loaded DNAsomes (2 μM versus 5 μM) (Figure 2.25). This result suggests that DNAsomes are efficient nanocarriers for multi-drug delivery, particularly for siRNA.

2.5. Conclusion

In conclusion, we have created Y-DNA-based amphiphiles that are anisotropic, branched, and multivalent, which allow us to conjugate each molecule with multiple functionalities in a highly controlled fashion. To the best of our knowledge, this is the first time branched DNA amphiphiles have been created for drug delivery. These Y-DNA amphiphiles self-assemble into novel core-shell liposome-like DNAsomes with finely-tunable sizes. Although this study made use of Y-DNA amphiphiles, more highly-branched DNA could also be utilized for increased multivalency. These DNAsomes are natural and effective vectors for multi-drug delivery (in particular, siRNA), representing novel multifunctional carriers for future biomedical applications.

REFERENCES

1. R. Langer, *Nature* 1998, *392*, 5.
2. D. Luo, W. M. Saltzman, *Nat Biotechnol* 2000, *18*, 33.
3. M. E. Davis, Z. G. Chen, D. M. Shin, *Nat Rev Drug Discov* 2008, *7*, 771.
4. A. K. Salem, P. C. Searson, K. W. Leong, *Nature Materials* 2003, *2*, 668.
5. F. Gu, L. Zhang, B. A. Teply, N. Mann, A. Wang, A. F. Radovic-Moreno, R. Langer, O. C. Farokhzad, *Proc. Natl. Acad. Sci. U. S. A.* 2008, *105*, 2586.
6. C. C. Lee, J. A. MacKay, J. M. J. Frechet, F. C. Szoka, *Nature Biotechnology* 2005, *23*, 1517.
7. Y. Hu, P. U. Atukorale, J. J. Lu, J. J. Moon, S. H. Um, E. C. Cho, Y. Wang, J. Chen, D. J. Irvine, *Biomacromolecules* 2009, *10*, 756.
8. A. Akinc, A. Zumbuehl, M. Goldberg, E. S. Leshchiner, V. Busini, N. Hossain, S. A. Bacallado, D. N. Nguyen, J. Fuller, R. Alvarez, A. Borodovsky, T. Borland, R. Constien, A. de Fougerolles, J. R. Dorkin, K. N. Jayaprakash, M. Jayaraman, M. John, V. Koteliansky, M. Manoharan, L. Nechev, J. Qin, T. Racie, D. Raitcheva, K. G. Rajeev, D. W. Y. Sah, J. Soutschek, I. Toudjarska, H. P. Vornlocher, T. S. Zimmermann, R. Langer, D. G. Anderson, *Nature Biotechnology* 2008, *26*, 561.
9. V. P. Torchilin, *Nature Reviews Drug Discovery* 2005, *4*, 145.
10. Y. C. Tseng, S. Mozumdar, L. Huang, *Advanced Drug Delivery Reviews* 2009, *61*, 721.
11. A. P. Griset, J. Walpole, R. Liu, A. Gaffey, Y. L. Colson, M. W. Grinstaff, *J. Am. Chem. Soc.* 2009, *131*, 2469.
12. H. Mok, S. H. Lee, J. W. Park, T. G. Park, *Nat Mater*, *9*, 272.
13. Y. Wang, S. Gao, W. H. Ye, H. S. Yoon, Y. Y. Yang, *Nat Mater* 2006, *5*, 791.

14. A. M. Chen, M. Zhang, D. Wei, D. Stueber, O. Taratula, T. Minko, H. He, *Small* 2009, *5*, 2673.

15. N. C. Seeman, *Nature* 2003, *421*, 427.

16. F. A. Aldaye, A. L. Palmer, H. F. Sleiman, *Science* 2008, *321*, 1795.

17. Y. He, T. Ye, M. Su, C. Zhang, A. E. Ribbe, W. Jiang, C. D. Mao, *Nature* 2008, *452*, 198.

18. H. Yan, X. Zhang, Z. Shen, N. C. Seeman, *Nature* 2002, *415*, 62.

19. T. H. LaBean, *Nature* 2009, *459*, 331; f) R. P. Goodman, I. A. T. Schaap, C. F. Tardin, C. M. Erben, R. M. Berry, C. F. Schmidt, A. J. Turberfield, *Science* 2005, *310*, 1661.

20. S. Rinker, Y. Ke, Y. Liu, R. Chhabra, H. Yan, *Nature nanotechnology* 2008, *3*, 418.

21. U. Feldkamp, B. Sacca, C. M. Niemeyer, *Angew. Chem.* 2009, 121, 6110; *Angew. Chem., Int. Ed.* 2009, *48*, 5996.

22. Y. Li, Y. D. Tseng, S. Y. Kwon, L. D'Espaux, J. S. Bunch, P. L. McEuen, D. Luo, *Nature Materials* 2004, *3*, 38.

23. Y. Li, Y. T. Cu, D. Luo, *Nat Biotechnol* 2005, *23*, 885.

24. S. H. Um, J. B. Lee, N. Park, S. Y. Kwon, C. C. Umbach, D. Luo, *Nat Mater* 2006, *5*, 797.

25. S. Um, J. Lee, S. Kwon, Y. Li, D. Luo, *Nature Protocols* 2006, *1*, 995.

26. J. B. Lee, Y. H. Roh, S. H. Um, H. Funabashi, W. Cheng, J. J. Cha, P. Kiatwuthinon, D. A. Muller, D. Luo, *Nature nanotechnology* 2009, *4*, 430.

27. Ambion *Silencer*® siRNA Starter Kit Instruction Manual http://www.ambion.com/index.html

28. R. D. Leapman, N. W. Rizzo, *Ultramicroscopy* 1999, *78*, 251.

29. K. Kalyanasundaram, J. K. Thomas, *J. Am. Chem. Soc.* 1977, *99*, 2039.

30. J. H. Jeong, T. G. Park, *Bioconjug Chem* 2001, *12*, 917.

31. E. S. Andersen, M. Dong, M. M. Nielsen, K. Jahn, R. Subramani, W. Mamdouh, M. M. Golas, B. Sander, H. Stark, C. L. Oliveira, J. S. Pedersen, V. Birkedal, F. Besenbacher, K. V. Gothelf, J. Kjems, *Nature* 2009, *459*, 73.

32. Y. Dorsett, T. Tuschl, *Nat Rev Drug Discov* 2004, *3*, 318.

33. A. Fire, S. Xu, M. K. Montgomery, S. A. Kostas, S. E. Driver, C. C. Mello, *Nature* 1998, *391*, 806.

34. S. M. Elbashir, J. Harborth, W. Lendeckel, A. Yalcin, K. Weber, T. Tuschl, *Nature* 2001, *411*, 494.

35. E. Bernstein, A. A. Caudy, S. M. Hammond, G. J. Hannon, *Nature* 2001, *409*, 363.

36. K. A. Woodrow, Y. Cu, C. J. Booth, J. K. Saucier-Sawyer, M. J. Wood, W. M. Saltzman, *Nat Mater* 2009, *8*, 526.

37. D. M. Dykxhoorn, C. D. Novina, P. A. Sharp, *Nat Rev Mol Cell Biol* 2003, *4*, 457.

38. T. Holen, M. Amarzguioui, E. Babaie, H. Prydz, *Nucleic Acids Res* 2003, *31*, 2401.

39. H. Liang, D. Harries, G. C. Wong, *Proc. Natl. Acad. Sci. U. S. A.* 2005, *102*, 11173.

40. H. Lv, S. Zhang, B. Wang, S. Cui, J. Yan, *J Control Release* 2006, *114*, 100.

41. A. Lakkaraju, J. M. Dubinsky, W. C. Low, Y. E. Rahman, *J. Biol. Chem.* 2001, *276*, 32000.

42. S. D. Patil, D. G. Rhodes, *Nucleic Acids Res* 2000, *28*, 4125.

43. Y. Mo, L. Y. Lim, *J Pharm Sci* 2004, *93*, 20.

44. M. M. Zegers, K. J. Zaal, I. S. C. van, K. Klappe, D. Hoekstra, *Mol Biol Cell* 1998, *9*, 1939.

CHAPTER 3

Photocrosslinked DNA Nanospheres for Drug Delivery*

*Young Hoon Roh[1], Jong Bum Lee[1], Shawn J. Tan[1], Bojeong Kim[1], Hyeongsu Park[1], Edward J. Rice[1], Dan Luo[1] "Photocrosslinked DNA Nanospheres for Drug Delivery". *Macromol. Rapid Commun. 31*, 1207–1211 (2010).

[1]Department of Biological and Environmental Engineering, Cornell University Ithaca, New York, 14850, USA

3.1. Abstract

DNA has been employed as both a genetic and a generic material. X-shaped DNA (X-DNA) in particular has four branched arms, providing multivalent functionalities that can allow for simultaneous multiple crosslinking. Here we report the synthesis of four acrylate-functionalized X-DNA monomers that can be further photocrosslinked to form monodisperse and tunable DNA nanospheres. In particular, the size and surface charge of these nanospheres were precisely controlled in a linear fashion, simply by tuning the monomer concentration in the reaction. The morphology and surface properties of the nanospheres were characterized using FT-IR, HPLC, TEM, AFM, zeta potential, and DLS analysis. *In vitro* studies in mammalian cells revealed that these DNA nanospheres demonstrated significant efficacy in the delivery of doxorubicin. These results highlight the potential of using DNA as material building blocks to design novel nanocarriers with properties tailored for the delivery of drugs in general and DNA/RNA in particular.

3.2. Introduction

Non-viral drug delivery systems have attracted significant interest for their therapeutic potential.[1, 2] Recent progress in the field have led to the development of nanocarriers based on a variety of different materials such as lipids,[3, 4] polymers,[5, 6] and inorganic nanoparticles.[7] Nevertheless, it remains a challenge to design a delivery system with highly tunable and controllable features such as uniform size and precise surface charge. DNA is particularly suitable for this purpose, as it is a highly versatile biological polymer that can be manipulated precisely down to the molecular level using techniques from the existing molecular biology toolbox.[8] Although DNA exists naturally in a linear topology, recent progress in the field of DNA nanomaterials has led to the development of branched topologies that allows for the construction of novel

materials.[9–11] In particular, the fabrication of several sophisticated three-dimensional DNA nanostructures, including tetrahedra, buckyballs,[12] and boxes with controllable lids,[13] have also been reported.

By using branched DNA building blocks in conjunction with enzymatic ligation, our group has developed a wide range of novel DNA-based materials. These include dendrimer-like DNA[14, 15] and DNA hydrogels[16] for biotechnological applications such as multiplexed detection and sensing[17–19] as well as cell-free protein production.[20] These materials were assembled from highly monodisperse and anisotropic DNA building blocks[17] that provide significant control over multi-functionalization. Based on these earlier works, here we have designed four-armed, X-shaped DNA building blocks (X-DNA) with four photoreactive groups that were crosslinked to generate monodisperse DNA nanospheres. Notably, these nanospheres were assembled via a rapid crosslinking and enzyme-free remote activation process, while maintaining the key advantages of monodispersity and tunability of DNA nanomaterials.

In more detail, we report the photoactivated assembly of DNA nanospheres from X-DNA monomers that were specifically designed to anneal from four single-stranded DNA (ssDNA) containing partially complementary sequences with terminal modifications (Figure 3.1). In particular, the 5′-ends of these ssDNA were modified to contain a primary amine group that was used to conjugate photoreactive poly(ethylene glycol) acrylate groups (PEGA) to the oligonucleotides. Subsequently, the ssDNA–PEGA was annealed to assemble photocrosslinkable X-DNA monomers that can rapidly generate monodisperse DNA nanospheres within minutes upon UV illumination.

Notably, we precisely tuned the size of the nanospheres simply by adjusting the concentration of the X-DNA monomers. Interestingly, the monodisperse building

blocks photoassembled into nanospheres that were monodisperse as well, with an extremely high crosslinking efficiency and yield. In addition, these DNA nanospheres exhibited a significantly enhanced delivery efficacy of doxorubicin over free drug to mammalian cells. This work demonstrates the high-yield synthesis of novel photocrosslinked monodisperse DNA nanospheres with tunable size control that make them ideal candidates as effective drug delivery carriers.

3.3. Materials and Methods

3.3.1. Functionalization of photoreactive groups onto DNA building blocks

The DNA sequences were designed and synthesized based on previous work.[15] All oligonucleotides were commercially synthesized with standard desalting (Integrated DNA Technologies, Coralville, Iowa). The DNA sequences used in this experiment are listed in Table 3.1. Briefly, oligonucleotides were dissolved in annealing buffer (10×10^{-3}M Tris, pH 8.0, 1×10^{-3}M EDTA, and 50×10^{-3}M NaCl) to a final concentration of 0.2 mM. PEGA succinimidyl carboxy methyl ester (Nektar, Huntsville, Alabama) was conjugated to each arm of the ssDNA building blocks in a 5:1 molar ratio by mixing in a sterile 0.5 mL microcentrifuge tube. The reaction mixture was incubated for 4 h at room temperature. High performance liquid chromatography (HPLC) was performed to remove non-reacted products and impurities through an XBridge C18 column equipped with a photodiode array detector for UV detection at 260 nm (Waters Corp., Milford, Massachusetts). A gradient of 0–50% acetonitrile in 0.1 M triethylammonium acetate (TEAA, pH 7.0) at a flow rate of 1.0 mL · min^{-1} was used. After HPLC purification, gel electrophoresis was conducted to confirm the synthesis of the photocrosslinkable X-DNA–PEGA. Gel electrophoresis of HPLC fractions was conducted at a constant voltage of 90 V for 60 min (3% agarose gel).

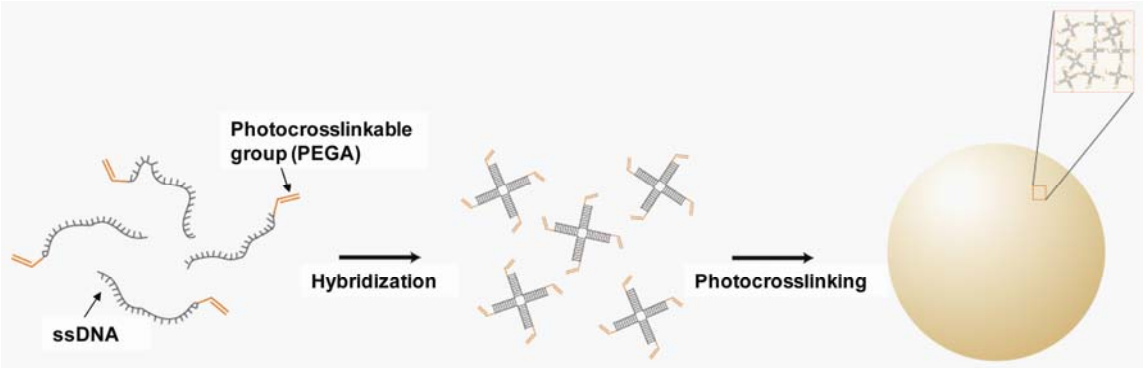

Figure 3.1. Schematic illustration of the construction of DNA nanospheres. DNA building blocks and DNA nanosphere are not drawn to scale. The resulting DNA nanospheres possess the capability and capacity to store drugs. PEGA, poly(ethylene glycol) acrylate.

Table 3.1. Oligonucleotide sequences of ssDNA used to generate X-DNA building blocks for photocrosslinked DNA nanospheres.

Strand	Segment
X01	5'- /NH_2/ CGA CCG ATG AAT AGC GGT CAG ATC CGT ACC TAC TCG - 3'
X02	5'- /NH_2/ CGA GTA GGT ACG GAT CTG CGT ATT GCG AAC GAC TCG -3'
X03	5'- /NH_2/ CGA GTC GTT CGC AAT ACG GCT GTA CGT ATG GTC TCG -3'
X04	5'- /NH_2/ CGA GAC CAT ACG TAC AGC ACC GCT ATT CAT CGG TCG -3'

3.3.2. Preparation of DNA nanospheres via photopolymerization

The solution mixture of X-DNA–PEGA was put into a 96-well plate and photopolymerization was carried out for 10 min upon exposure to a UV light source (8 $mW \cdot cm^{-2}$) in the presence of 1-[4-(2-hydroxyethoxy)phenyl]-2-hydroxy-2-phenylpropan-1-one (Ciba Specialty Chemicals, Tarrytown, New York), a photoinitiator, using a XL-1000 UV crosslinker (Spectronic Corp., Westbury, New York). After polymerization, the DNA nanospheres were collected and frozen using a FreeZone 4.5 freeze-dry system (Labconco Corp., Kansas City, Missouri).

3.3.3. Fourier Transform Infrared Spectroscopy (FT-IR)

To characterize the conjugation of PEGA and amine modified ssDNA, FT-IR spectra were obtained with a Mattson Galaxy GL5020 FT-IR spectrometer (Madison, Wisconsin). The spectra were scanned in the transmission mode from 4 000 to 500 cm^{-1} with 100 scans per point and a resolution of 4 cm^{-1}. Each 100 μL sample was pressed between two BaF_2 windows.

3.3.4. Morphology study of the DNA nanospheres

For the transmission electron microscopy (TEM) imaging experiment, a 5 μL drop of the DNA nanospheres (1 μM) was placed onto a sheet of parafilm and covered with a Petri dish for 7 min at room temperature. The spheres were then picked up by touching the drop with a formvar/carbon-coated TEM grid (Electron Microscopy Sciences, Fort Washington, Pennsylvania), and were left covered with a Petri dish for another 3 min. The sample was subsequently stained with 2% uranyl acetate for 1 min. The grid was then blotted with a filter paper and allowed to dry in air. The grids were visualized at a voltage of 120 kV using a FEI Philips TECNAI 12 (FEI Company, Hillsboro, Oregon), after rotary coating with Pt/C. For the scanning electron

microscopy (SEM) imaging experiment, a 10 μL drop of the DNA nanospheres was placed onto a silicon wafer and was allowed to dry in air for 2 h at room temperature. The surface of nanospheres was then examined at a voltage of 2 kV using a Leo 1550 Field Emission SEM (Carl Zeiss AG, Oberkochen, Germany). For atomic force microscopy (AFM) imaging, a 5 μL DNA nanosphere solution was placed onto the mica surface (Ted Pella, Inc., Redding, California) that was previously functionalized with aminopropyltriethoxysilane. The spheres were then allowed to adsorb to the mica surface for 20 min. The mica was then rinsed in Milli-Q water. Tapping-mode AFM images were taken in air using a Dimension 3100 AFM (Veeco, Inc., Plainview, New York).

3.3.5. Dynamic Light Scattering (DLS) and Zeta Potential measurement

The particle size and surface charge of DNA nanospheres were measured using a Zetasizer Nano ZS (Malvern Instruments, Worcestershire, UK). The nanospheres were dispersed in deionized water and all measurements were carried out at room temperature. Each parameter was measured in triplicate and the average hydrodynamic diameters and surface charges of DNA nanospheres were calculated.

3.3.6. Cell culture

Chinese hamster ovary (CHO) cells were cultured at 37 °C with 5% CO_2 in Ham's F-12K Nutrient Mixture, Kaighn's Modification supplemented with L-glutamine, 10% fetal bovine serum, and 1% penicillin/streptomycin.

3.3.7. Cell cytotoxicity evaluation (MTT)

The cytotoxicity of different formulations of DNA nanospheres and doxorubicin (Sigma–Aldrich) was evaluated using MTT cell viability assay (ATCC,

Manassas, Virginia). Absorbance was measured using a Synergy 4 Hybrid multi-mode microplate reader (Biotek Instruments, Inc., Winooski, Vermont) equipped with a specific monochrome filter at 570 nm. The cell viability of each sample was calculated by normalization of the absorbance to that of control cells.

3.4. Results and discussions

3.4.1. Characterization of photocrosslinkable X-DNA

3.4.1.1. Evaluation of ssDNA-PEGA conjugates

The ssDNA–PEGA conjugates were obtained via a reaction between the amine groups of ssDNA and the activated ester groups of the PEGA molecules (Figure 3.2). The final conjugated product was purified from the unreacted reagents using HPLC. The spectrum in Figure 3.3a shows two distinct peaks from HPLC which were further evaluated using gel electrophoresis (Figure 3.3b), distinguishing the initial ssDNA (Lane 1) from the ssDNA–PEGA conjugate (Lane 2). The results from gel electrophoresis also confirmed the successful generation of X-DNA–PEGA (Lane 3) from annealing the purified ssDNA–PEGA conjugates.

FT-IR spectroscopy was used to verify the conjugation of PEGA to ssDNA. Analysis of the amine-modified ssDNA with respect to the unmodified ssDNA revealed a band at approximately 1640 cm^{-1}, which corresponds to the N-H bending vibration for the amine group (Figure 3.4). Furthermore, the spectrum for ssDNA-PEGA revealed bands at 1670 cm^{-1} and 1640 cm^{-1}, which corresponds to the amide I band (C=O stretching vibration) and an amide II band (N-H bending vibration) respectively. Additionally, an alkane band (-CH_2- and -CH_3) at 2920 cm^{-1} was observed in the ssDNA-PEGA conjugates. The presence of these bands indicates the successful conjugation of PEGA with the amine functional group of ssDNA.

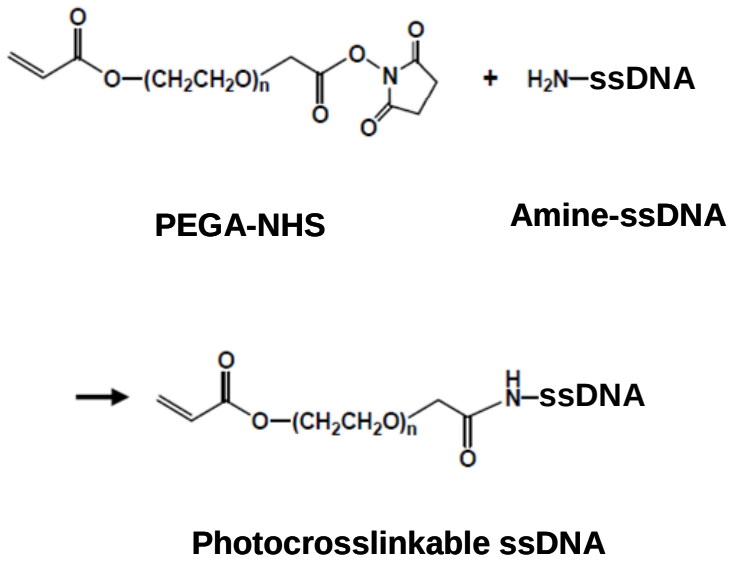

Figure 3.2. Synthesis of ssDNA–PEGA conjugates. The amine modified group of ssDNA was used to conjugate photoreactive poly(ethylene glycol) acrylate group (PEGA) to the oligonucleotide.

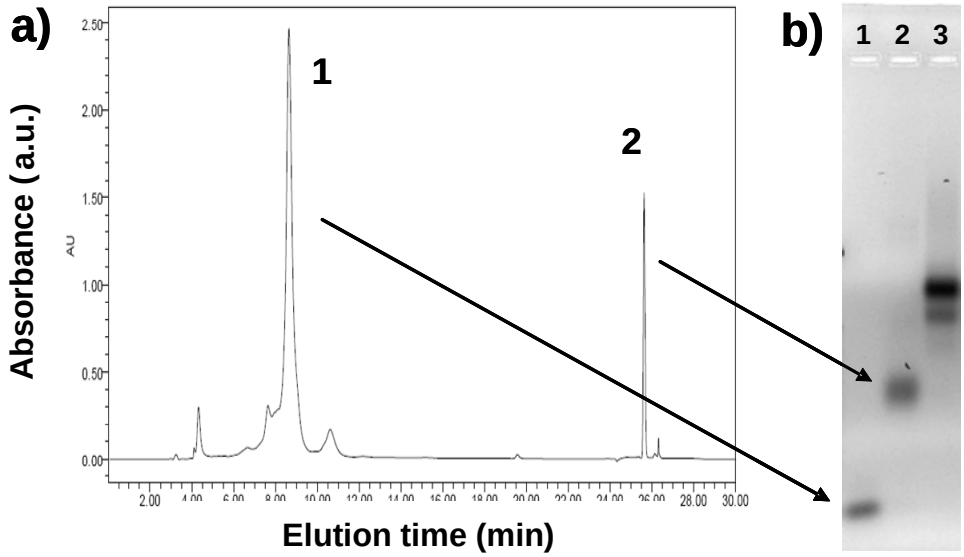

Figure 3.3. (**a**) HPLC chromatogram of products formed in the reaction of ssDNA and PEGA, indicating that the separation of unreacted ssDNA (1), and ssDNA–PEGA conjugate (2) was achieved. (**b**) Electrophoretic mobility shift of ssDNA and X-DNA building blocks. Lanes 1–3 indicate ssDNA, ssDNA–PEGA conjugate, and X-DNA–PEGA, respectively.

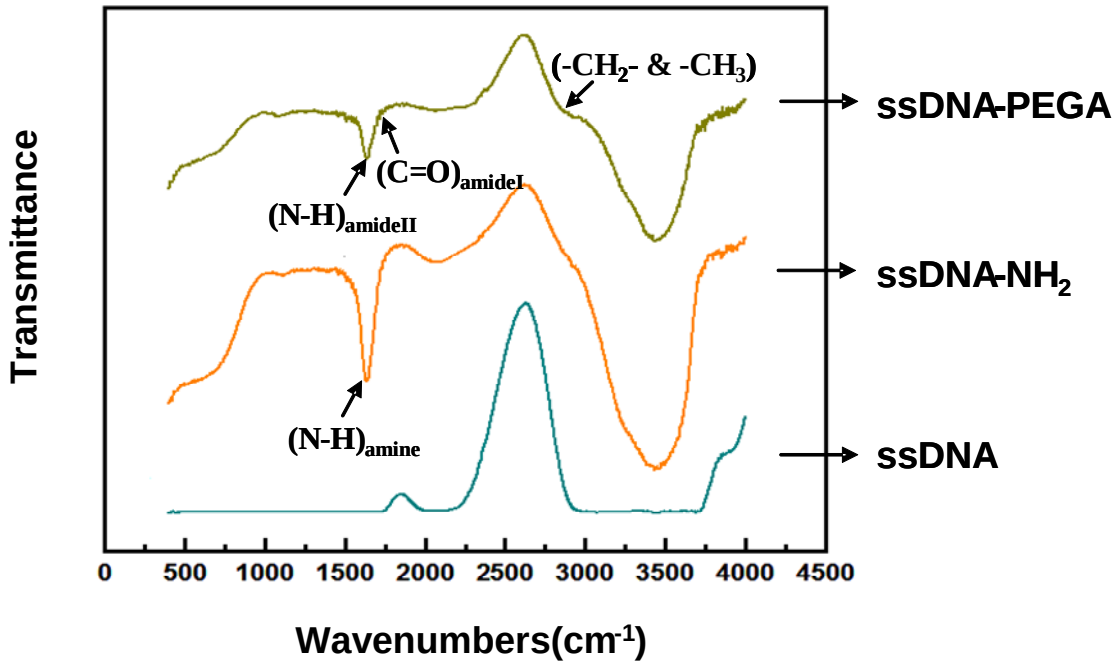

Figure 3.4. FT-IR spectra of ssDNA, amine-modified ssDNA, and PEGA-modified ssDNA indicating successful conjugation of PEGA onto ssDNA.

3.4.2. Characterization of DNA nanospheres

3.4.2.1. Morphology study of DNA nanospheres

DNA nanospheres were obtained by photocrosslinking the purified X-DNA–PEGA monomer. The morphology of these DNA nanospheres was then investigated using electron microscopy and scanning probe microscopy (Figure 3.5). TEM imaging revealed the formation of spherical nanostructures with diameters of 260 ± 35 nm (n = 16) from X-DNA–PEGA monomers (Figure 3.5a). At higher magnifications, we observed that these nanospheres possessed a textured surface (Figure 3.5b). SEM (Figure 3.5c) and AFM (Figure 3.5d) imaging also confirmed the presence of nanospheres with diameters of approximately 300 nm, which were consistent with TEM observations.

3.4.2.2. The controllability of DNA nanospheres

Interestingly, the size of DNA nanospheres can be controlled by varying the concentration of X-DNA building blocks. DLS analysis of DNA nanospheres generated from different concentrations of X-DNA revealed a linear relationship between nanosphere diameter and monomer concentration (Figure 3.6). In particular, we tuned the size of the nanospheres from 225 to 540 nm linearly simply by adjusting the concentration of X-DNA from 100 nM to 1 pM. AFM imaging further confirmed the DLS measurements as well as the formation of nanospheres (Figure 3.7). In addition, zeta potential measurements showed a slightly increasing surface charge (from −31.1 ± 0.3 to −24.3 ± 0.3 mV) that corresponds to the increase in concentration of X-DNA building blocks (Figure 3.8). These results suggest that the smaller DNA nanospheres contain less negatively charged DNA, resulting in relatively lower negative surface charge. The monomer peak (≈6 nm) from DLS data was not observed in the size distribution for the nanosphere samples after photocrosslinking, indicating

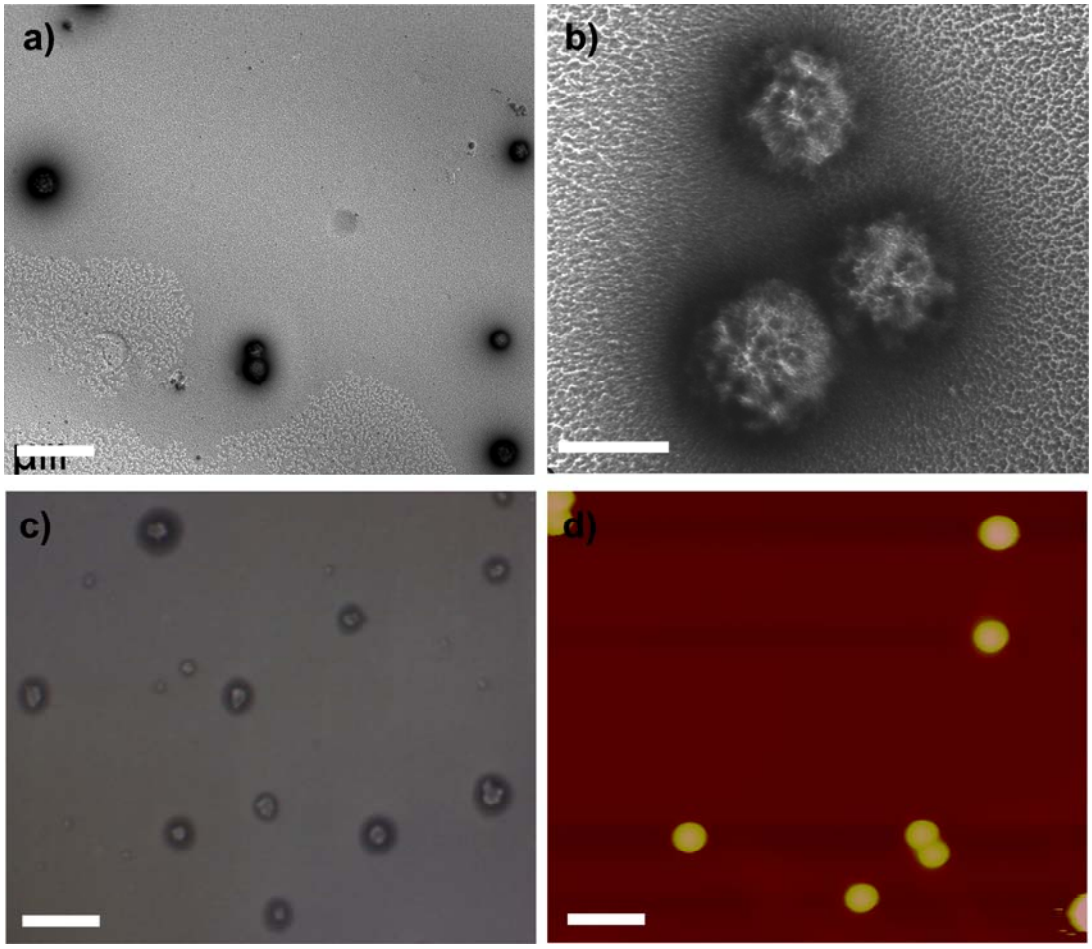

Figure 3.5. (**a** and **b**) TEM images of photocrosslinked DNA nanospheres. (**c**) SEM image of DNA nanospheres. (**d**) AFM image of DNA nanospheres. The scale bars are 1 μm for (a), (c), and (d) and 200 nm for (b).

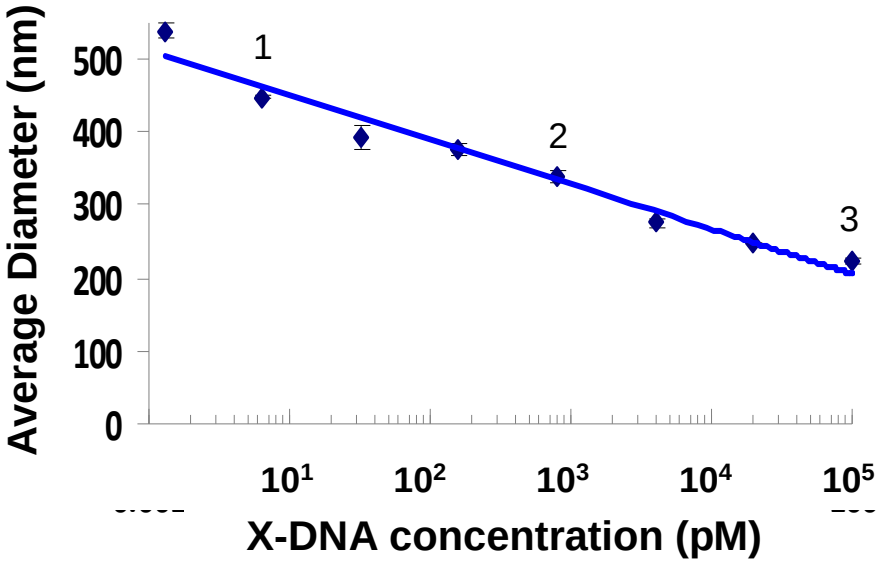

Figure 3.6. Average diameter of DNA nanospheres measured as a function of X-DNA monomer concentration.

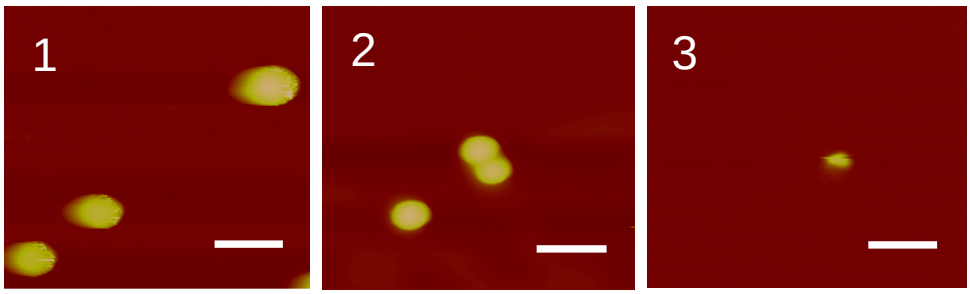

Figure 3.7. AFM images corresponding to the samples labeled (1), (2), and (3) in (a), indicating the presence of spherical particles with varying sizes. The scale bar is 500 nm.

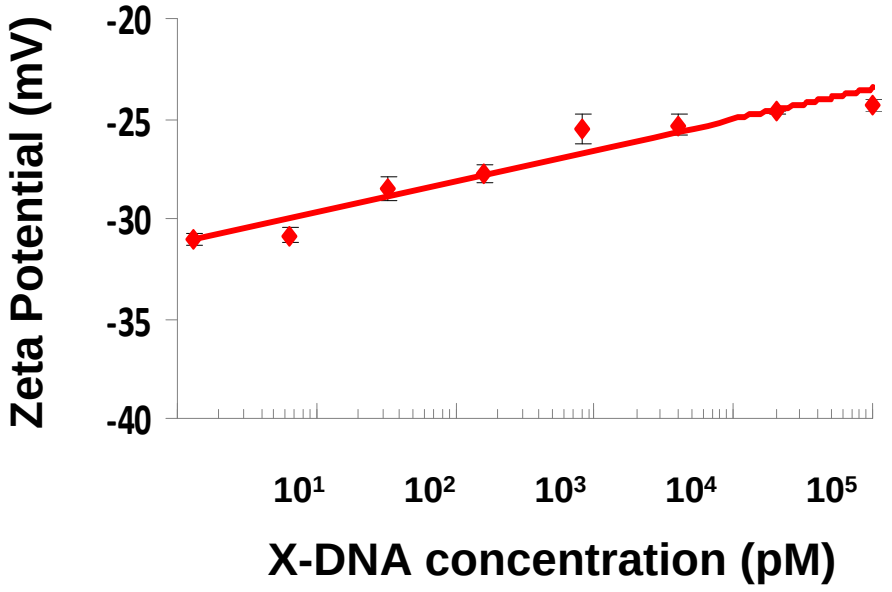

Figure 3.8. Zeta potential of DNA nanospheres as a function of X-DNA monomer concentration.

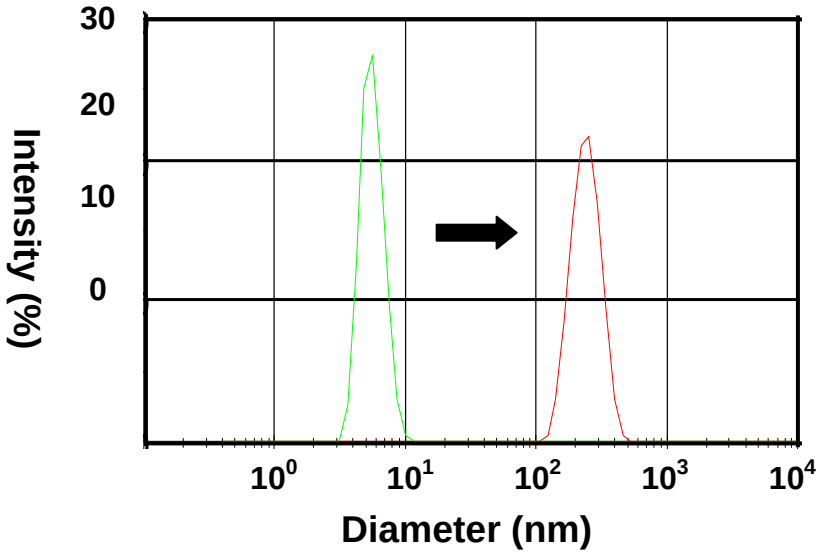

Figure 3.9. Size distribution of DNA nanospheres before and after photo-polymerization (overlay of two independent DLS measurements).

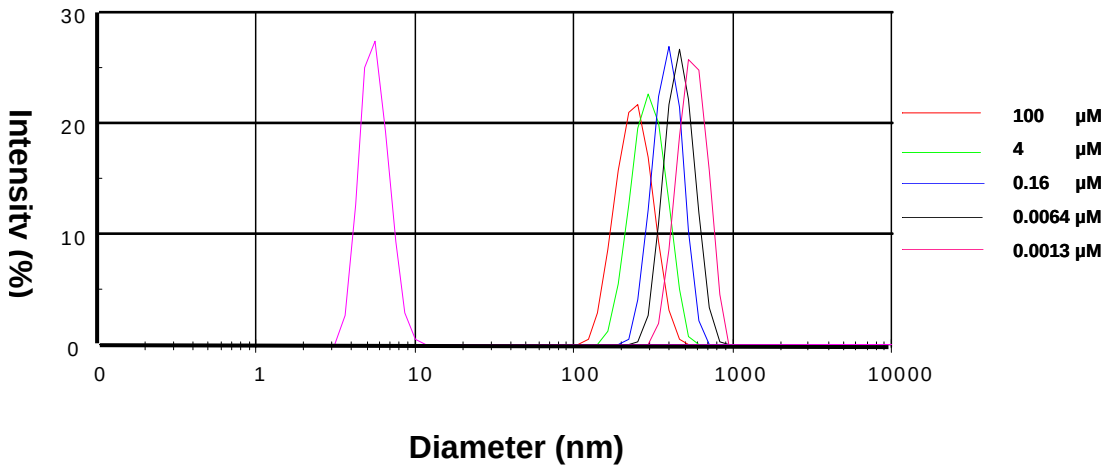

Figure 3.10. DLS size distribution data showing the size controllability and monodispersity of DNA nanospheres. The monomer peak at ~6 nm is not observed in the samples of DNA nanospheres generated from varying X-DNA monomer concentrations.

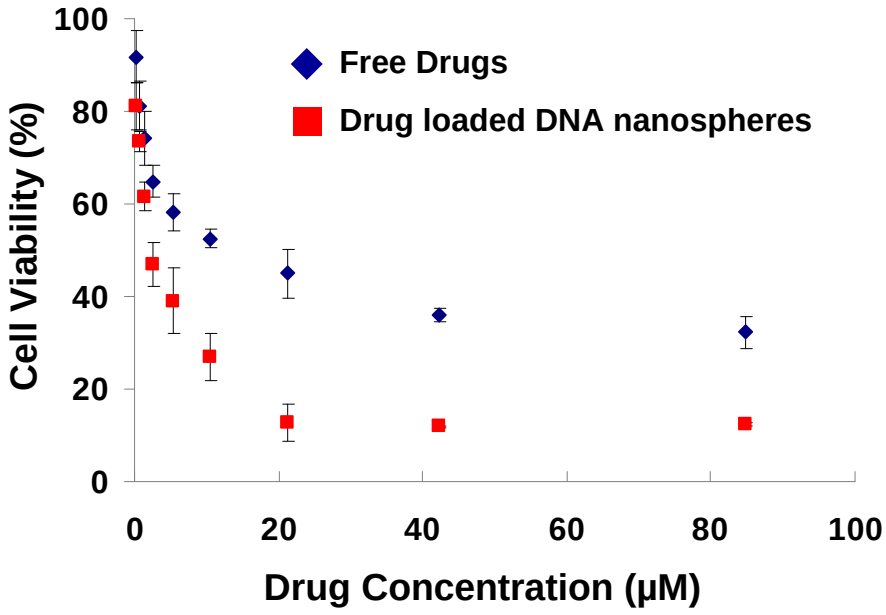

Figure 3.11. Viability of CHO cells after 48 h of incubation with free Dox and Dox-loaded DNA nanospheres. Error bars indicate standard deviation with $n = 3$.

an extremely high crosslinking efficiency of close to 100% (Figure 3.9), thus eliminating the need for any additional purification steps after photocrosslinking. The size distribution data also suggests that the DNA nanospheres were monodisperse in solution with a polydispersity index (PDI) of ≤ 0.05 across all samples (Figure 3.10).

3.4.3. Application of DNA nanospheres

3.4.3.1. Drug delivery efficiency of DNA nanospheres

To explore the potential application of DNA nanospheres as drug delivery vectors, doxorubicin (Dox) was used as a model drug and was encapsulated within DNA nanospheres. We achieved a relatively high drug loading efficiency of 62% (w/w, data not shown). The Dox-loaded nanospheres were then delivered to CHO cells and the delivery efficacy was evaluated based on cell viability studies with free Dox as a control. Importantly, DNA nanospheres loaded with Dox demonstrated a significantly lower IC_{50} (the concentration of Dox that kills 50% of the cells) compared with free Dox (14 vs. 2×10^{-6}M) (Figure 3.11). In addition, DNA nanospheres alone showed no cytotoxicity (data not shown).

3.5. Conclusion

In summary, we have created a novel class of DNA materials that can be synthesized by rapid photocrosslinking upon UV illumination. Unlike earlier works that involve enzymatic ligation of DNA building blocks, we can remotely activate the crosslinking of branched DNA. The material properties of the resulting DNA nanospheres, such as size and surface charge, can be precisely tuned in a linear fashion for applications such enhanced drug delivery. We envision that these photoassembled DNA nanospheres can also be utilized in other drug delivery applications that require rapid and remote assembly.

REFERENCES

1. D. Luo, W. M. Saltzman, *Nat Biotech* 2000, *18*, 33.
2. D. Peer, J. M. Karp, S. Hong, O. C. Farokhzad, R. Margalit, R. Langer, *Nat Nano* 2007, *2*, 751.
3. V. P. Torchilin, *Nat Rev Drug Discovery* 2005, *4*, 145.
4. Akinc, Akin et al *Nat Biotech* 2008, *26*, 561.
5. C. C. Lee, J. A. Mackay, J. M. Frechet, F. C. Szoka, *Nat Biotech* 2005, *23*, 1517.
6. A. K. Salem, P. C. Searson, K. W. Leong, *Nat Mater* 2003, *2*, 668.
7. M. De, P. S. Ghosh, V. M. Rotello, Applications of Nanoparticles in Biology *Adv Mater* 2008, *20*, 4225.
8. D. Luo, *Materials Today* 2003, *6*, 38.
9. N. C. Seeman, *Angewandte Chemie International Edition* 1998, *37*, 3220.
10. J. J. Storhoff, C. A. Mirkin, *Chemical Reviews* 1999, *99*, 1849.
11. T. H. LaBean, H. Li, *Nano Today* 2007, *2*, 26.
12. Y. He, T. Ye, M. Su, C. Zhang, A. E. Ribbe, W. Jiang, C. Mao, *Nature* 2008, *452*, 198.
13. E. S. Andersen, M. Dong, M. M. Nielsen, K. Jahn, R. Subramani, W. Mamdouh, M. M. Golas, B. Sander, H. Stark, C. L. P. Oliveira, J. S. Pedersen, V. Birkedal, F. Besenbacher, K. V. Gothelf, J. Kjems, *Nature* 2009, *459*, 73.
14. Y. Li, Y. D. Tseng, S. Y. Kwon, L. d'Espaux, J. S. Bunch, P. L. McEuen, D. Luo, *Nat Mater* 2004, *3*, 38.
15. S. H. Um, J. B. Lee, S. Y. Kwon, Y. Li, D. Luo, *Nat. Protocols* 2006, *1*, 995.
16. S. H. Um, J. B. Lee, N. Park, S. Y. Kwon, C. C. Umbach, D. Luo, *Nat Mater* 2006, *5*, 797.

17. J. B. Lee, Y. H. Roh, S. H. Um, H. Funabashi, W. Cheng, J. J. Cha, P. Kiatwuthinon, D. A. Muller, D. Luo, *Nat Nano* 2009, *4*, 430.

18. Y. Li, Y. T. H. Cu, D. Luo, *Nat Biotech* 2005, *23*, 885.

19. U. Feldkamp, B. Saccà, Christof M. Niemeyer, *Angewandte Chemie International Edition* 2009, *48*, 5996.

20. N. Park, S. H. Um, H. Funabashi, J. Xu, D. Luo, *Nat Mater* 2009, *8*, 432.

CHAPTER 4

Photocrosslinked Nucleic Acid Hydrogels and Their Application *

---

*Young Hoon Roh[1], Dan Luo[1] "Photo-crosslinked Nucleic Acid Hydrogels". *PCT/US2009/052795*.

*Young Hoon Roh[1], Bojeong Kim[1], Mark R. Hartman[1], Edward J. Rice[1], Songming Peng[1], Dan Luo[1] "Photocrosslinked DNA Hydrogels for Cell-free Protein Expression". *Paper in preparation* (2011).

*Young Hoon Roh[1], Michael J. Campolongo[1], Shawn J. Tan[1], Mark R. Hartman[1], Dan Luo[1] "Nanopatterning of DNA Coated Nanoparticles via Photocrosslinking". *Paper in preparation* (2011).

[1]Department of Biological and Environmental Engineering, Cornell University Ithaca, New York, 14850, USA

4.1. Abstract

DNA has been utilized as both a genetic and a generic material. In particular, DNA hydrogels provide biocompatible, biodegradable and cost effective way to form desired sizes and shapes. Here we report rapid and new methods to construct three-dimensional networked hydrogel structures from branched DNA-based building blocks via photocrosslinking. The advantages of this approach are that the gelling process is easily achieved within several minutes and the mechanical strength of the resulting gel matrixes can be dramatically improved. Several different shapes and formats of photocrosslinked DNA hydrogels are described. Furthermore, their applications for cell-free protein production are discussed. Fine tuning of each system has its own benefits in terms of protein yield, format, and stability. These results demonstrate that our photo-crosslinked DNA hydrogels can be tailored as a novel material for bio-related applications, particularly in protein engineering.

4.2. Introduction

Photopolymerization is widely used to make relatively simple hydrogels.[1] DNA is a highly efficient material that can be controlled by various molecular tools, such as enzymes.[2] Previously, we developed DNA hydrogels, DNA nanobarcodes, and dendrimer-like DNA nanostructures entirely from programmable self-assembled, branched DNA through enzyme ligation.[3-6] Our DNA hydrogels have been used as fundamental components in a variety of therapeutic applications.[7] Recently, an enzyme-catalyzed DNA hydrogel has been used for cell-free protein synthesis, controlled drug delivery, and cell and tissue culture applications.[8-11] Although an enzyme-ligated approach to synthesizing DNA gels can yield a biocompatible, biodegradable, and inexpensive means to manipulating a product, this approach may use several hours of reaction time to produce a gel with soft gel properties.

Here we report a method for rapidly producing DNA hydrogels using photo-crosslinking of branched DNA-based structures. The X-shaped DNA building blocks, which have at least one portion of the branched nucleic acid molecules are conjugated with a photoreactive group (biocompatible polymer, poly(ethylene glycol) (PEG)). The crosslinked nucleic acid molecules can form a three-dimensional structure and nucleic acid hydrogel. The hydrogel can posses various structures, including a micro thin film, micro pad, micro thin fiber, nanosphere or a microsphere. The networked structures are fabricated by emulsification, photolithography, microfluidic synthesis, micromolding, or micro-electrospinning combining with photocrosslinking. This photocrosslinking method can also allow for the coating of DNA hydrogel on the surface of a substrate within 10 minutes or less.

Various hydrogel matrices can be produced, depending on UV exposure time, photoinitiator concentration, and the properties of the DNA building blocks. The geometric pattern also provides pore size controllability by selecting from other polymer group (e.g. PEGDA) and varying the polymer concentration. These photo-crosslinked hydrogels can also have improved mechanical properties including increased hydrogel strength. These aspects make photocrosslinked DNA hydrogels and particles valuable in constructing DNA gels with improved functions.

X-shaped DNA building blocks with photoreactive portions were also conjugated onto gold nanoparticles (AuNP) to obtain modified AuNP-DNA conjugates after photoreaction. A variety of other nanoparticles can be used as well. Fine tuning of DNA hydrogel coated nanoparticles is easily accomplished by adjusting the initial DNA concentrations, reaction time and types of monomers, thus allowing the hydrogels to be tailored for specific applications. These photocrosslinked hydrogels can be utilized in novel bio-related applications, such as cell-free protein synthesis, surface chemistry and controlled drug delivery.

4.3. Materials and Methods

4.3.1. Synthesis of photocrosslinkable DNA building block

The DNA sequences for synthesizing functionalized branched DNA building blocks are designed and listed in Table 4.1 and Table 4.2. All oligonucleotides were commercially synthesized with standard desalting (Integrated DNA Technologies, Coralville, Iowa). The photocrosslinkable X-DNAs were prepared following the same procedures as described in our previous publications.[12] Briefly, oligonucleotides were dissolved in annealing buffer (10×10^{-3}M Tris, pH 8.0, 1×10^{-3}M EDTA, and 50×10^{-3}M NaCl) to a final concentration of 0.2 mM. PEGA succinimidyl carboxy methyl ester (Nektar, Huntsville, Alabama) was conjugated to each 5' end of the ssDNA in a 4:1 molar ratio by mixing in a sterile 1.5 mL microcentrifuge tube. The reaction mixture was incubated for 4 h at room temperature. Next, the ssDNA-PEGA conjugate was purified via High Performance Liquid Chromotography (HPLC) to remove non-reacted products. An XBridge C18 column was used with a photodiode array detector for UV detection at 260 nm (Waters Corp., Milford, Massachusetts). A gradient of 0–70% acetonitrile in 0.1 M triethylammonium acetate (TEAA, pH 7.0) at a flow rate of 0.5 mL · min^{-1} was used. Photocrosslinkable X-DNA was constructed by mixing four ssDNA-PEGA components (with the same molar ratio) in sterile Milli-Q water with a final concentration of 40 mM for each oligonucleotide. Hybridizations were performed according to the following procedures: (i) Denaturation at 95 °C for 2 min. (ii) Cooling at 65 °C and incubation for 2 min. (iii) Annealing at 60 °C for 5 min. and (iv) Further annealing at 60 °C for 0.5 min with a continuous temperature decrease at a rate of 1 °C per min. The annealing steps were repeated a total of 40 times. The final annealed products were stored at 4 °C.

Table 4.1. Oligonucleotide sequences of the DNA building blocks for photo-crosslinked DNA hydrogels

Strand	Segment 1	Segment 2
X01	5'- /NH_2/	CGA CCG ATG AAT AGC GGT CAG ATC CGT ACC TAC TCG - 3'
X02	5'- /NH_2/	CGA GTA GGT ACG GAT CTG CGT ATT GCG AAC GAC TCG -3'
X03	5'- /NH_2/	CGA GTC GTT CGC AAT ACG GCT GTA CGT ATG GTC TCG -3'
X04	5'- /NH_2/	CGA GAC CAT ACG TAC AGC ACC GCT ATT CAT CGG TCG -3'

Table 4.2. Oligonucleotide sequences of the DNA building blocks for hybridization with linearized plasmid.

Strand	Segment
X01	5'- /NH_2/ CGA CCG ATG AAT AGC GGT CAG ATC CGT ACC TAC TCG - 3'
X02	5'- /p/ CGA GTA GGT ACG GAT CTG CGT ATT GCG AAC GAC TCG GGCC -3'
X03	5'- /NH_2/ CGA GTC GTT CGC AAT ACG GCT GTA CGT ATG GTC TCG -3'
X04	5'- /NH_2/ CGA GAC CAT ACG TAC AGC ACC GCT ATT CAT CGG TCG -3'

Sticky ends (corresponding to ApaI restriction sequence 5'-GGCC-3') are in red text. The sequences considered internal to the X-DNA are in black text and can remain unchanged for use with any gene.

4.3.2. Synthesis of photocrosslinked DNA hydrogel

The purified photocrosslinkable DNA conjugates were further photo-polymerized to from DNA hydrogels under ultraviolet (UV) irradiation (8 mW cm^{-2}) in an aqueous solution of 5 wt % photoinitiator Irgacure (Ciba Geigy) using a UV crosslinker (Spectronics Corporation, XL-1000).

4.3.3. Fabrication of micropatterned DNA gel

A micro-meter scale DNA gel pad are made by casting the DNA pre-gel solution into a PDMS mold that was fabricated with precisely defined dimensions by soft lithography or photolithography. The dimensions of the micropads were 1 mm × 1 mm × 20 μm, and 400 μm × 200 μm × 20 μm. A DNA pre-gel solution (10 μL) was dropped onto a 3-aminopropyltriethoxysilane (APTES) modified glass slide, and the PDMS mold was placed over the solution. After photocuring for 30 mins at room temperature, the PDMS mold was peeled off. To visualize the DNA gel micro-patterns, the molded gel was stained with the DNA specific dye SYBR I, and the fluorescence image was taken by a fluorescence microscope.

4.3.4. Mechanical property of photocrosslinked DNA-Polymer hydrogel

The mechanical property measurements were performed on a Dynamic Mechanical Analyzer (DMA 2980, TA Instruments, Inc). The hydrogel was clamped between a parallel-plate compression clamp with a diameter of 1.0 cm. The compressive modulus test was conducted on a cylindrical shaped DNA gel with 7.0 mm in diameter and 3.0 mm thick.

4.3.5. Morphology study of photocrosslinked DNA hydrogel

For SEM imaging, strips cut from the dried DNA gel were placed into the top of the SEM holder with carbon tape and metal-coated with Au/Pd to obtain high resolution images.

4.3.6. Gel-electrophoresis

Gel electrophoresis was performed to confirm the polymerization of the PEG and DNA. Gel electrophoresis of hydrogel fractions were conducted at a constant voltage of 100 volts for 60 min (3 % agarose gel).

4.3.7. Fourier transform infrared spectroscopy (FT-IR)

To characterize the conjugation of PEG and X-DNA, FT-IR microspectra were conducted with Galaxy series FT-IR 5000 (GL5020, Mattson, Arizona). The spectra were scanned in the absorbance mode from 4000 to 500 cm^{-1} with 100 scans per point and resolution of 4 cm^{-1}. Each sample of 150 µl was squeezed between two BaF_2 windows.

4.3.8. Preparation of linear *Renilla* luciferase reporter gene

The plasmid DNA (pDNA) was PCR-amplified from the pRL-Null vector (Promega, Madison, WI) in competent *Escherichia coli* and purified by an Eppendorf Perfectprep® Plasmid Mini Kit (Westbury, NY). Two primers were designed for PCR amplification: ATG CCA TGG CTT CGA AAG TTT ATG ATC CAG and TAC CCC GGG TTA TTG TTC ATT TTT GAG AAC TCG C. The amplified and purified Rluc gene was inserted into the *Nco* I and *Sma* I sites of the expression vector pIVEX1.3WG (Roche) to generate pIVEX1.3RL (for wheat germ lysate). The plasmids were linearized with the restriction enzyme *Apa* I (Promega, Madison, WI) which cuts the plasmid at a single site before the T7 promoter for P-gels expression.

The size of the entire plasmid is 4,134 bp, and the size of luciferase gene is 1,331 bp including the T7 promoter, 3' UTR and 5' UTR.

4.3.9. Protein expressions

Protein expressions were carried out by using coupled transcription and translation system (Roche) following the procedures described by the manufacturer. For example, the photocrosslinked DNA hydrogel containing specifically pre-defined amounts of plasmids were first delivered to the expression solution. For control SPS, the same amounts of linear plasmids were directly added to the expression solution. The reaction volume was kept in a volume of 50 μl and the feeding solution in a volume of 1 ml. The protein expression reaction was carried out in the Proteomaster (Roche) in 24 °C with 900 r.p.m. of shaking. After incubation for a specific time, all reaction samples were stored at -80 °C before assay.

4.3.10. Protein assays

The detailed methods for protein assays are described in our previous paper.[9] The protein expression yield was measured based on functional assays such as measuring luminescence or fluorescence. The luciferase activity was evaluated by the *Renilla Luciferase* Assay System (Promega, Madison, WI) and assayed by a luminometer.

4.3.11. Synthesis of gene photocrosslinked DNA hydrogels for protein expression

Photocrosslinkable X-DNA building blocks and linear plasmids (genes) were first mixed at a pre-determined molar ratio in the presence of photoinitiator Irgacure (Ciba Geigy) to form the photocrosslinkable gene precursor. For example in case of an X-DNA/plasmid ratio of 2,000:1, we used 35.0 mM of X-DNA and 17.5 nM of

plasmid. Then the mixtures of photocrosslinkable DNA building blocks and plasmid of interest was photopolymerized with UV light (8 mW cm^{-2}) in an aqueous solution using a UV crosslinker (Spectronics Corporation, XL-1000) for 10 min.

4.4. Results and discussions

4.4.1. Characterization of photocrosslinked DNA hydrogel

These DNA gels can be formed into pre-selected and different shapes at a macroscopic scale. In addition, DNA hydrogels can also be molded into complicated shapes at microscopic scale. Figure 4.1-3 illustrates micropatterning of DNA gels. A micrometer-sized DNA hydrogel in a given shape is fabricated using traditional photolithography and microfluidic devices. These DNA hydrogels repeatedly return to their original shapes even after successive drying and hydrating without collapsing to films or powders.

4.4.2. Characterization of photocrosslinked DNA-Polymer hydrogel

4.4.2.1. Morphology study of DNA–PEG hydrogels

Various shapes of DNA-PEG hydrogels can be generated in the millimeter size (i.e. macroscopic). FT-IR spectra and electrophoretic mobility shift of photo-crosslinked DNA-PEG hydrogels indicated successful crosslinking between DNA and PEG (Figure 4.4-6).

The morphology and structure of the DNA-PEG hydrogel were investigated using a variety of visualization methods including fluorescence microscopy, FE-SEM, and confocal microscopy. Digital camera and fluorecence images revealed that swollen photocrosslinked DNA-PEG hydrogels with rectangular, round, triangular, cross, and star shapes were successfully fabricated within a defined mould (Figure 4.7). In the swollen state, the structure of a DNA-PEG hydrogel differs drastically

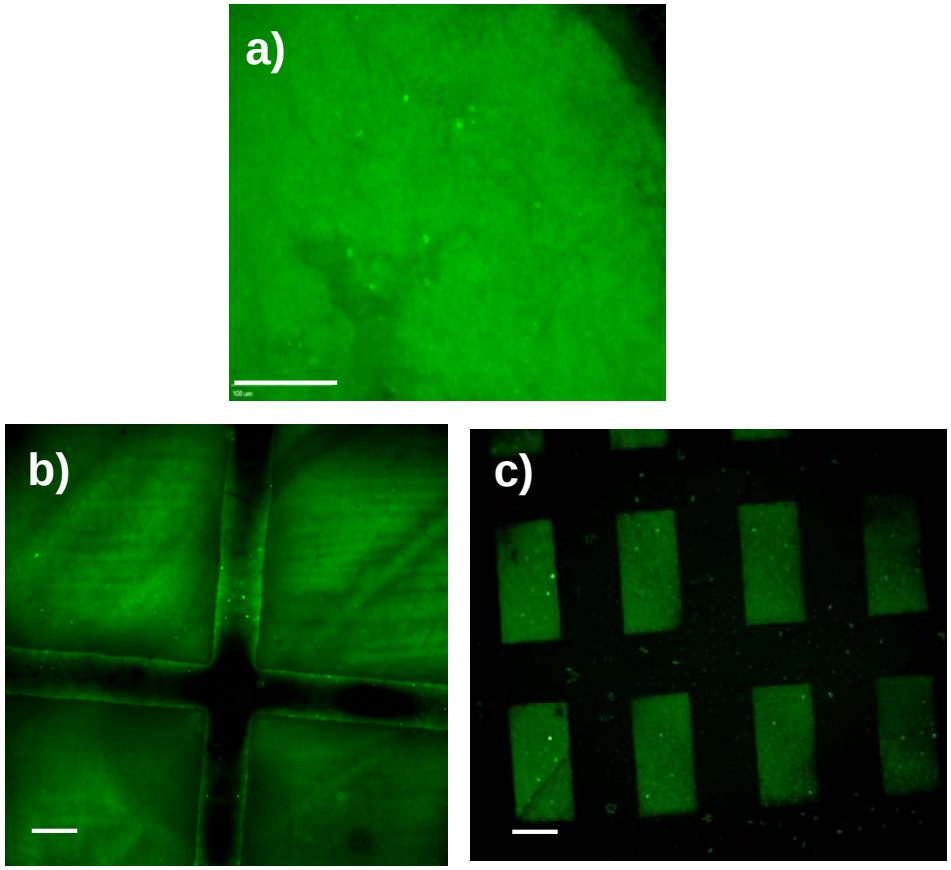

Figure 4.1. Microscopy images of photocrosslinked DNA gels stained with a DNA-specific fluorescent dye, SYBR I (green). (**a**) Fluorescence microscopy image of bulk DNA gel stained with SYBR I. The scale bar is 100 μm. (**b-c**) Fluorescence microscopy images of micropatterned DNA gels with different size patterns (1 mm × 1 mm × 20 μm, (**b**) and 400 μm × 200 μm × 20 μm, (**c**)). The scale bars are 200 μm.

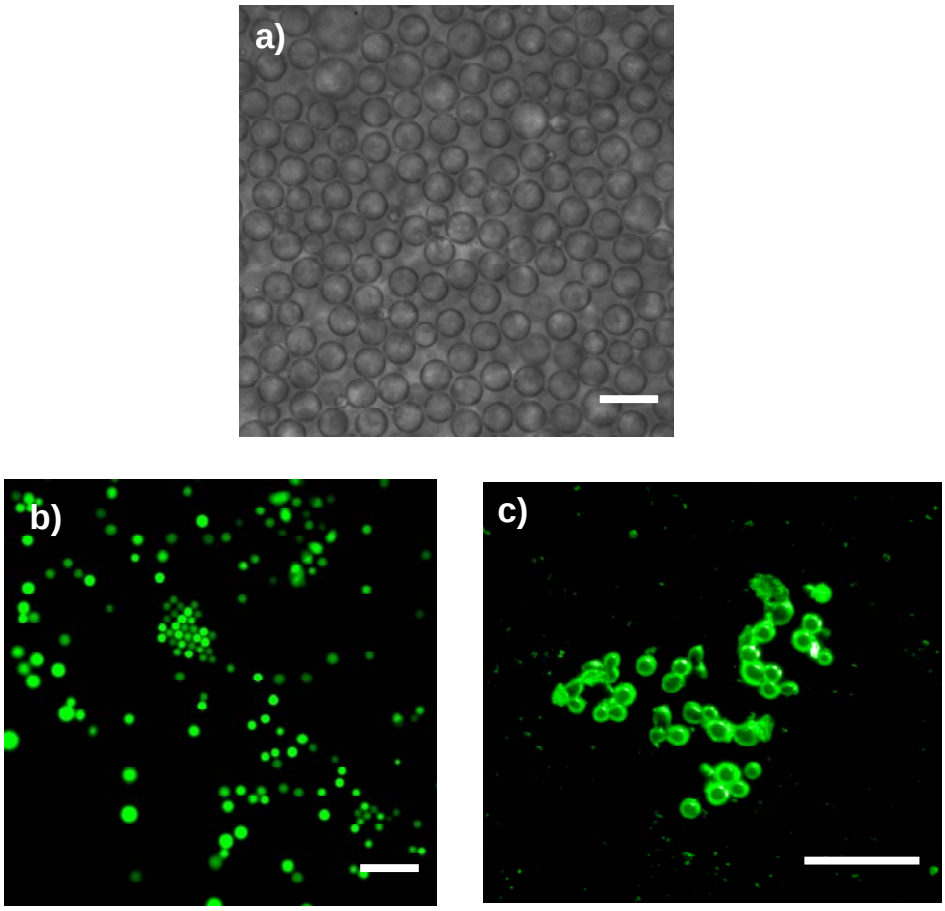

Figure 4.2. Microscopy images of DNA microdroplets combined with photo-polymerization. (**a**) Microscopy image of the water/oil emulsion. (**b-c**) Fluorescence microscopy images of DNA microdroplets after water extraction. The scale bars are 50 μm. Droplets were stained with DNA-specific fluorescent dyes: SYBR I (green).

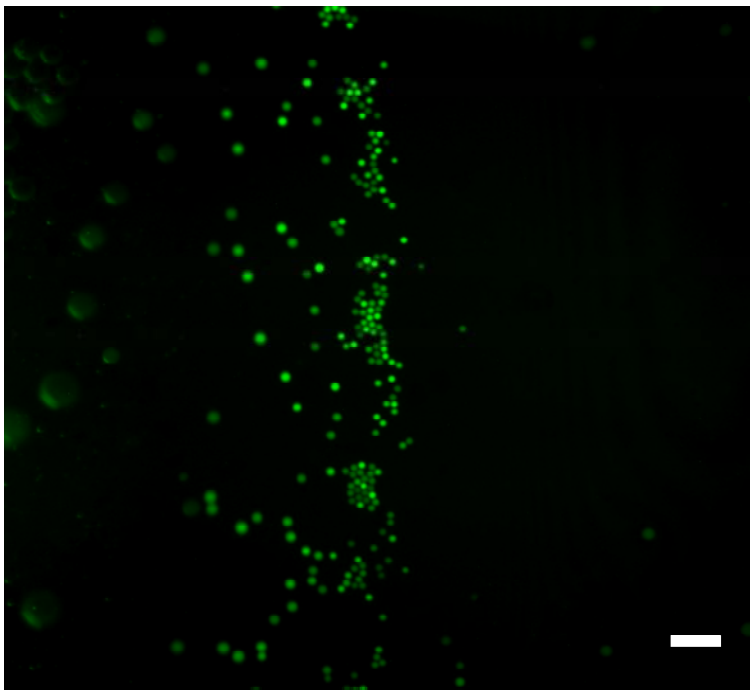

Figure 4.3. Microscopy image of DNA microdroplets combined with photo-polymerization. Fluorescence microscopy image of DNA microdroplets was taken during water-extraction process. The scale bar is 50 μm. DNA microdroplets were stained with DNA-specific fluorescent dyes: SYBR I (green).

with different combinations of DNA and PEG monomers. The more detailed inner structures of the DNA-PEG hydrogels are further evaluated using scanning electron microscopy (SEM) (Figure 4.8). After placing the sample on silicon wafer and mounting it on aluminum stab using double-sided tape, the interior morphological structure of photocrosslinked PEG-DNA hydrogels as a function of DNA-polymer ratio was analyzed using SEM.

The pore structure of photocrosslinked PEG-DNA hydrogels varied according to the PEG content. The increase in PEG content resulted in more compact structure of the hydrogels with thicker walls and smaller pore formation. The result corresponds to the fact that the hydrophilic composition affects the formation of interchain crosslink by increasing crosslink density of hydrogels. The imaging results also demonstrate that the amount of monomers have a significant effect on a pore size of the final DNA hydrogels. More importantly, by selecting different shapes of DNA and PEG monomers and by adjusting the lengths of branched arms, one can design different DNA hydrogels with desired structural properties.

4.4.2.2. Mechanical property of DNA-PEG hydrogels

In order to investigate the effect of the DNA-polymer ratio (PEG wt%) on the properties of photocrosslinked DNA-PEG hydrogel, dynamic mechanical analysis measurements were employed (Figure 4.9). Dynamic mechanical analysis measurements of the newly synthesized photocrosslinked PEG-DNA hydrogel were performed using DMA in a compression mode at room temperature. Stress [MPa] and strain [m/m] were recorded automatically by the system. A sample with 6.35 mm in diameter and thickness ranged from 0.21 mm to 5.15 mm was used. The compressive moduli were calculated from the slope of initial portion of stress vs. strain curve of each hydrogel. The compressive moduli of photocrosslinked PEG gel, photocrossliked

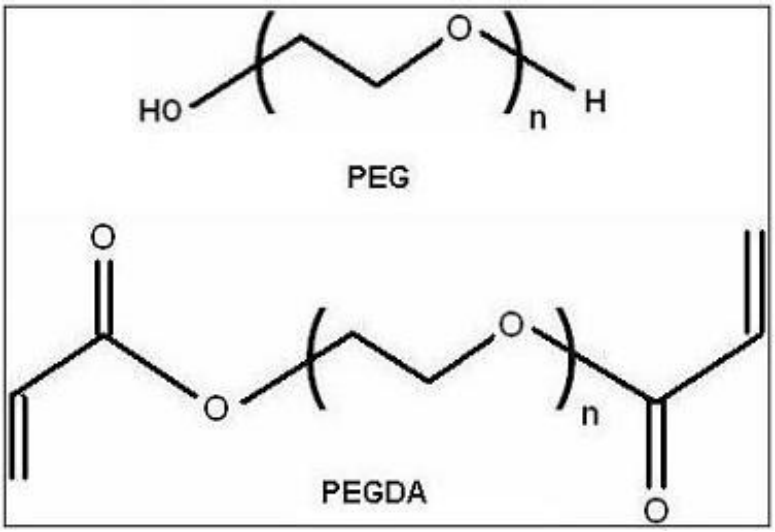

Figure 4.4. Chemical structures of polyethylene glycol (PEG) and polyethylene glycol diacrylate (PEGDA).

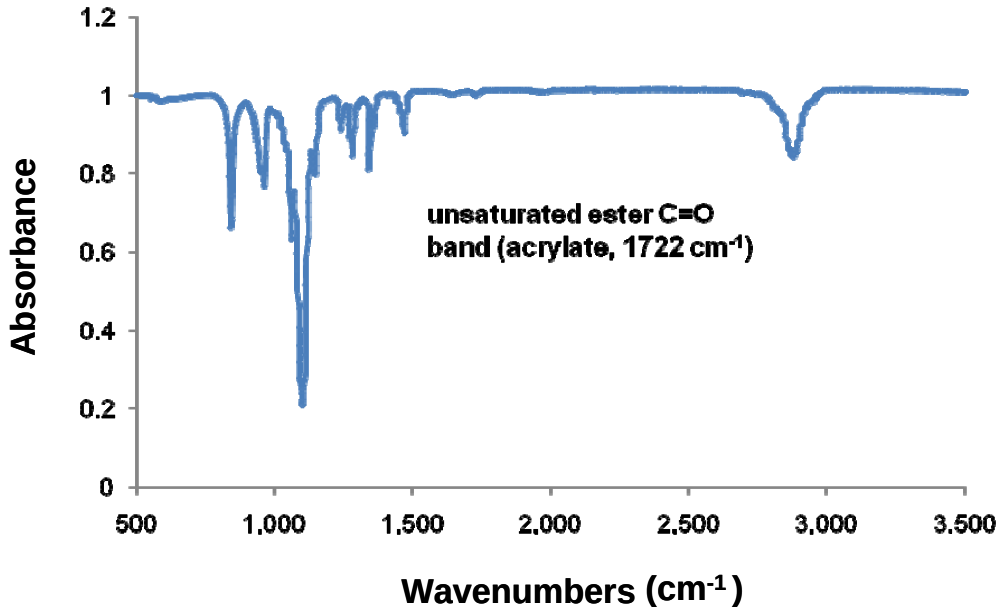

Figure 4.5. FT-IR spectra of photocrosslinked DNA-PEG hydrogel indicate successful crosslinking between DNA and PEG.

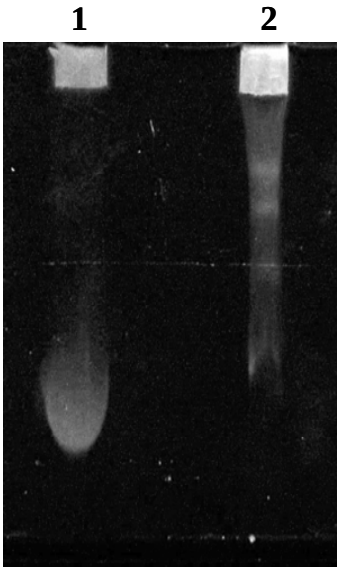

Figure 4.6. Mobility shift of photocrosslinked DNA-PEG hydrogel. Gel electrophoresis of hydrogel fractions were conducted at a constant voltage of 90 volts for 60 min (3 % agarose gel). PEG hydrogels were photocrosslinked with X-DNA which has non-photocrosslinkable groups (Lanes 1) and photocrosslinkable groups (Lanes 2).

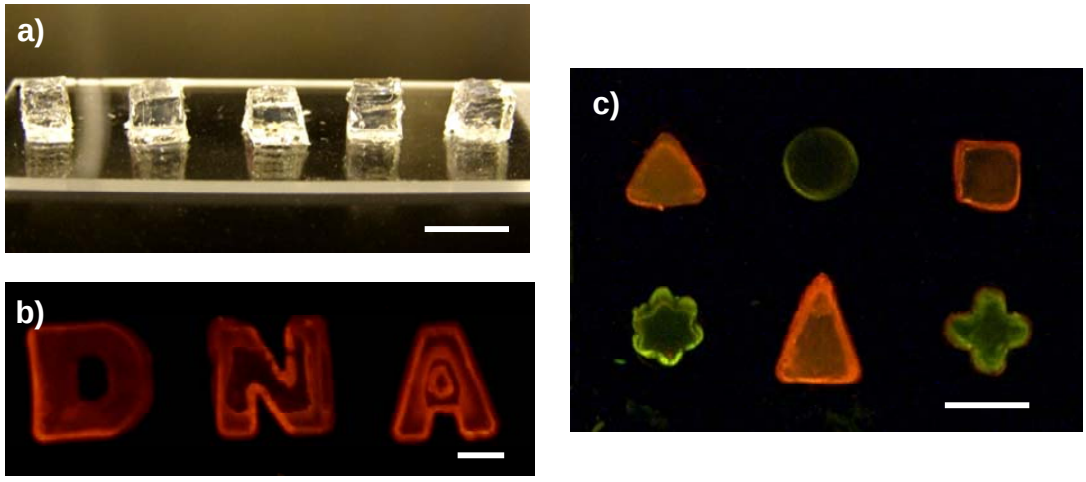

Figure 4.7. Digital amera and fluorecence images of a different type of swollen photocrosslinked DNA-PEG hydrogels fabricated in a defined mould. (**a**) The size is 7.0 mm in one side and 7.0 mm in height. The scale bar is 1 cm. (**b**) Gels patterned in DNA shapes at centimetre scale (the scale bar is 1 cm). (**c**) Gels with different patterns: triangular, circular, rectangular, star and cross. Gels were stained with DNA-specific fluorescent dyes: Gel Red (red color) and Gel Green (green color).

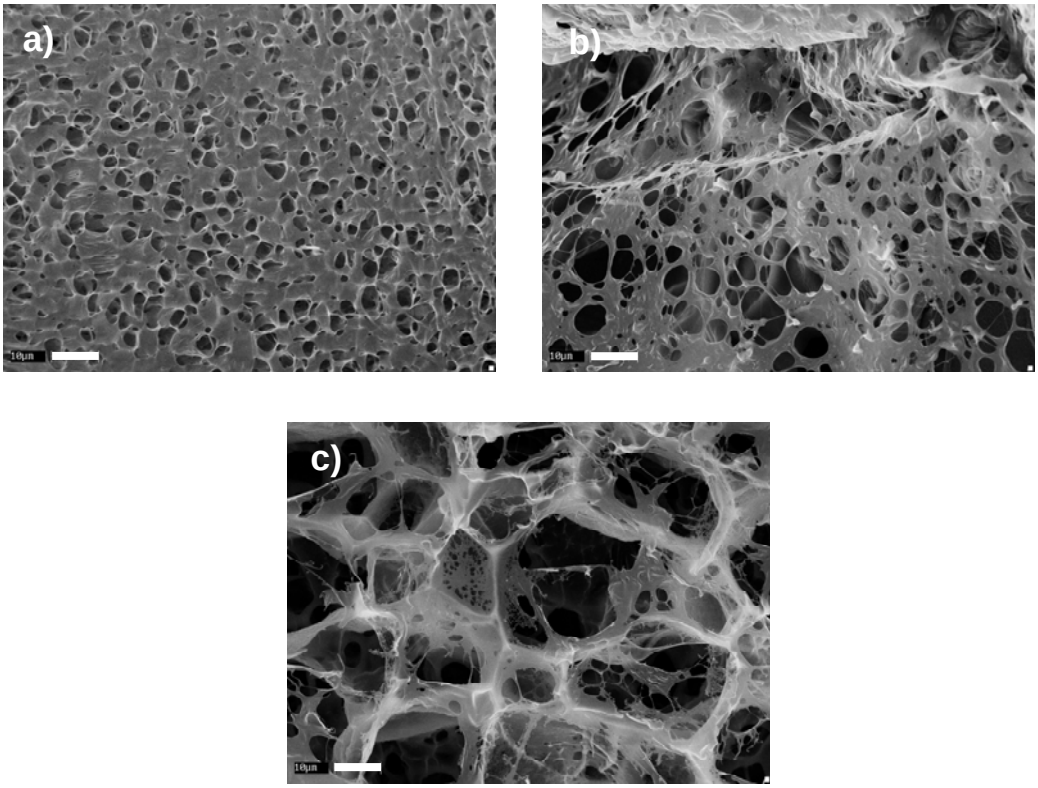

Figure 4.8. SEM images of photocrosslinked DNA-PEG hydrogels. The pore size of DNA-PEG hydrogels can be manipulated by changing the ratios of X-DNA monomers and PEGDA monomers. The scale bars are 10 μm.

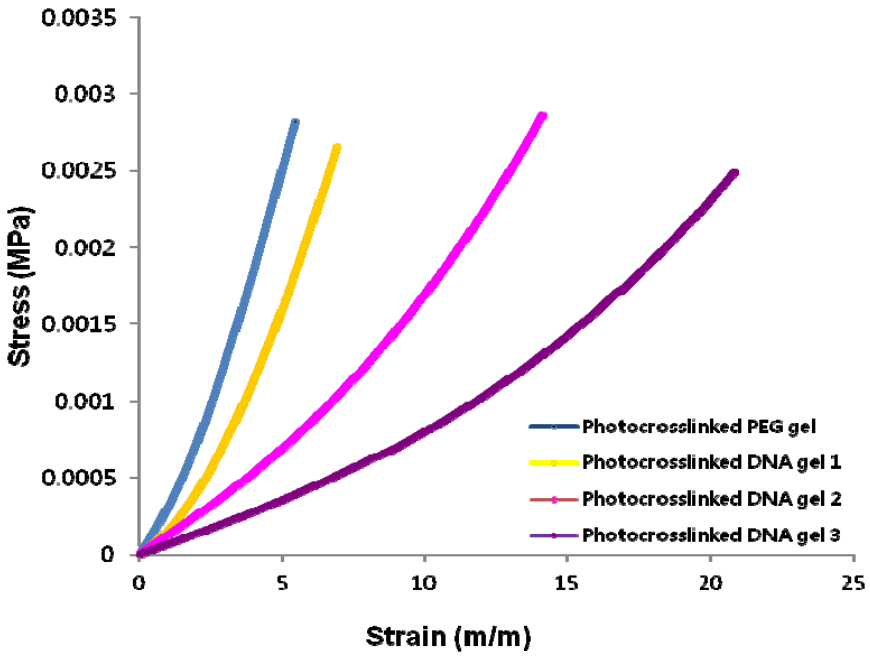

Figure 4.9. Mechanical property of photocrosslinked DNA-PEG hydrogel. The comparison of the stress and strain of a photopolymerized DNA-PEG compared to a PEG hydrogel.

Table 4.3. Mechanical property of photocrosslinked DNA-PEG hydrogel. The comparison of the stress and strain of a photopolymerized DNA-PEG compared to a PEG hydrogel.

	d/dx | x=0	Compressive Modulus
Photocrosslinked PEG gel	$-3E\text{-}07x^4 - 1E\text{-}06x^3 + 7E\text{-}05x^2 + 0.0002x + 1E\text{-}05$	0.0002
Photocrosslinked DNA gel 1	$-2E\text{-}08x^4 - 2E\text{-}06x^3 + 5E\text{-}05x^2 + 0.0001x + 9E\text{-}07$	0.0001
Photocrosslinked DNA gel 2	$-4E\text{-}09x^4 + 3E\text{-}07x^3 + 2E\text{-}06x^2 + 0.0001x + 5E\text{-}06$	0.0001
Photocrosslinked DNA gel 3	$-1E\text{-}09x^4 + 2E\text{-}07x^3 - 5E\text{-}07x^2 + 7E\text{-}05x - 4E\text{-}06$	0.00007

DNA gel 1, photocrossliked DNA gel 2, photocrossliked DNA gel 3 were calculated to be 0.0002, 0.0001, 0.0001 and 0.00007, respectively (Table 4.3).

The denser network structure shown in SEM images and the higher compressive modulus in DMA measurement data demonstrated that the increase in PEG feed ratio leads to higher crosslinking density and tighter network structure owing to the higher amounts of reactive functionalities (acrylate groups) in the reaction mixture. The increase in concentration of PEG caused an increase in the network yield and thus higher mechanical strength.

4.4.3. Characterization of photocrosslinked DNA hydrogel coated particles

A networked matrix of X-DNA building blocks can be integrated into the nano and micro sized particles (Figure 4.10). Particles can be changed for use with any type (e.g. silica, polystyrene, magnetic, gold) and size (e.g. micro and nano). The morphology and structure of the DNA hydrogel coated particles were investigated via a fluorescence microscopy, confocal microscopy, and FE-SEM. Confocal microscopy and SEM images of photocrosslinked DNA hydrogel coated beads, exhibiting the efficient DNA coating onto polystyrene beads (Figure 4.11-13). The size ranges of core materials were from 10 μm to 1 μm. Moreover, multi-layered DNA gels onto particles were successfully synthesized by allowing additional photoreactions. DIC (Differential interference contrast) and fluorescence microscopy images of multi-layered DNA gels onto particles revealed a successful multiple-coating onto magnetic beads (from 1 μm to 300 nm) (Figure 4.14-15). DLS size distribution result showed the size controllability and monodispersity of DNA coated nanoparticles even after multiple photoreactions (Figure 4.16). Two thiol-modified X-DNA building blocks were also designed and prepared for conjugation onto the AuNP (Figure 4.17). Size distribution data exhibited the efficient DNA coating onto AuNP (Figure 4.18).

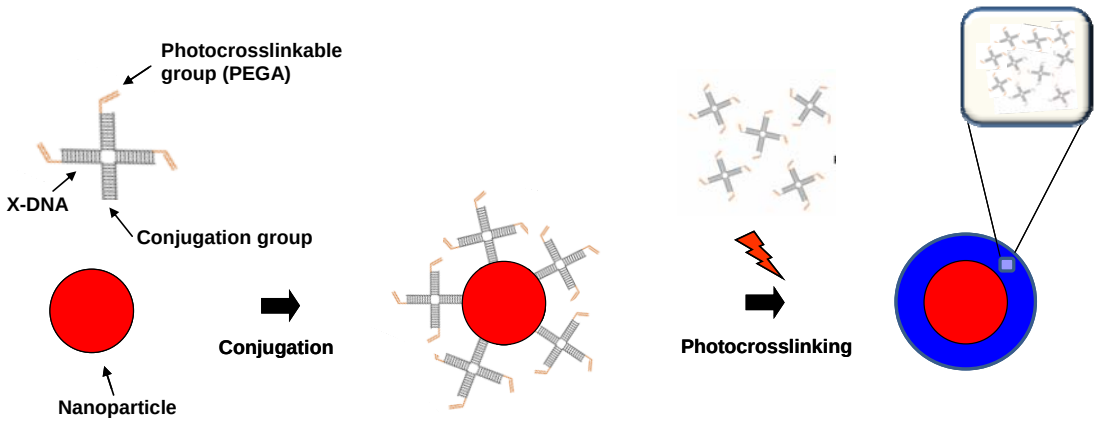

Figure 4.10. Schematic drawing of a networked matrix of X-DNA building blocks integrated into the nano and micro sized particles. Particles can be changed for use with any type and size. X-DNA building blocks and particles are not drawn to scale.

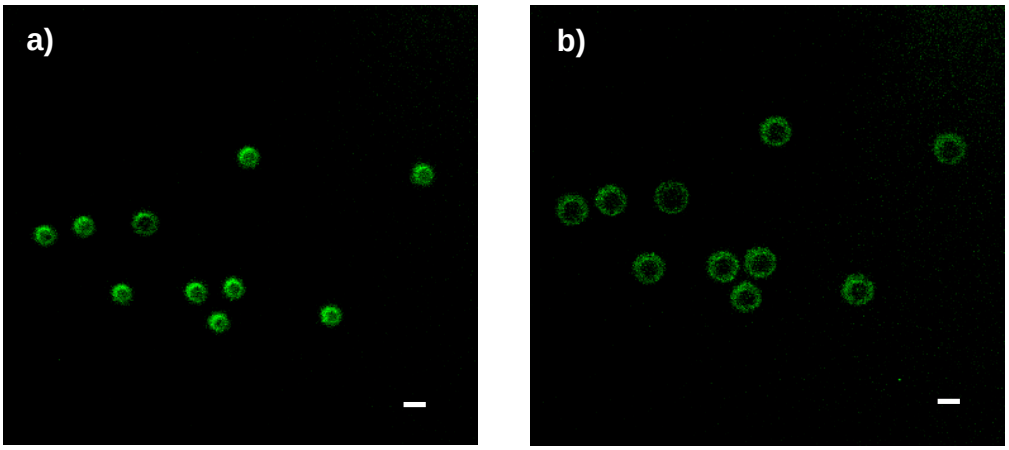

Figure 4.11. Confocal microscopy images of photocrosslinked DNA hydrogel coated beads, demonstrating the efficient DNA coating onto polystyrene beads. The average size of bead is 10 μm. Images were taken with different Z-directional slices (top view: (**a**) and center: (**b**)). DNA was stained with specific fluorescent dyes (SYBR I: green color). The scale bars are 10 μm.

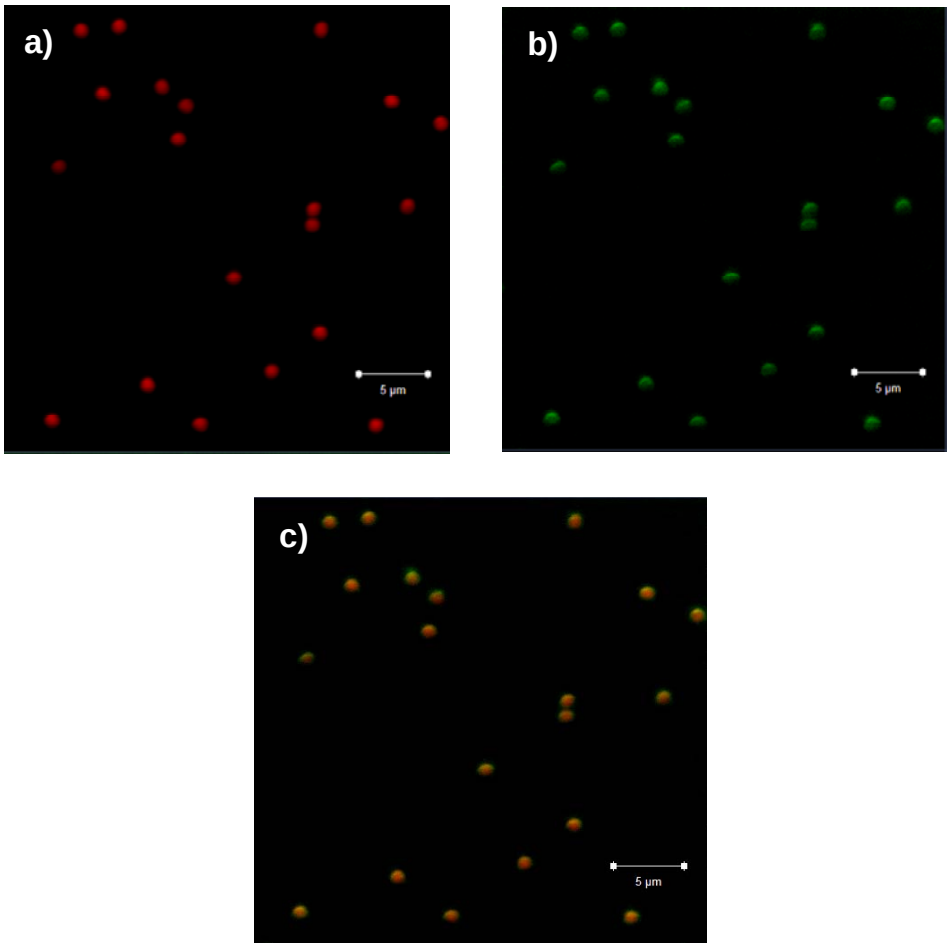

Figure 4.12. Confocal microscopy images of photocrosslinked DNA hydrogel coated particles, exhibiting the efficient DNA coating onto polystyrene beads. The average size of particles is 1 µm. Polystyrene bead (**a**, red color) and DNA (**b**, green color) were pre-stained with specific fluorescent dyes and overlaid (**c**, yellow color). The scale bars are 5 µm.

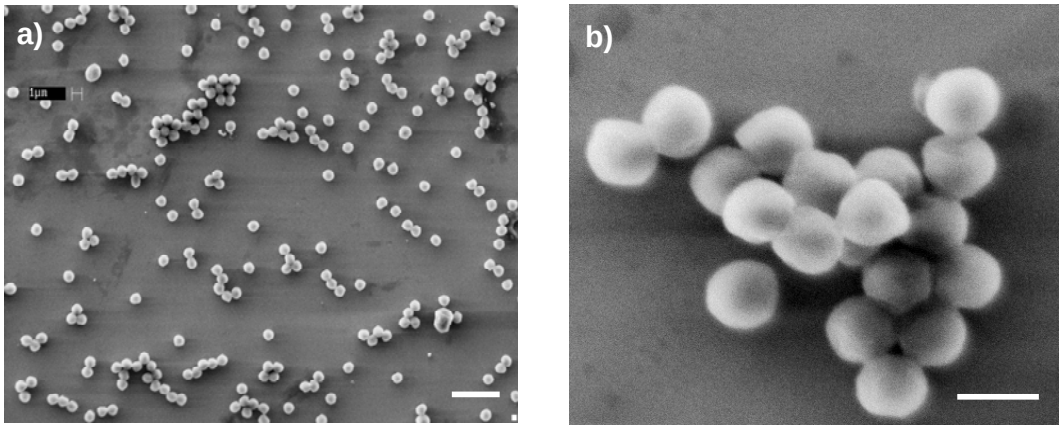

Figure 4.13. SEM images of photocrosslinked DNA hydrogel coated particles. The average size of particles is 1 μm. The scale bars are 5 μm (**a**) and 1 μm (**b**).

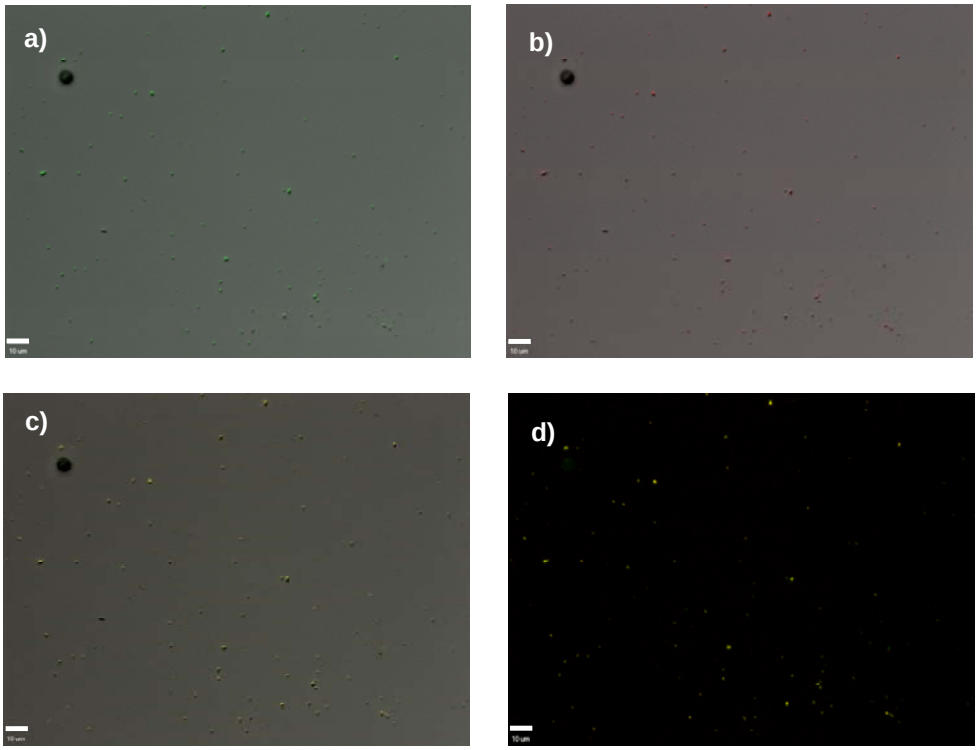

Figure 4.14. Microscopy images of multi-layered and photocrosslinked DNA gels onto nanoparticles. (**a-c**) DIC (Differential interference contrast) microscopy images of photocrosslinked DNA hydrogels after multiple coating onto magnetic beads. Specific fluorescent dyes modified DNA (**a-b**, green and red color) was utilized for each reaction and overlaid (**c**, yellow color). (**d**) Fluorescence microscopy image of photocrosslinked DNA gels coated onto magnetic beads. The average size of magnetic beads is 700 nm. The scale bars are 10 μm.

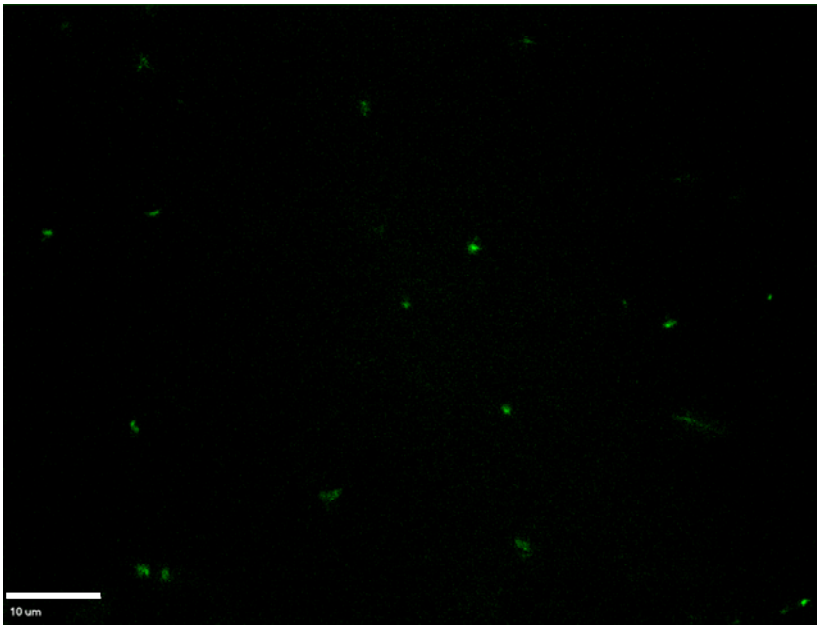

Figure 4.15. Fluorescence microscopy image of photocrosslinked DNA gels coated onto magnetic beads. The average size of magnetic beads is 300 nm. The scale bar is 10 μm.

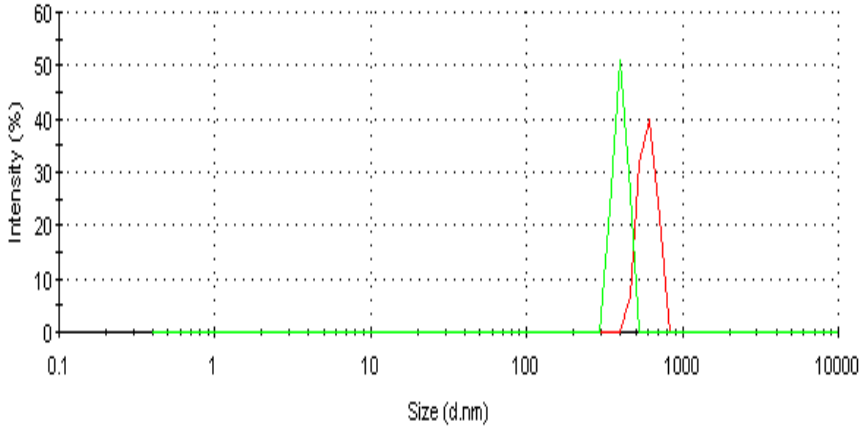

Figure 4.16. DLS size distribution of DNA coated nanoparticles after multiple photoreactions. Size distribution data shows the size controllability and monodispersity of DNA coated nanoparticles. The average size of nanoparticles before photoreaction is 300 nm.

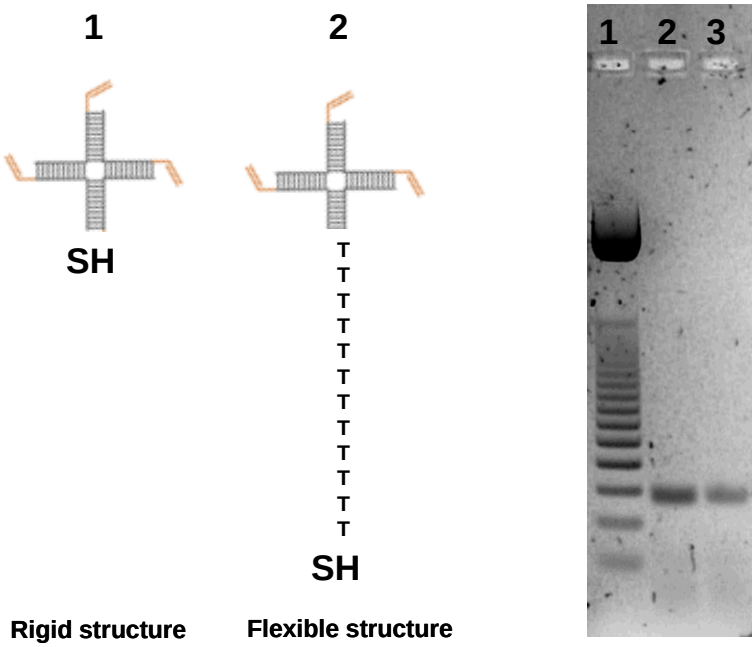

Figure 4.17. (**a**) Two different X-DNAs were designed and prepared for AuNP conjugation. (**b**) Electrophoretic mobility shift of thiol-modified X-DNA building blocks for conjugation onto the AuNP. Lanes 1–3 indicate ladder (100 bp), two different types of X-DNA respectively.

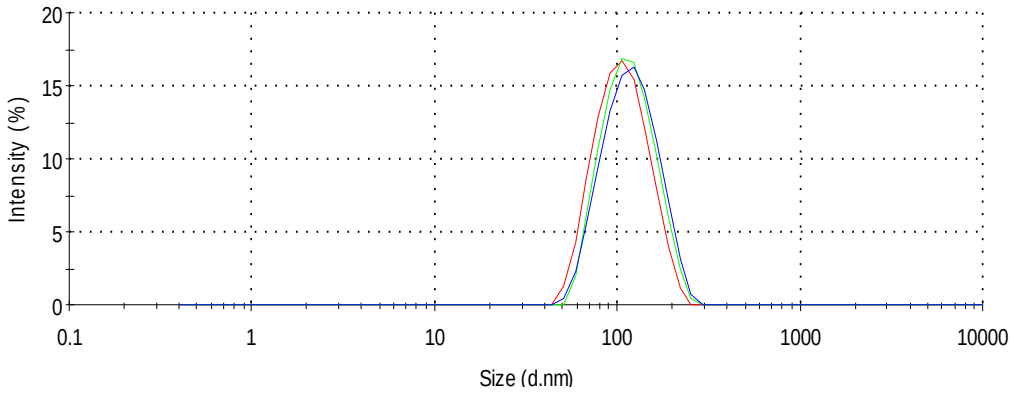

Figure 4.18. DLS size distribution of DNA coated nanoparticles during photoreaction. Size distribution data exhibit the efficient DNA coating onto AuNP. The average size of AuNP (original) is 101.6 nm. The average size of AuNP after thiol-modified X-DNA conjugation is 116.1 nm. The average size of DNA coated AuNP after photoreaction is 130.3 nm.

4.4.4. Application of photocrosslinked DNA hydrogel

4.4.4.1. Evaluation of protein expression from photocrosslinked DNA hydrogel

A new DNA hydrogel for protein production was constructed by utilizing two types of nucleic acids: linearized plasmid and X-shaped DNA (X-DNA) building blocks. The linearized plasmid vector containing a gene for *Renilla luciferase* was used to photocrosslink with X-DNA monomers, incorporating the gene into the DNA hydrogel (Figure 4.19). *Renilla luciferase* is a 36 kDa monomeric protein and does not require a post-translational modification for activity. The linearized plasmid vectors were prepared by digesting the vector at a single site using *Apa I* restriction enzyme. The X-DNA building blocks were prepared through complimentary hybridization of four different oligonucleotides after functionalization (photocrosslinkable group). The gel electrophoresis result showed a complete linearization of the circular DNA after *Apa I* digestion and also the attachement of photocrosslinkable groups by either using PCR method or hybridization (Figure 4.20).

The photocrosslinking of X-DNA to linearized plasmids was performed using one of two methods to link the *Renilla luciferase* genes to the DNA hydrogels. In one method, the genes were crosslinked onto DNA building blocks wherein the genes were pre-modified with one or more photoresponsive moities. In the following step, both photocrosslinkable genes and DNA-building blocks were combined together via photoreaction. In the second approach, DNA building blocks with partial photocrosslinkable groups and sticky-ends were first hybridized with linearized gene sequences via hybridization. Then additional photocrosslinkable DNA building blocks were incorporated to create DNA hydrogels. Using either approach, methods were carried out for protein production.

In vitro expression of *Renilla luciferase* (Rluc) protein from photocrosslinked protein-producing gels consist of genes as part of the gel scaffolding was conducted

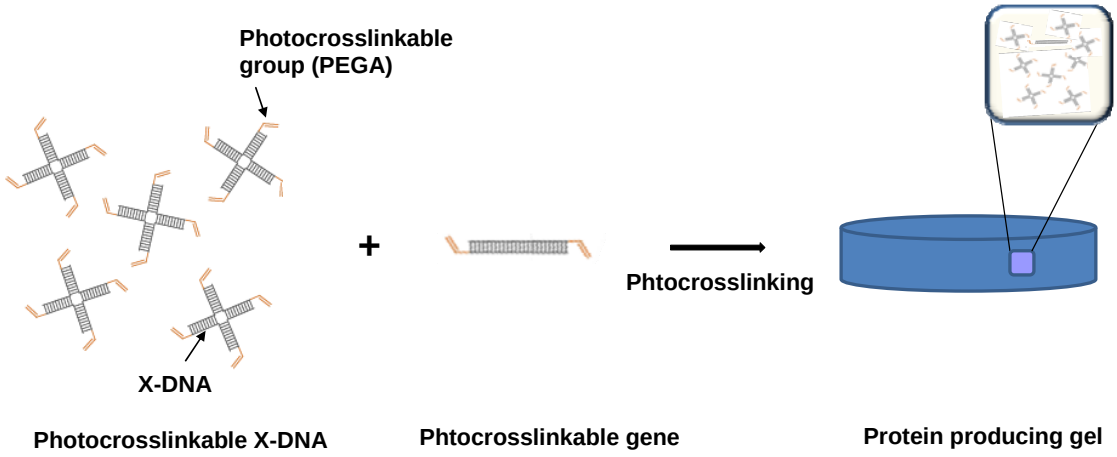

Figure 4.19. A schematic outline for cell-free protein production using photo-crosslinked nucleic acid hydrogels.

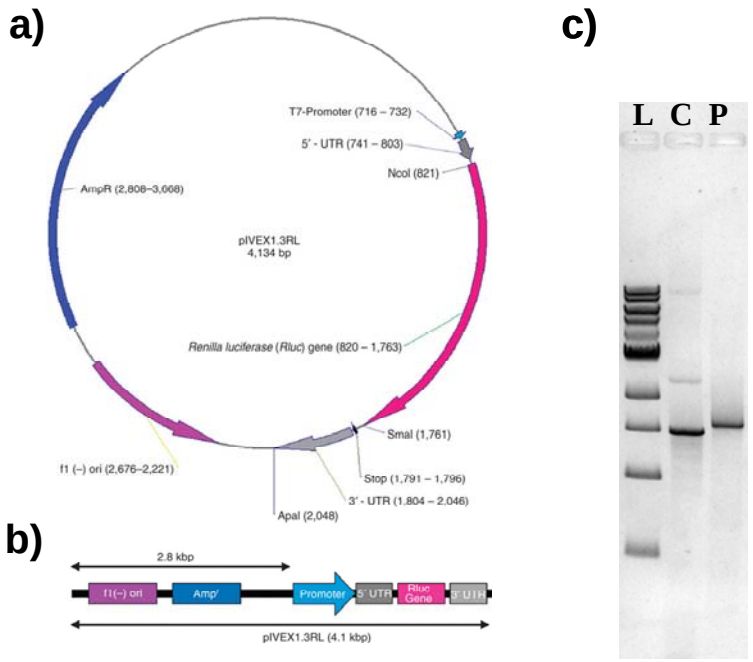

Figure 4.20. Schematic plasmid map of pIVEX 1.3RL. (**a**) Circular, the gene (*Renilla luciferase* (Rluc)) is located downstream from the T7 promoter, between *Nco*I and *Sma*I restriction sites. The *Apa*I restriction site is used to linearize the plasmid. (**b**) A complete linearization of the circular DNA after *Apa* I digestion. (**c**) Electrophoretic migration shift of linearized *Renilla luciferase* (Rluc) plasmid before and after functionalization (photo-crosslinkable group). Lanes L, C, and P correspond to Ladder (1kb), linearlized luciferase gene (before functionalization), and photocrosslinkable gene respectively. Reprinted by permission from Macmillan Publishers Ltd: Nature protocols (11), copyright (2009).

using a coupled gene transcription and translation kit (Roche). Conventional cell-free systems are solution phase systems (SPS), in which the gene templates are dispersed in solution. Here, SPS was used as a benchmark to evaluate the productivity (efficiency and yield) of protein produced using photocrosslinked P-gels. We produced Rluc protein with the photocrosslinked P-gel using the same conditions as those for the SPS. The results showed that a functional protein expression in DNA gel form had an efficiency about 72 times fold increases greater than solution based systems (Figure 4.21). In terms of volumetric yield, the photocrosslinked P-gel produced up to about 1 mg/ml of functional protein. Because the DNA gel is composed only of DNA, there were no non-specific bindings that may have caused lower protein expression in other solid phase systems.

4.4.4.2. Evaluation of photocrosslinked DNA-Polymer hydrogel for protein production

In previously reported P-gel system, the protein yielding matrixes can be re-used at least 3 times and can last 7 days before the gel micropads are degraded by nucleases from lysates. However, by linking the nucleic acid based matrices with at least one copolymer or additional compound, mechanically stronger gels were constructed. Here the crosslinking with PEG is utilized to make stronger gels, where PEG is attached onto the DNA strands by direct crosslinking PEG with DNA in the gel. The effect of PEG polymer on *Renilla Luciferase* expression was determined by varying the DNA/PEG ratios of plasmid photopolymerized to the hydrogels in the reaction (Figure 4.22). The same amounts of the plasmid were utilized in enzyme-ligased P-gel as a control reaction. The results demonstrated that DNA-PEG hydrogels produced a similar amount of protein (80-90 % yield compare to enzyme-catalyzed P-gel system) with improved reusability.

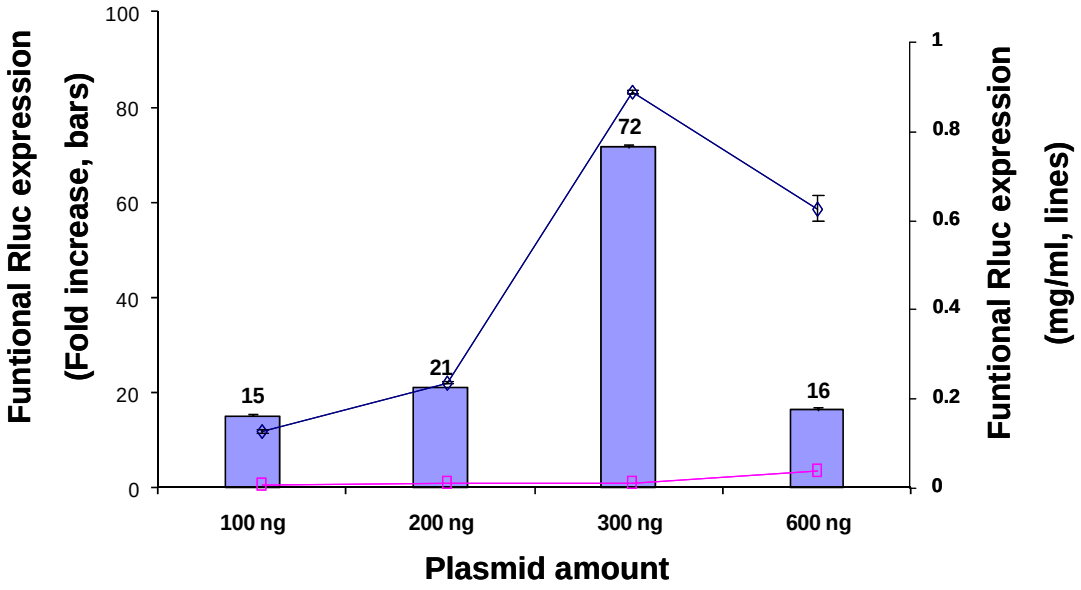

Figure 4.21. Effect of the total gene amounts on functional protein expression via photocrosslinked DNA hydrogels. The functional Rluc expression was determined by varying the concentration of plasmid photo-polymerized to the DNA hydrogels in the reaction (Blue lines). The same amounts of the plasmid were used in solution phase systems (SPS) control reactions (Red lines). In terms of volumetric yield, the photo-crosslinked P-gel produced up to about 1 mg/ml of functional protein. The bars indicate the fold-change in functional protein expression efficiency compared to SPS.

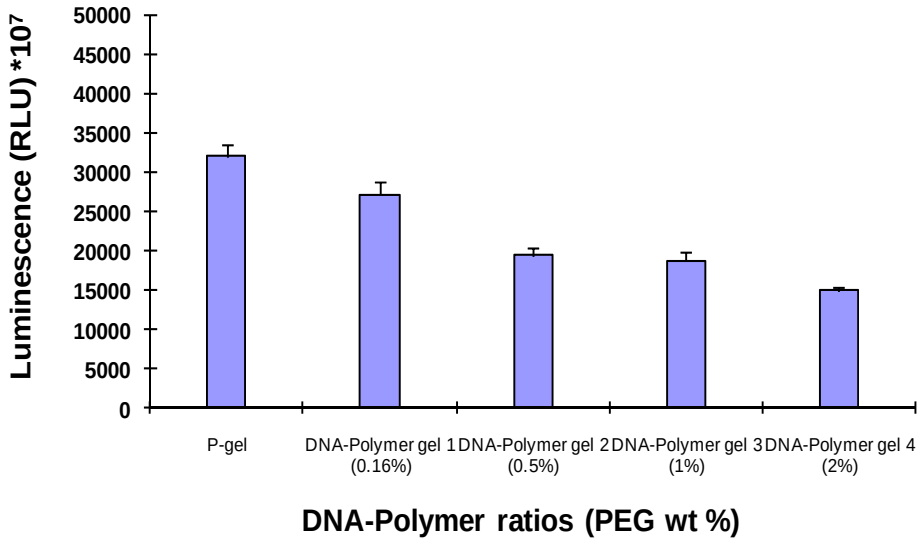

Figure 4.22. Effect of the additional crosslinker on functional protein expression. The effect of PEG polymer on *Renilla Luciferase* expression was determined by varying the DNA/PEG ratios of plasmid photopolymerized to the hydrogels in the reaction. The same amounts of the plasmid were utilized in enzyme-ligased P-gel as a control reaction.

4.4.4.3. Evaluation of protein expression from various formats of photocrosslinked DNA gels

Different formats of photocrosslinked DNA hydrogels for protein expression were prepared (Figure 4.23, 25). Using these systems we have performed protein expression experiments to optimize and achieve sufficient protein yield. For example, in the case of DNA nanospheres, protein expression of *Renilla Luciferase* was optimized by changing X-DNA/gene ratios (Figure 4.24). We obtained maximum yield with a 3000:1 ratio. In addition, photocrosslinked DNA hydrogel coated particles were examined to produce protein. Two different sizes of particles were prepared for protein production and the amount of protein yield was compared with control SPS. According to our data, enhanced protein yield was obtained from DNA hydrogel coated particles (20-30 fold increase from control).

We also tried protein expression by varying different parameters such as bead types (magnetic, silica, polystyrene), bead sizes (1 μm, and 5 μm), DNA monomers concentration, and coating thickness. For example, in the case of DNA concentration, we optimized by changing X-DNA amount during photoreaction (Figure 4.26). Two different sizes of nanoparticles (the average nanoparticle size are around 1 μm and 5 μm) were prepared to produce protein and the protein amount of *Renilla Luciferase* was compared with control SPS (Figure 4.27). When we changed to larger size of bead (5 μm) we could improve protein yield. Interestingly when we changed DNA coating thickness onto nanoparticles by varying the number of photoreation, yield was much increased compared to thinner one (Figure 4.28). Based on results we achieved, bead size, surface areas and/or DNA coating thickness are important factors to determine protein yield.

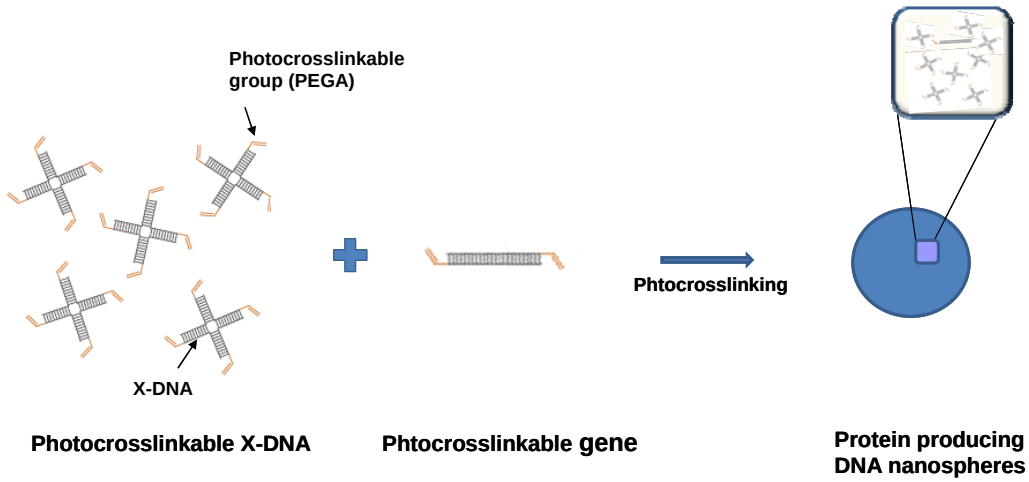

Figure 4.23. Schematic illustration of the construction of photocrosslinked DNA nanospheres for cell-free protein production.

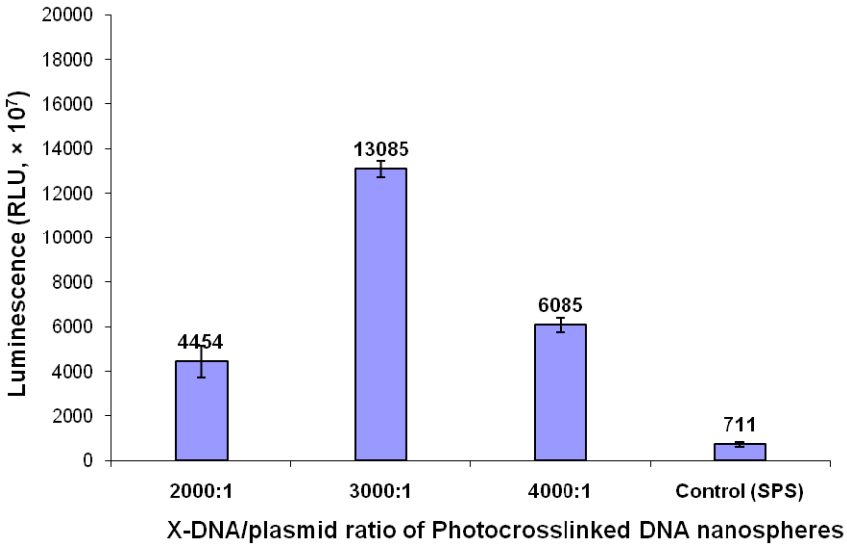

Figure 4.24. Effect of the crosslinker (X-DNA) and plasmid ratio of photocrosslinked DNA nanospheres on functional *Renilla Luciferase* expression.

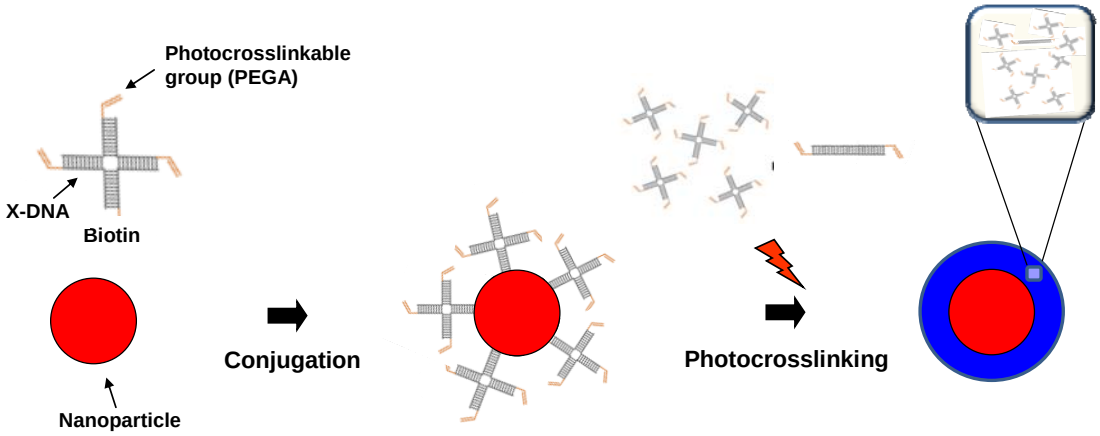

Figure 4.25. Schematic illustration of the synthesis of DNA hydrogels coated particles via photocrosslinking for cell-free protein production.

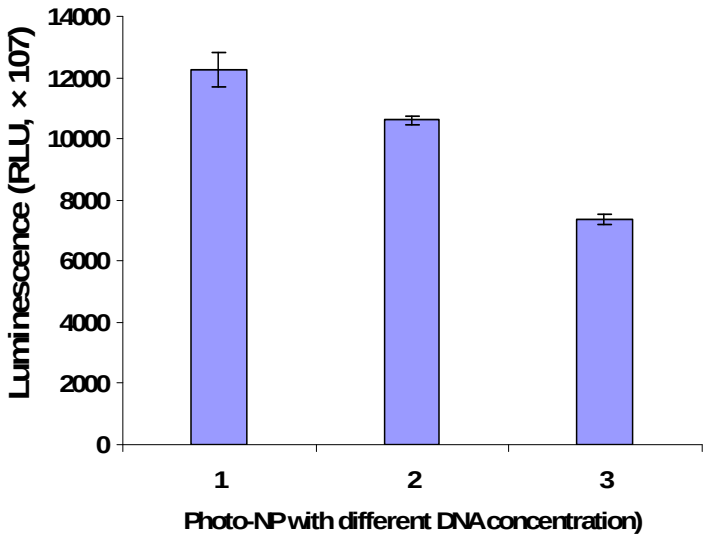

Figure 4.26. Effect of the crosslinker concentration of photocrosslinked DNA hydrogels coated nanoparticles on functional protein expression. The effect of photocrosslinked DNA hydrogel coated nanoparticles on *Renilla Luciferase* expression was determined by changing the X-DNA amount during photoreaction.

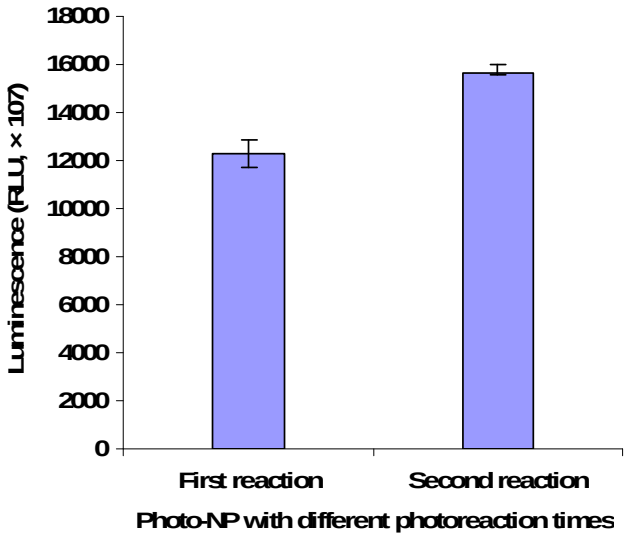

Figure 4.27. Effect of the coating thickness of photocrosslinked DNA hydrogel-coated nanoparticles on functional protein expression. Two different thicknesses of DNA coating were prepared by varying the extent of photoreaction.

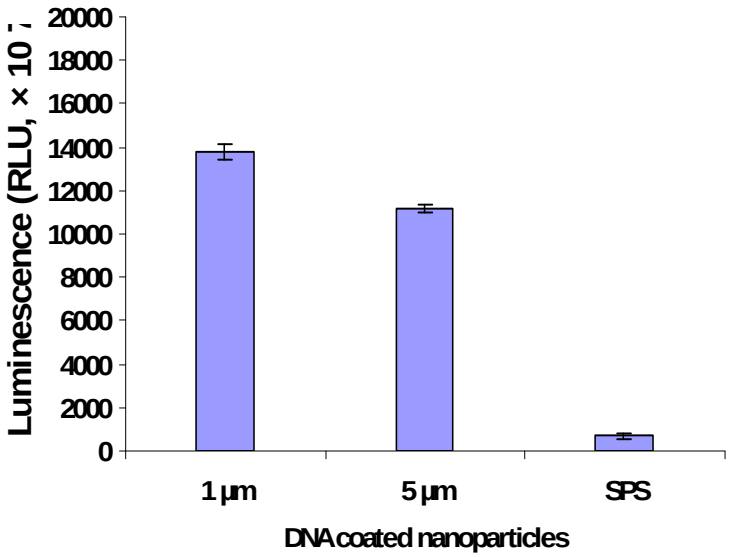

Figure 4.28. Effect of the particle size of photocrosslinked DNA hydrogels coated nanoparticles on functional protein expression. Two different sizes of particles (the average particle size are around 1 µm and 5 µm) were prepared to produce protein and the amount of *Renilla Luciferase* was compared with control SPS.

4.5. Conclusion

In summary, newly developed photocrossliked DNA hydrogels with different formats were constructed from branched DNA building blocks. By designing a matrix comprising different nucleic acid molecules, as well as nucleic acid molecules of different shape, sequence or length, a designer gel can be utilized to produce for any target drug, including any bioactive agent, cells, viruses, small molecules, peptides, polypeptides and antibodies. Indeed, these DNA hydrogels demonstrate improved mechanical properties corresponding to the polymer chemistry, suggesting industrially-feasible applications in, for example, protein engineering.

REFERENCES

1. Peppas et al., Hydrogels in Biology and Medicine: From Molecular Principles to Bionanotechnology. Adv. Mater. 18:1345-60 (2006)
2. Luo, D. The Road from Biology to Materials. Mater. Today 6:38-43 (2003)
3. Y. Li, Y. D. Tseng, S. Y. Kwon, L. d'Espaux, J. S. Bunch, P. L. McEuen, D. Luo, *Nat Mater 3*, 38 (2004)
4. Y. Li, Y. T. Cu, D. Luo, *Nat Biotechnol 23*, 885 (2005).
5. S. H. Um, J. B. Lee, S. Y. Kwon, Y. Li, D. Luo, *Nat. Protocols 1*, 995 (2006)
6. J. B. Lee, Y. H. Roh, S. H. Um, H. Funabashi, W. Cheng, J. J. Cha, P. Kiatwuthinon, D. A. Muller, D. Luo, *Nat Nano 4*, 430 (2009)
7. U. Feldkamp, B. Saccà, Christof M. Niemeyer, *Angewandte Chemie International Edition 48*, 5996 (2009)
8. S. H. Um, J. B. Lee, N. Park, S. Y. Kwon, C. C. Umbach, D. Luo, *Nat Mater 5*, 797 (2006)
9. N. Park, S. H. Um, H. Funabashi, J. Xu, D. Luo, *Nat Mater 8*, 432 (2009)
10. A pH-Triggered, Fast-Responding DNA Hydrogel Enjun Cheng, Yongzheng Xing, Ping Chen, Yang Yang, Yawei Sun, Dejian Zhou, Lijin Xu, Qinghua Fan, and Dongsheng Liu *Angewandte Chemie* 41, 7796–7799 (2009)
11. Nokyoung Park et al *Nature Protocols* **4**, - 1759 - 1770 (2009)
12. Y. H. Roh, J. B. Lee, S. J. Tan, B. Kim, H. Park, E. J. Rice, D. Luo *Macromol. Rapid Commun. 31*, 1207–1211 (2010)

CHAPTER 5

Future work

5.1. Multi-drug delivery systems via DNAsomes

Based on previous achievements, DNAsomes are particularly suited for multi-functionalization in a finely-controlled fashion due to their multivalency, monodispersity, anisotropicity, and the rich chemistry of DNA bioconjugation. Moreover DNAsomes demonstrated a universal approach to construct multi-drug delivery vectors for simultaneous co-delivery. Therefore future work on DNAsomes can be further extended by selecting combinations of various functional types (targeting moieties, proteins, tracer dyes, or antibodies) along with nucleic acids (aptamers, genes, siRNA, or antisense nucleic acids).

5.2. Nanopatterning of photocrosslinked DNA nanospheres and DNA coated nanoparticles

Recently nanoparticle-based 1D nanowires, 2D superlattices, and 3D dry crystals were successfully fabricated by using ssDNA as a nano-organizer.[1-3] Photocrosslinked DNA nanospheres and DNA coated nanoparticles were utilized for superlattice-nanopatterning within PDMS moulds through a local dewetting process (Figure 5.1). Instead of using ssDNA-capped nanoparticles, branched DNA-modified nanoparticles were utilized for nanopatterning. Spatial regulation between nanoparticles or nanospheres can be achieved by controlling the thickness of DNA-coating layers through multiple photoreactions.

A PDMS mould was designed to offer defined structures and sizes, and a nano-sized DNA hydrogel was obtained through a photoreaction. According to size distribution results from DLS, photocrosslinked DNA nanospheres with 230 nm average size were successfully synthesized (Figure 5.2). Then these nano-sized gels were further transferred to the PDMS mould and arrayed by controlling moulding pressures. Under low moulding pressure the edge dewetting patterning tendency

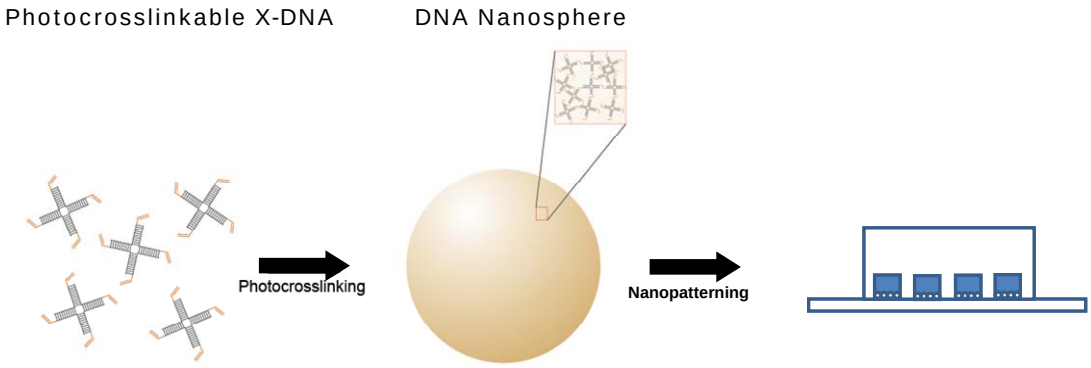

Figure 5.1. A schematic outline for superlattice-nanopatterning of photocrosslinked nucleic acid hydrogels using a PDMS mould for moulding microdroplets.

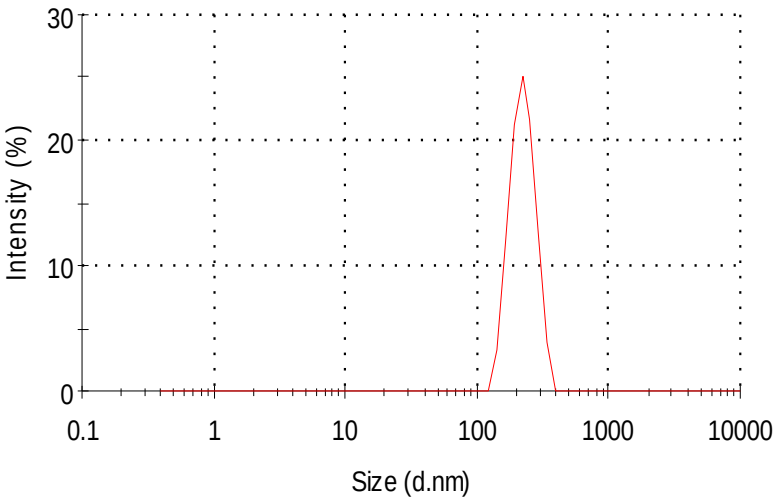

Figure 5.2. DLS size distribution of DNA nanospheres after photoreactions. The average size of DNA nanospheres is 230 nm.

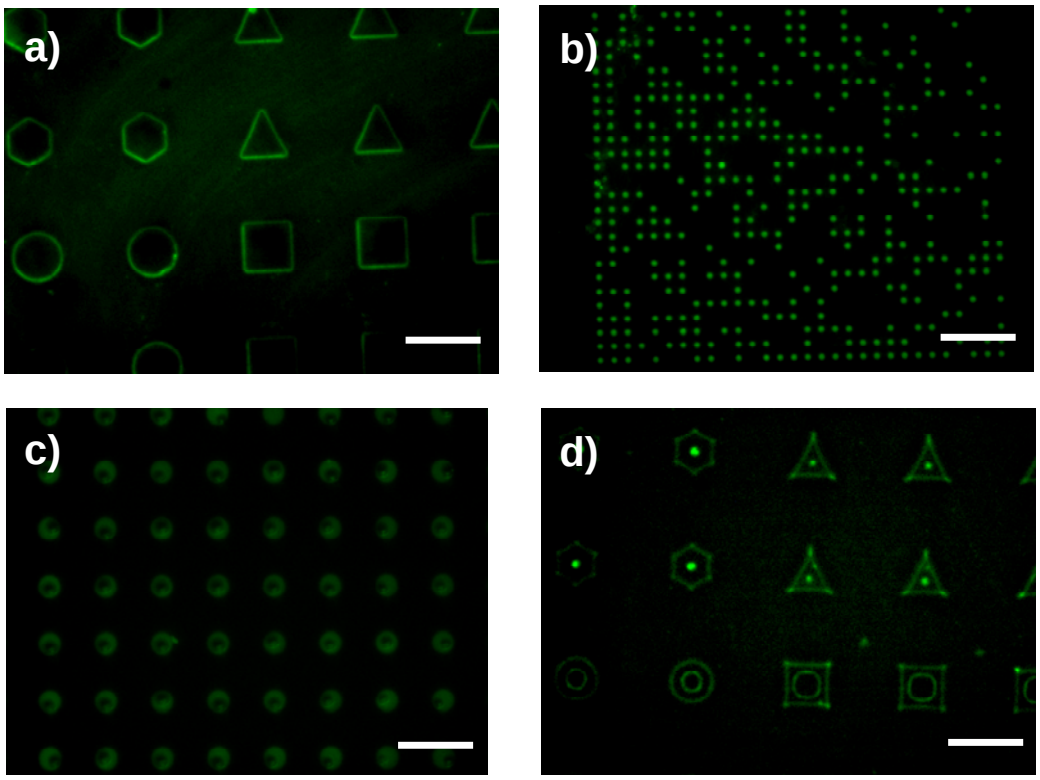

Figure 5.3. Microscopy images of micro-patterned DNA hydrogels combined with photo-polymerization. (**a-c**) Fluorescence microscopy images of different sizes and shapes of micro-patterned DNA hydrogels. (**d**) Fluorescence microscopy image of multi-layered and micro-patterned DNA hydrogels after additional photoreaction. The scale bars are 20 μm. Gels were pre-stained with the DNA-specific fluorescent dye: SYBR I (green).

occurred, and under high moulding pressure centre dewetting occurred (Figure 5.3). More complicated, multiple-layered and micro-patterned structures can be obtained by allowing additional photoreactions during dewetting process (Figure 5.3d). To enhance the patterning capability, we considered several parameters including micromould geometry, moulding pressures, gel concentration, and additional photoreactions during the dewetting process. Notably these DNA gels-based nanomaterials can be utilized for the signal enhancement effect of SERS by attaching multiple functional moieties onto branched DNA building blocks. In addition these micropatterned DNA hydrogels have a great potential in cell culture for tissue engineering.

5.3. Functionalized DNA hydrogels via photocrosslinking

The results from the DNA-PEG hydrogel showed that desired structural property and higher mechanical strength were manipulated by selecting the ratios between DNA and PEG monomers and by adjusting the types of branched arms. Similar to DNA-PEG hydrogel, DNA hydrogel can chemically interact with a wide range of synthetic and natural polymers by photoreaction. Therefore, the investigation of functionalized DNA-polymer hydrogel with improved gel properties has great potential in real-world applications.

REFERENCES

1. Cheng, W., Park, N., Walter, M.T., Hartman, M.R. & Luo, D. Nanopatterning self-assembled nanoparticle superlattices by moulding microdroplets. *Nat. Nano.* **3**, 682-690 (2008).
2. Cheng, W., Campolongo, M.J., Cha, J.J., Tan, S.J., Umbach, C.C., Muller, D.A. & Luo, D. Free-standing nanoparticle superlattice sheets controlled by DNA. *Nat. Mater.* **8**, 519-525 (2009).
3. Cheng, W., Hartman, Mark R., Smilgies, D.-M., Long, R., Campolongo, Michael J., Li, R., Sekar, K., Hui, C.-Y. & Luo, D. Probing in real time the soft crystallization of DNA-capped nanoparticles. *Angew. Chem. Intl. Ed.* **49**, 380-384 (2010).